SCIENCE CHINA Materials REVIEWS

mater.scichina.com link.springer.com

Published online 10 October 2020 | https://doi.org/10.1007/s40843-020-1456-x
Sci China Mater 2020, 63(11): 2153–2188

SPECIAL TOPIC: Advanced Photocatalytic Materials

Nanostructured CdS for efficient photocatalytic H_2 evolution: A review

Rongchen Shen[1†], Doudou Ren[1†], Yingna Ding[2], Yatong Guan[2], Yun Hau Ng[3*], Peng Zhang[4*] and Xin Li[1*]

ABSTRACT **Cadmium sulfide (CdS)-based photocatalysts have attracted extensive attention owing to their strong visible light absorption, suitable band energy levels, and excellent electronic charge transportation properties. This review focuses on the recent progress related to the design, modification, and construction of CdS-based photocatalysts with excellent photocatalytic H_2 evolution performances. First, the basic concepts and mechanisms of photocatalytic H_2 evolution are briefly introduced. Thereafter, the fundamental properties, important advancements, and bottlenecks of CdS in photocatalytic H_2 generation are presented in detail to provide an overview of the potential of this material. Subsequently, various modification strategies adopted for CdS-based photocatalysts to yield solar H_2 are discussed, among which the effective approaches aim at generating more charge carriers, promoting efficient charge separation, boosting interfacial charge transfer, accelerating charge utilization, and suppressing charge-induced self-photocorrosion. The critical factors governing the performance of the photocatalyst and the feasibility of each modification strategy toward shaping future research directions are comprehensively discussed with examples. Finally, the prospects and challenges encountered in developing nanostructured CdS and CdS-based nanocomposites in photocatalytic H_2 evolution are presented.**

Keywords: solar fuel, nanostructured cadmium sulfide-based photocatalysts, modification strategies, hydrogen production, photocharge utilization

INTRODUCTION

Rapid urbanization and industrialization have led to a shortage of global energy resources, while significant amounts of harmful and toxic chemical pollutants are being discharged into the environment [1–5]. This necessitates research on environment-friendly technologies to solve the aforementioned environmental and energy crises. Tremendous efforts have been devoted toward developing technologies for producing clean and sustainable energy [6–9]. Among the available renewable energy options, solar energy conversion into chemical fuels has been extensively studied in recent decades [10–14]. Solar energy can become the greenest and most abundant energy source on earth if efficient harvesting and conversion are enabled [15–20]. Among the proposed technologies, visible-light-activated semiconductor photocatalytic technology has been considered one of the most promising strategies for simultaneously overcoming the challenges of environmental pollution and global energy shortage [21–26]. Visible-light semiconductor photocatalytic technologies can convert solar energy into valuable chemical fuels, such as clean H_2 and renewable hydrocarbon fuel, from water splitting, as well as from the photoreduction of CO_2 [27–36]. Concurrently, photocatalytic technology can be used for environmental purification *via* photocatalytic degradation of various harmful chemical pollutants [37–51]. The increasing public awareness of the impacts of global warming and energy shortages has led to efforts that promote research

[1] Key Laboratory of Energy Plants Resource and Utilization, Ministry of Agriculture and Rural Affairs, College of Forestry and Landscape Architecture, South China Agricultural University, Guangzhou 510642, China
[2] College of Materials and Energy, South China Agricultural University, Guangzhou 510642, China
[3] School of Energy and Environment, City University of Hong Kong, Hong Kong SAR, China
[4] State Center for International Cooperation on Designer Low-Carbon & Environmental Materials (CDLCEM), School of Materials Science and Engineering, Zhengzhou University, Zhengzhou 450001, China
† These two authors contributed equally to this work.
* Corresponding authors (emails: Xinliscau@yahoo.com (Li X); yunhau.ng@cityu.edu.hk (Ng Y); zhangp@zzu.edu.cn (Zhang P))

on new sustainable energy sources [52–55]. Hydrogen (H_2)—a clean energy carrier—has attracted widespread attention as an alternative to fossil fuel to reduce the current environmental pollution and energy crisis [45,56–61]. Carbon-free H_2 can either be used in a typical internal combustion engine to power vehicles or to generate electricity through fuel cells. Presently, H_2 is mainly acquired through the steam reforming of methane using natural gas, which relies on the use of nonrenewable fossil products [62–64].

Since Fujishima and Honda [65] first discovered the photoelectrochemical splitting of H_2O using a Pt/TiO_2 electrode in 1972, solar H_2 generation *via* artificial photosynthesis has rapidly emerged as a promising method to convert and store solar energy in the form of carbon-free H_2. Over the past few decades, photocatalytic water splitting for H_2 evolution has been studied in several systems, including organic–inorganic hybrid, molecular material-based homogeneous, and semiconductor-based heterogeneous systems [19,66–70]. The field of solar H_2 is rapidly expanding and involves multidisciplinary approaches, including the following branches: (1) understanding the fundamental photocatalytic mechanisms and constructing efficient photocatalytic systems [71–76]; (2) developing heterogeneous photocatalytic and homogeneous molecular-photosensitizer systems [19,77–79]; and (3) designing novel semiconductor photocatalysts with unique structures and properties [80–82]. The synergy among all these disciplines plays a key role in improving the efficiencies of photocatalytic systems.

The overall photocatalytic H_2O splitting reaction ($2H_2O \rightarrow 2H_2 + O_2$) requires a positive Gibbs energy change of 237.13 kJ mol^{-1}, corresponding to a minimum energy of 1.23 eV [83]. The basic processes of overall photocatalytic water splitting include three steps (Fig. 1a): (1) light absorption, (2) charge excitation from the valence band (VB) to the conduction band (CB) of the semiconductors to form electron–hole (e^-–h^+) pairs, and (3) migration of photoexcited charge carriers (e^-–h^+ pairs) to surface active sites to react with H_2O to generate O_2 and H_2 [10,84–86]. During step 3, e^-–h^+ recombination readily occurs, resulting in poor photocatalytic activity for overall water splitting. Notably, the CB, VB, and bandgap energies play crucial roles in influencing the photocatalytic performance of semiconductor photocatalysts [11,87]. The standard reduction potentials for the half-reactions of O_2 and H_2 evolution are described in Equations (1) and (2), respectively.

$$2H_2O \rightarrow 4H^+ + 4e^- + O_2 \text{ (pH 0, } E^0 = +1.23 \text{ V } \textit{vs.} \text{ NHE (normal hydrogen electrode))}, \quad (1)$$

$$4H^+ + 4e^- \rightarrow 2H_2 \text{ (pH 0, } E^0 = 0 \text{ V } \textit{vs.} \text{ NHE)}. \quad (2)$$

Over the past few years, numerous semiconductor photocatalysts have been developed for photocatalytic H_2 evolution water splitting, such as metal-free compounds (g-C_3N_4 [11,88–94], SiC [78,95,96], and 6,13-pentacenequinone [97]), inorganic solid solutions ($Zn_xCd_{1-x}S$ [98–103], $ZnIn_2S_4$ [104–108], $Bi_{1-x}In_xTaO_4$ [109], HNb_x-$Ta_{1-x}WO_6$ [59], and $Mn_xCd_{1-x}S$ [110,111]), oxynitrides ($BaTaO_2N$ [112], $LaTaON_2$, and TaON [113]), sulfides (ZnS [114–117], $NiCo_2S_4$ [118], Cu_2ZnSnS_4 [119], MoS_2 [120–123], $CuInS_2$ [124–127], and CdS [128–130]), selenides (WSe_2 [131], $CoSe_2$ [132], CdSe [133–135]), and metal oxides ($SrTiO_3$ [136–138], Ga_2O_3 [139], Fe_2O_3 [140–142], Cu_2O [143,144], ZrO_2 [145], TiO_2[146–149], ZnO [150–152], Ta_2O_5 [153,154], and CoO_x [155]). Among them, CdS is considered one of the most promising photocatalysts for H_2 production due to its ex-

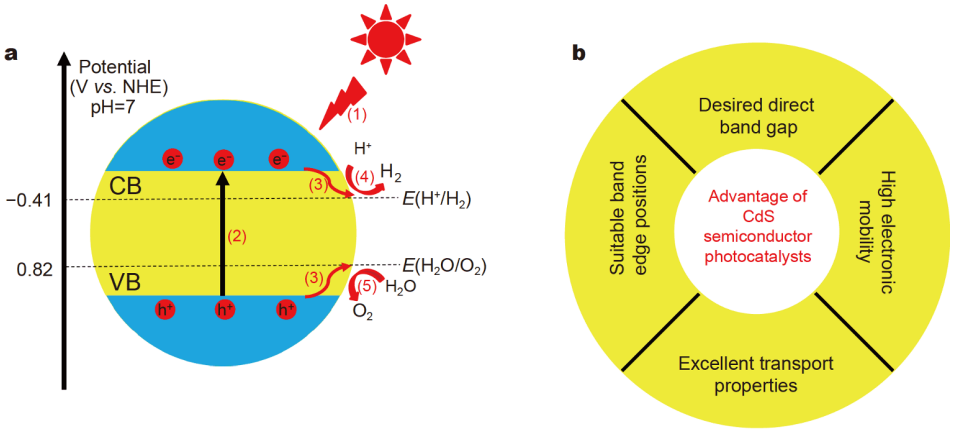

Figure 1 (a) Schematic of the main processes for photocatalytic H_2O splitting on a semiconductor photocatalyst that typically include: (1) light absorption, (2) charge excitations, (3) charge transfer, (4) H_2 evolution, and (5) O_2 evolution. (b) Advantages of CdS semiconductor photocatalysts.

cellent photoresponse in visible light, which is empowered by its suitable bandgap, high stability, as well as low material and synthesis costs [156–158]. A few review papers have reported the progress in the use of inorganic cocatalysts, construction of heterojunctions, and charge transfer behaviors in heterogeneous photocatalytic H_2 production systems [159,160]. In recent years, some review papers have also discussed different classes of semiconductor photocatalysts, including g-C_3N_4 [12] and TiO_2 [161,162], for photocatalytic H_2 production. However, there are only limited comprehensive reviews on the development of photocatalytic H_2 generation systems using CdS-based photocatalysts.

CdS—a classical and vital II–VI photo-semiconductor with a bandgap of 2.4 eV—has been extensively investigated as a promising photocatalyst owing to its several fundamental advantages, including excellent charge transport properties, ideal direct bandgap, high electronic mobility, and suitable band edge positions [17,163,164] (Fig. 1b). The CdS surface can be conveniently functionalized with a variety of ligands, which not only render the CdS-based photocatalysts hydrophobicity or hydrophilicity, but also offer selectivity for interaction with other relevant functional materials [165]. Furthermore, CdS evinces efficient photocatalytic performances under visible light (wavelength <520 nm). It also has excellent charge carrier transportation capacities, which can efficiently facilitate the migration of photoexcited h^+ and e^- in a timely manner, thereby prolonging the lifetime of the photoexcited carriers and resulting in higher photocatalytic activity [166].

It is evident from Fig. 2a that research on H_2 has rapidly expanded in recent years due to its attractiveness and sustainability. Notably, CdS has recently emerged as a hot research topic owing to its application in nanoscale optoelectronic devices and the potential merits of its known fundamental physical properties (Fig. 2b). The development of CdS photocatalysts has been a significant component of energy and environmental research over the past few years. In 1981, Kalyanasundaram *et al.* [167] reported the production of photocatalytic H_2 and oxygen (O_2) in stoichiometric proportions from overall water splitting in an aqueous suspension of CdS loaded with Pt and RuO_2 under visible light. In 2007, one-dimensional (1D) CdS nanowires (NWs) synthesized *via* a solvothermal method in ethylenediamine were found to exhibit a higher rate of photocatalytic H_2 production in the mixed aqueous solution of Na_2S and Na_2SO_3 as sacrificial re-

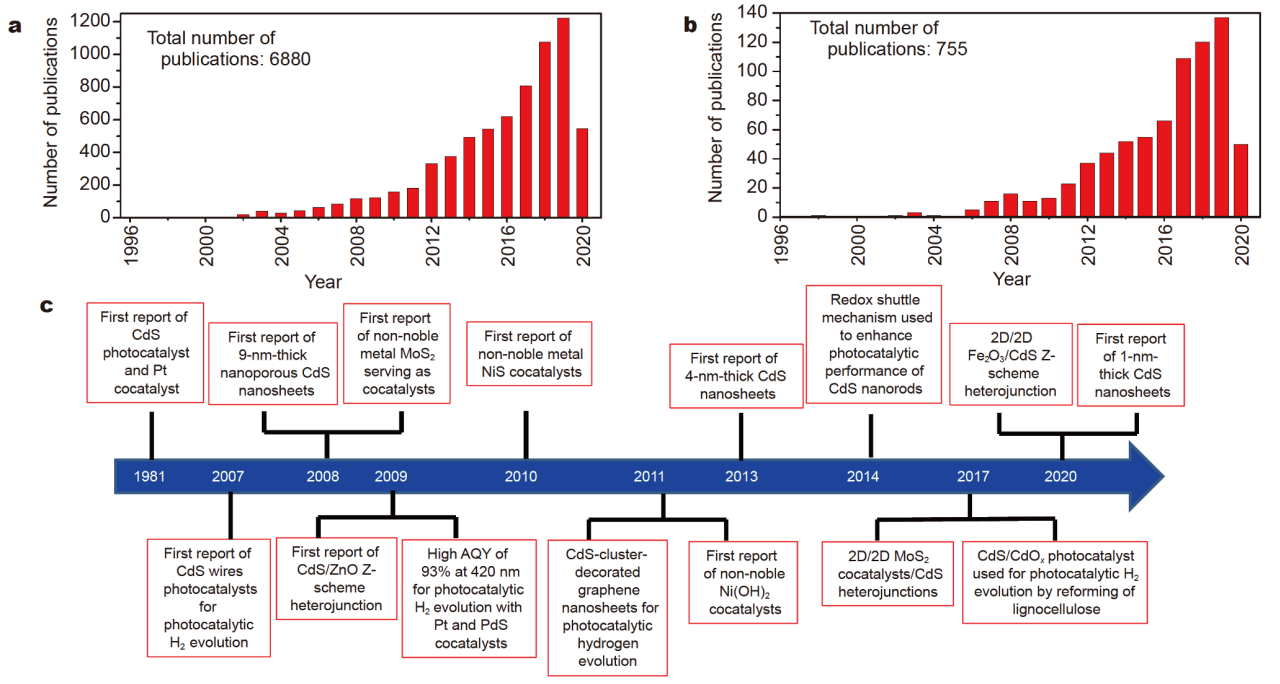

Figure 2 (a) Number of publications since 1996 on photocatalytic H_2-production cocatalysts involving the use of "photo* or light*" and "hydrogen* or H_2 or H-2". (b) Number of publications since 1996 on photocatalytic CdS-based H_2-production cocatalysts involving the use of "CdS* or Cadmium sulfide*" and "hydrogen* or H_2 or H-2. (Reorganized from ISI Web of Science Core Collection, date of information search: May 16, 2020). (c) The roadmap of the development of CdS-based photocatalysts for H_2 generation.

agents [168]. Meanwhile, CdS nanosheets with engineered thicknesses have been fabricated by different methods [169–172]. Subsequently, various noble-metal or non-noble-metal cocatalysts, such as Pt–PdS [173], MoS_2 [166], NiS [174], $Ni(OH)_2$ [175] and Ni_3C [176], have been applied in photocatalytic H_2 evolution over CdS-based photocatalysts. Additionally, various CdS-based composite photocatalysts, such as ZnO/CdS [177], CdS/WO_3 [178], CdS/α-Fe_2O_3 Z-scheme heterojunction [179], CdS-cluster/graphene [180] and two-dimensional (2D) layered hybrid CdS nanosheets/MoS_2 heterojunctions [66], have also been reported for enhanced photocatalytic H_2 evolution. Despite the significant development, there are only a handful of reviews on CdS-based semiconductor photocatalysts [17,181]. Therefore, a comprehensive review on the strategies to promote CdS-based semiconductors' photocatalytic performances is essential for further development of solar H_2.

An excellent CdS-based photocatalyst must be inexpensive, efficient, visible-light-driven, stable with fast kinetics, and highly efficient in photocatalytic H_2 evolution (Fig. 3). To achieve these goals, a great deal of effort has been devoted toward enhancing stability, reducing cost, improving charge separation and light absorption, as well as accelerating H_2 evolution kinetics. Herein, we mainly concentrate on the manipulation of the charge carriers of nanostructured CdS for efficient photocatalytic H_2 evolution (Fig. 4). This includes strategies for generating more charge carriers, promoting efficient charge separation, boosting interfacial charge transfer, accelerating charge utilization, and suppressing charge-induced self-photocorrosion. All these modification strategies are thoroughly discussed in this review. Exploring the important progress in this project may facilitate a new opportunity toward designing CdS-based nanostructured semiconductor photocatalysts for efficient photocatalytic H_2 evolution.

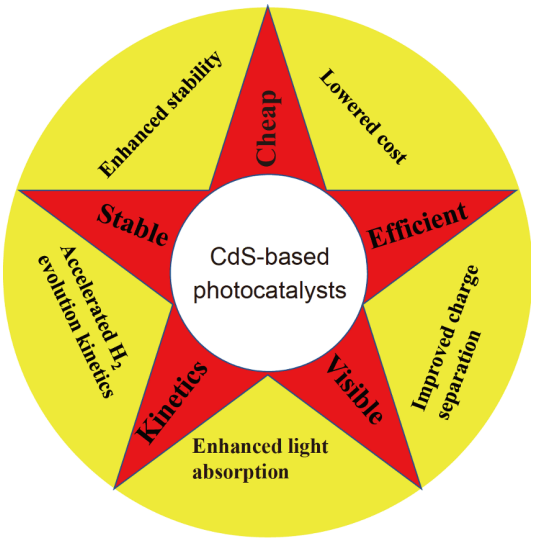

Figure 3 Factors governing the photocatalytic H_2 evolution efficiency of CdS-based photocatalysts and the corresponding engineering and modification strategies.

GENERATING MORE AVAILABLE CHARGE CARRIERS IN NANOSTRUCTURED CdS

Sensitization with dyes and plasmonic metals

As mentioned above, the application of nanostructured CdS for photocatalytic H_2 generation has been attracting considerable attention [182,183]. It is generally accepted that the ideal water-splitting bandgap for semiconductor photocatalysts is ~2.0 eV, wherein an adequate portion of visible light can be harvested to generate sufficient e^- and h^+ with thermodynamic driving forces for photocatalytic redox reactions. However, the bandgap of CdS is 2.4 eV, which ensures the sole utilization of solar light with a wavelength shorter than 520 nm. Various methods have been developed to increase the visible-light absorption of CdS-based photocatalysts to generate more available charge carriers. Sensitized semiconductor photocatalysts have been widely used in photoelectrochemistry. Dye sensitization is also a promising strategy to promote photocatalytic H_2 production over CdS-based semiconductor materials, whereby the dye molecules normally do not exhibit photocatalytic H_2 production activities [184,185]. The effectiveness of this step is determined by choosing a suitable dye, light source, and e^- donor. Dye photosensitization can extend the visible-light absorption range of CdS-based photocatalysts, thereby improving the photon-harvesting efficiency. With increased light absorption, an extra population of excited e^- from the dye molecules that may speed up charge transfer is presented, resulting in highly efficient photoelectric conversion [186,187]. Through this method, the photoexcited e^- from the dye molecules with a suitable lowest unoccupied molecular orbital level can pass into the CB of CdS-based semiconductors, thereby contributing additional charges for reactions. Compared with hybridized inorganic materials serving as cocatalysts, metal-free organic dyes display a stronger visible-light absorption capacity, which makes them suitable for enhancing photocatalytic H_2 production activities [185]. Based on the sensitization strategy, semiconductor photocatalysts with narrow

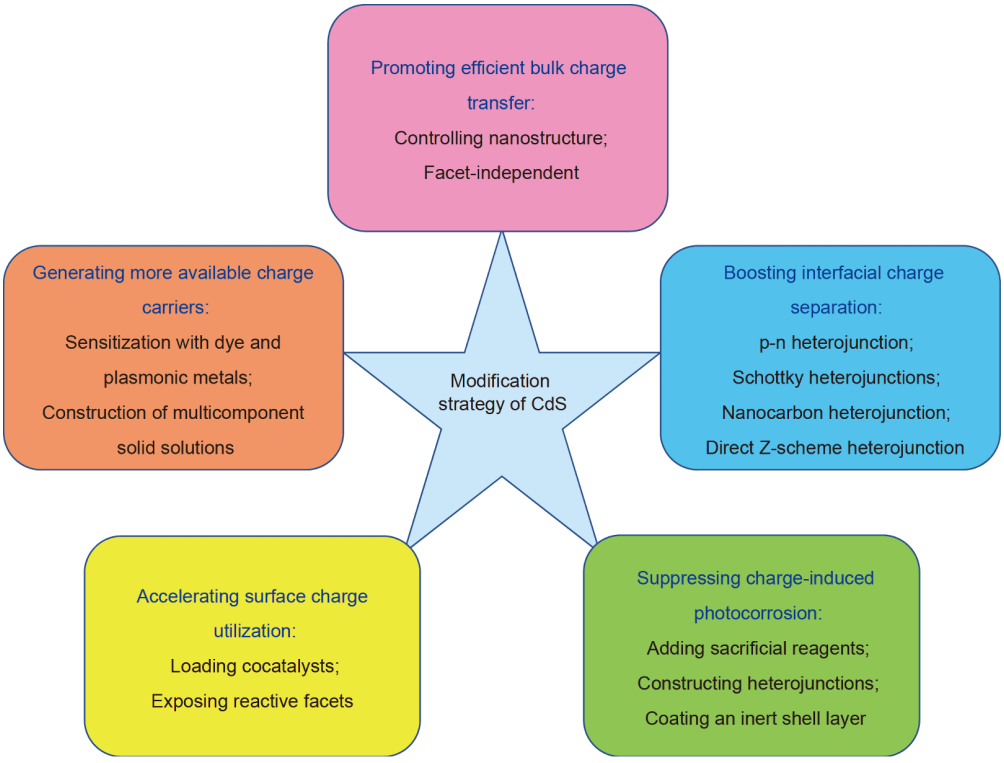

Figure 4 Engineering the charge carriers of nanostructured CdS for efficient photocatalytic H_2 evolution through different modification strategies.

bandgaps, such as graphene quantum dots and conjugated polymers [188,189], have been extensively studied and are considered as good photosensitizer candidates for enhancing the visible-light-driven photocatalysis of CdS-based semiconductors.

Furthermore, coupling CdS photo-semiconductors with other plasmonic metals has been extensively applied in visible-light-driven water splitting activities. The plasmonic energy transfer from the metal to the semiconductor can enhance photocatalytic performances *via* light scattering, near-field enhancement, hot-electron injection, and resonant energy transfer. For example, Ma *et al.* [190] reported multi-interfacial plasmon coupling with CdS for efficient photocatalytic H_2 evolution (Fig. 5a). The (Au/AgAu)@CdS core–shell photocatalysts exhibited excellent photocatalytic performances owing to the strong plasmonic light absorption and near-field enhancement induced by the multi-interfacial plasmon coupling, which could significantly enhance the light-harvesting efficiency from the ultraviolet to the near-infrared region (Fig. 5b and c). Meanwhile, as the number of Au/AgAu gaps increased, light harvesting gradually improved. The four-gap Au/AgAu hybrids displayed the highest extinction intensity and the broadest absorption band, accompanied by the red-shifting of the localized surface plasmon resonance peaks to 576 nm (Fig. 5d–g). Consequently, the (Au/AgAu)@CdS core–shell photocatalysts exhibited an excellent H_2 evolution performance of 4.71 mmol g^{-1} h^{-1}, which was 47.2 times higher than that of pure CdS photocatalyst [190]. It is envisaged that the combination of various sensitization strategies can be feasibly designed and applied to enhance the photocatalytic H_2 evolution of CdS-based semiconductors [191]. In the future, all these sensitization strategies are expected to be coupled with CdS-based cocatalysts and thoroughly studied with respect to the mechanisms.

Construction of multicomponent solid solutions

In addition to the extended visible-light absorption, adjusting the CB and VB redox potentials to achieve higher driving forces of the photoexcited charge carriers is another effective strategy. Notably, the fabrication of multicomponent solid-solution CdS-based photocatalysts provides a platform to fully maximize the advantages of the different components to generate more available charge carriers with considerable energetic redox potentials for photocatalytic reactions. Moreover, the bandgap energy (E_g) of multicomponent solid-solution photocatalysts can

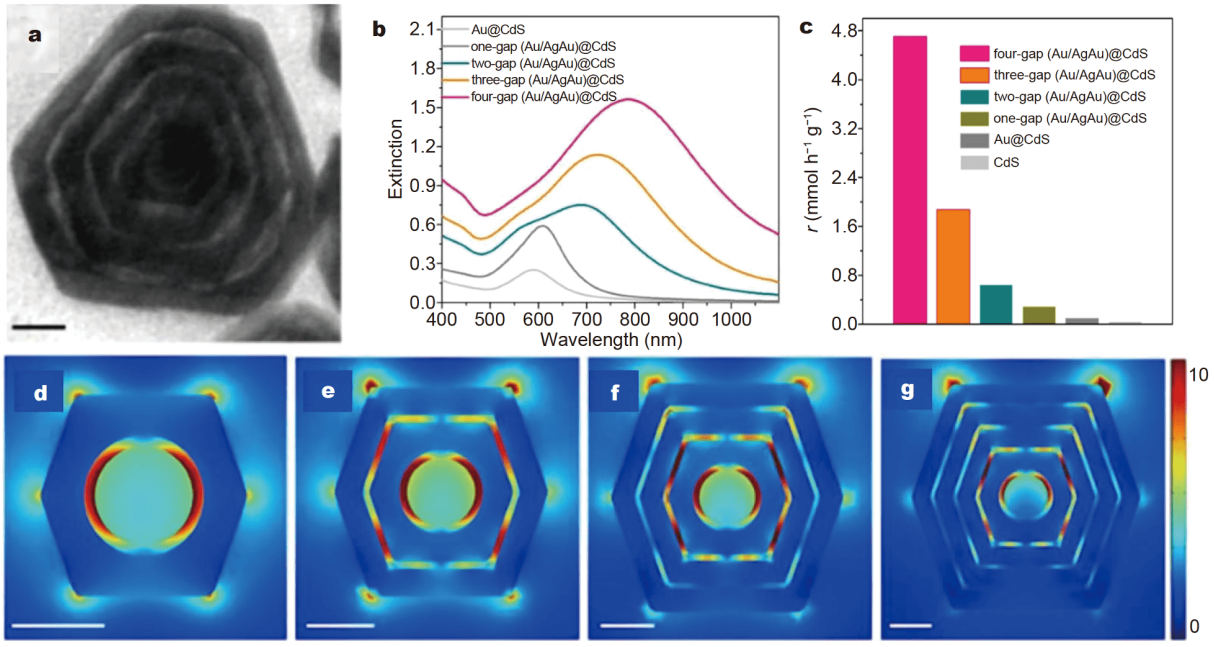

Figure 5 (a) Transmission electron microscopy (TEM) image of (Au/AgAu)@CdS core–shell hybrids. (b) Extinction spectra of Au@CdS and multigap (Au/AgAu)@CdS core–shell hybrids. (c) Photocatalytic H_2 evolution rates of different samples. (d–g) Calculated local electric field distributions of one-, two-, three-, and four-gap Au/AgAu hybrids. Reprinted with permission from Ref. [190]. Copyright 2020, Royal Society of Chemistry.

be continuously tuned by controlling their constituent stoichiometry, which will be rather helpful to achieve an optimized balance between visible-light absorption and redox potential. In recent years, doping transitional metal ions (e.g., Ni^{2+} [192], Cu^{2+} [193], Mn^{2+} [194, 195] and Zn^{2+} [196–200]) with CdS to construct CdS-based solid-solution photocatalysts has proven to be effective for improving photocatalytic water splitting for H_2 evolution. Compared with the original CdS, solid solutions, such as $Zn_xCd_{1-x}S$ and $Mn_xCd_{1-x}S$, possess some specific advantages, such as tunable band edge positions and bandgap width, more active sites, and better electrical conductivity [201,202]. Additionally, in long-term photocatalytic reactions, the construction of solid-solution photocatalysts can inhibit photocorrosion during visible-light irradiation [195,203,204].

Among the solid solutions, Zn-doped CdS ternary alloys ($Zn_xCd_{1-x}S$) have received ample attention in the past few years owing to the crystal structure similarity shared by both ZnS and CdS. A well-matched coordination mode between ZnS and CdS can be established [205,206]. However, most reports on $Zn_xCd_{1-x}S$ solid solutions reveal the morphological features of micro-/nano-spheres or irregular particles. In a recent example, Han *et al.* [207] fabricated 1D cubic $Cd_{0.8}Zn_{0.2}S$ solid-solution NWs *via* a facile solvothermal method. Thioglycolic acid (TGA) served as both the template agent and S source. The TGA revealed a "levelling effect" to nullify the disparity in the physicochemical properties of metal ions *via* its carboxyl and hydrosulfonyl groups, leading to the formation of a cubic $Cd_{0.8}Zn_{0.2}S$ solid solution with a cylindrical morphology. Owing to the doping of Zn into the lattice of the CdS semiconductor, the absorption edges of the $Cd_{0.8}Zn_{0.2}S$ semiconductor are extended to longer wavelengths than those of the CdS semiconductor [208]. In other words, with increasing Zn content in the $Zn_xCd_{1-x}S$ semiconductor, its VB and CB levels shift to more positive and negative positions, respectively. Notably, a higher photo-semiconductor CB level induces a stronger reducing ability, which is pivotal for efficient H_2 generation. Hence, the $Cd_{0.8}Zn_{0.2}S$ solid-solution photo-semiconductor displayed enhanced H_2 generation activity compared with pure CdS (52.3 mmol h^{-1}, with Na_2S–Na_2SO_3 as a sacrificial agent).

Li *et al.* [111] prepared a $Mn_xCd_{1-x}S$ nanorod (NR) solid solution in a pure N_2 atmosphere through standard hot-injection synthesis. By adjusting the ratios of Cd and Mn, the E_g values of the $Mn_xCd_{1-x}S$ ($\boldsymbol{x}$ = 0–1) solid-solution photocatalysts could be controlled over a wide range (E_g = 2.21–3.43 eV). The improved photocatalytic H_2 generation performance of the $Mn_xCd_{1-x}S$ NR solid solution was attributed to the stronger oxidation and

reduction ability, charge separation efficiency, as well as light absorption. In particular, the $Mn_{0.5}Cd_{0.5}S$ NRs exhibited the highest photocatalytic H_2 generation rate of 26 mmol g^{-1} h^{-1} under visible-light irradiation, with an apparent quantum efficiency (AQE) of 30.3% at 400 nm. The photocatalytic performance of the solid-solution $Mn_xCd_{1-x}S$ NRs was evidently superior to that of the $Mn_xCd_{1-x}S$ solid solution and pristine CdS fabricated *via* the hydrothermal method [111]. The X-ray diffraction results proved that the sample formed a homogeneous $Mn_xCd_{1-x}S$ rather than a simple mixture of h-CdS and γ-MnS. The corresponding geometry supercell models for $Mn_xCd_{1-x}S$ are illustrated in Fig. 6a, while the CB and VB edges of the $Mn_xCd_{1-x}S$ NR photocatalysts are presented in Fig. 6b. It was apparent that the CB became more negative with increasing Mn content, thereby resulting in a significantly extended bandgap. The improved H_2 generation activity of the $Mn_{0.5}Cd_{0.5}S$ NR solid-solution photocatalysts could be ascribed to a suitable bandgap and an adjusted CB position. In addition, the separation and transfer capacity of photoexcited e^- and h^+ play a key role in photocatalytic H_2 generation. Fig. 6c displays the transient photocurrent response of the $Mn_{0.5}Cd_{0.5}S$ NRs under visible-light irradiation. Under the same conditions, the photocurrent of the $Mn_{0.5}Cd_{0.5}S$ NR solid solution was evidently higher than that of bare CdS and MnS. Unfortunately, the photocatalytic H_2 generation performance of these multicomponent solid solutions remains insufficient for satisfying the basic requirements for practical applications. Therefore, it is highly desirable to exploit other novel strategies to further enhance the photocatalytic H_2 generation performance of CdS-based solid-solution photocatalysts.

Although both the CB position and bandgap of CdS-based solid-solution semiconductor photocatalysts can be adjusted to a certain extent by tuning the value of *x* (stoichiometric ratio) to enhance the photocatalytic H_2 generation activity, the rapid recombination of photo-excited charges remains a crucial challenge that limits the further improvement of photocatalytic performances. The construction of CdS-based solid-solution photocatalysts results in a tunable bandgap, wherein these adjustable band potentials may lead to new photoredox reactions (beyond water splitting) and help in the chemical adsorption of specific reactants. Notably, the environmental concern of this type of composite semiconductor photocatalyst can also be assuaged by reducing the Cd content. In addition to constructing bimetallic solid solutions, the photocatalytic H_2 generation performance of CdS-based solid solutions can be further enhanced by intentionally introducing other transition metal ions.

PROMOTING EFFICIENT BULK CHARGE TRANSFER IN NANOSTRUCTURED CdS

In the past few years, efforts have been made to control the morphology, shape, and size of CdS with various

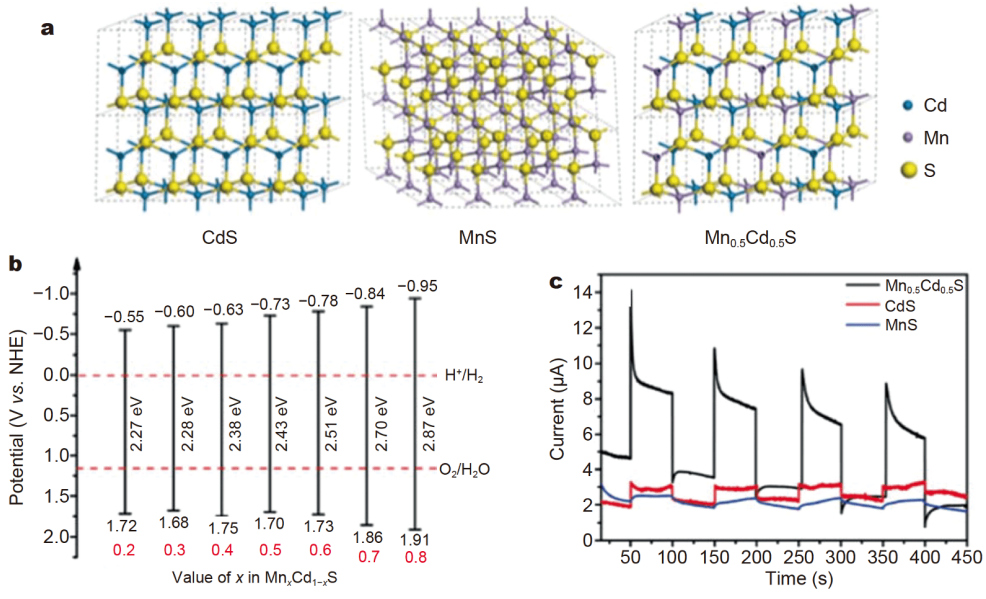

Figure 6 (a) Corresponding geometry supercell models for $Mn_xCd_{1-x}S$. (b) CB and VB of the $Mn_xCd_{1-x}S$ NRs solid solutions. (c) *I*–*t* curves of $Mn_{0.5}Cd_{0.5}S$, MnS, and CdS. Reprinted with permission from Ref. [111]. Copyright 2018, Elsevier.

nanostructures (NSs). Many studies have reported the photocatalytic performance of CdS semiconductor photocatalysts with unique NSs, such as the 0D, 1D, 2D, and 3D structures. Different NSs impose varying effects on the photocatalytic H_2 generation performance of CdS photocatalysts (Fig. 7). Notably, the photocatalytic H_2 generation performance of photocatalysts with different morphologies, structures, and sizes can be affected by different synthetic methods. Nevertheless, with regard to CdS and CdS-based nanocomposite photocatalysts, researchers have focused on environmentally friendly and low-cost synthetic methods. These approaches include sonochemical, solvothermal, chemical bath deposition, impregnation, template, and template-free methods. Some fabrication methods for CdS photo-semiconductors and CdS-based nanocomposites are listed in Table 1.

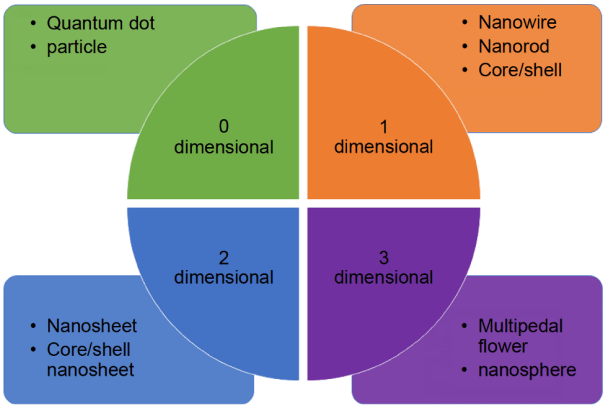

Figure 7 Descriptions of the morphologies of CdS photocatalysts.

Construction of 0D nanostructures

There are many synthetic approaches, such as solvothermal, combustion, sonochemical, biogenic synthesis, complex thermolysis, microwave-assisted polyol synthesis, and chemical precipitation methods, for constructing 0D CdS NSs [73,258–264]. Researchers suggest that although 0D CdS nanomaterials possess large surface area, they are susceptible to severe agglomeration, which reduces the photocatalytic efficiency.

Wang *et al.* [265] fabricated 0D CdS nanoparticles (NPs) modified with covalent triazine-based frameworks (CTF-1) in a controlled manner by means of a facile one-pot solvothermal synthesis. As the triazine unit of CTF-1 has an apparent Lewis property on its nitrogen sites, size-controlled and highly dispersed CdS NPs can be prepared and stabilized on CTF-1 layers. The morphology of the as-fabricated 0D CdS NP nanocomposites was investigated *via* scanning electron microscopy (Fig. 8a). The formation processes of the porous CTF-1 frameworks and the subsequent decoration with 0D CdS NPs to form CdS/CTF-1 nanocomposite are presented in Fig. 8b. Compared with bare CdS, the electrochemical impedance spectrum of CdS/5%CTF-1 displays a smaller semicircle, implying that CdS/CTF-1 possesses a reduced charge transfer resistance for photoinduced e^- (Fig. 8c). This result was further supported by the photoluminescence (PL) spectra, which were used to study the recombination rate of the photoexcited charge carriers (Fig. 8d). The PL peak intensity of CdS/5%CTF-1 was evidently lower than

Table 1 Synthesis methods for CdS nanostructures

Photocatalyst	Synthesis method	Morphology	Precursor materials	HER (mmol g^{-1} h^{-1})	AQE (420 nm)	Ref.
CdS–TiO_2	Hydrothermal	Nanodots	$Cd(CH_3COO)_2{\cdot}2H_2O$, dimethyl sulfoxide	1.5	11.9%	[209]
CdS	Hydrothermal synthesis	Nanoparticles	Graphdiyne, $Cd(Ac)_2{\cdot}2H_2O$	4.1	-	[210]
CdS	Hydrothermal	Nanoparticles	$Cd(CH_3COO)_2{\cdot}2H_2O$, DMSO	58.9	-	[211]
CdS	Solid-state	Nanoparticles	$Cd(Ac)_2{\cdot}2H_2O$, thioacetamide	1.15	16.5%	[212]
CdS	Microwave	Nanoparticles	$C_4H_{10}CdO_4{\cdot}2H_2O$, H_2NCSNH_2	11.4	-	[213]
CdS	Hydrothermal	Nanoparticles	$Cd(NO_3)_2{\cdot}4H_2O$, $NH_2CH_2CH_2NH_2$	0.56	-	[214]
CdS	Hydrothermal	Nanoparticles	$Cd(CH_3COO)_2$, Na_2S	14.2	8.7%	[215]
CdS	Hydrothermal	Nanoparticles	Na_2S, $Cd(CH_3COO)_2$	5.9	8.6%	[57]
CdS	Solvothermal	Nanoparticles	$CdCl_2{\cdot}2.5H_2O$, thiourea	1.89	-	[216]
CdS	Hydrothermal	Nanoparticles	$Cd(NO_3)_2{\cdot}4H_2O$, dimethyl sulfoxide	0.61	-	[217]
CdS	Hydrothermal	Nanoparticles	$Cd(NO_3)_2{\cdot}4H_2O$, thiourea	1.26	-	[218]
CdS/$CdWO_4$	Hydrothermal	Nanoparticles	CH_3CSNH_2, $Cd(CH_3COO)_2{\cdot}2H_2O$	9.17	-	[219]

(*Continued*)

Photocatalyst	Synthesis method	Morphology	Precursor materials	HER (mmol g^{-1} h^{-1})	AQE (420 nm)	Ref.
CdS	Directly reacting	Nanoparticles	Na_2S, $Cd(CH_3COO)_2$	5.89	19%	[220]
CdS	Hydrothermal	Nanoparticles	$NaS_2{\cdot}9H_2O$, $Cd(NO_3)_2{\cdot}4H_2O$	0.33	34.3%	[221]
CdS	Hydrothermal	Nanoparticles	$Cd(Ac)_2{\cdot}2H_2O$, CH_4N_2S	2.85	10%	[222]
CdS/Cu_2O/g-C_3N_4	Hydrothermal	Nanoparticles	Na_2S, $CdCl_2$	1.84	-	[223]
CdS–BCNNTs	Hydrothermal	Nanoparticles	$Cd(NO_3)_2{\cdot}4H_2O$, Na_2S	0.526	4.01	[224]
CdS/ZnS	Solvothermal	Nanorod	$CdCl_2{\cdot}2.5H_2O$, thiourea	24.1	9.3%	[225]
CdS/TiO_2	Solvothermal	Nanorod	$Cd(NO_3)_2$, thiourea	1.118	-	[226]
CdS@MoO_x	Solvothermal photodeposition	Nanorod	$Cd(NO_3)_2$, thiourea	5.42	-	[227]
CdS/g-C_3N_4	Solvothermal method	Core/shell nanowires	$Cd(NO_3)_2{\cdot}4H_2O$, thiourea	4.15	4.3%	[228]
CdS	Solvothermal	Nanowires	$CdCl_2{\cdot}2.5H_2O$, $(C_2H_5)_2NCSSNa$	0.15	44.9%	[229]
CdS	Self-templated synthesis	Nanoporous structures	$CdCl_2{\cdot}2.5H_2O$, NaOH, $Na_2S{\cdot}9H_2O$	27.33	60.34%	[169]
CdS	One-pot synthesis	Nanorods	$Cd(NO_3)_2{\cdot}4H_2O$, $CS(NH_2)_2$, H_2PtCl_6	10.29	-	[230]
CdS	Hydrothermal	Nanorods	$(CH_3CO_2)_2Cd{\cdot}xH_2O$, CH_4N_2S	15.56	-	[231]
CdS	Hydrothermal	Nanorods	$Cd(NO_3)_2{\cdot}4H_2O$, thioacetamide	24.15	-	[232]
CdS	Hydrothermal	Nanorods	$Cd(NO_3)_2{\cdot}4H_2O$, NH_2CSNH_2	15.55	6.9%	[233]
CdS	Hydrothermal	Nanorods	$Cd(NO_3)_2{\cdot}4H_2O$, thiourea	1.131	-	[234]
CdS	Hydrothermal	Nanorods	$CdCl_2{\cdot}2.5H_2O$, CH_4N_2S	106	29%	[235]
CdS	Hydrothermal	Nanorods	$CdCl_2{\cdot}2.5H_2O$, NH_2CSNH_2	4.64	11.8%	[236]
CdS	Hydrothermal	Nanorods	CdO, Na_2S	11.58	16.3%	[237]
CdS	Solvothermal	Nanorods	$CdCl_2{\cdot}2.5H_2O$, thiourea	3.5	-	[155]
CdS/Ti_3C_2	Hydrothermal	Nanorods	$Cd(NO_3)_2{\cdot}4H_2O$	2.407	35.6%	[238]
Pt–CdS/g-C_3N_4-MnO_x	Hydrothermal	Nanorods	$Cd(NO_3)_2{\cdot}4H_2O$	924,4	1.745%	[239]
CdS	Hydrothermal	Nanorods	$Cd(NO_3)_2$, NH_2CSNH_2	1.84	21.2%	[240]
CdS	Hydrothermal	Nanorods	$Cd(NO_3)_2$, thiourea	167.1	1.5%	[241]
CdS/ZnS	Solvothermal, chemical bath deposition	Nanorod	$CdCl_2$, CH_4N_2S	239	16.8%	[18]
CdS	Solvothermal,	Nanorod	$Cd(Ac)_2{\cdot}2H_2O$, CH_4N_2S	20.2	-	[242]
CdS	Directly reacting	Nanorod	$Cd(NO_3)_2$, thiourea	37.1	43%	[243]
CdS	Solvothermal	Nanorod	$Cd(NO_3)_2$, thiourea	0.206	-	[244]
CdS/g-C_3N_4	vapor deposition	Nanotubes	$CdCl_2{\cdot}2.5H_2O$	0.392	-	[245]
CdS	Hydrothermal	Nanosheets	$Cd(Ac)_2{\cdot}2H_2O$, sulfocarbamide, ethylenediamine	27.8	14.7%	[246]
CdS/GO	Hydrothermal	Nanosheets	$CdCl_2{\cdot}2.5H_2O$, DETA	10.5	29.5%	[247]
CdS	Hydrothermal	Nanosheet	$CdSO_4$, DL-dithiothreitol	1.293	-	[248]
CdS	Hydrothermal	Nanosheets	$CdCl_2{\cdot}2.5H_2O$, S powder	138.7	-	[249]
CdS–FeP	Hydrothermal	Nanosheets	$CdCl_2{\cdot}2.5H_2O$, S powder	18.63	11.2	[250]
CdS	Hydrothermal	Nanosheets	$CdCl_2{\cdot}2.5H_2O$, DETA	7.37	-	[251]
MoS_2/CdS	Two-step hydrothermal	Core/shell-like	Ammonium molybdate, thiourea	38.75	14.7%	[252]
CdS	Precipitation	Cubic-Phase	$Cd(NO_3)_2$, Na_2S, Na_2SO_3	18	-	[253]
CdS	One-pot wet-chemical	Nanocrystals	CdO	1.98	-	[254]
CdS	Hydrothermal	Nanospheres	$Cd(CH_3COO)_2{\cdot}2H_2O$, thiourea	4.65	7.31%	[255]
CdS	Hydrothermal	Nanospheres	$Cd(CH_3COO)_2$, thiourea	44.65	-	[256]
CdS	Hydrothermal	Nanospheres	$Cd(Ac)_2{\cdot}2H_2O$, thiourea	1.44	-	[257]

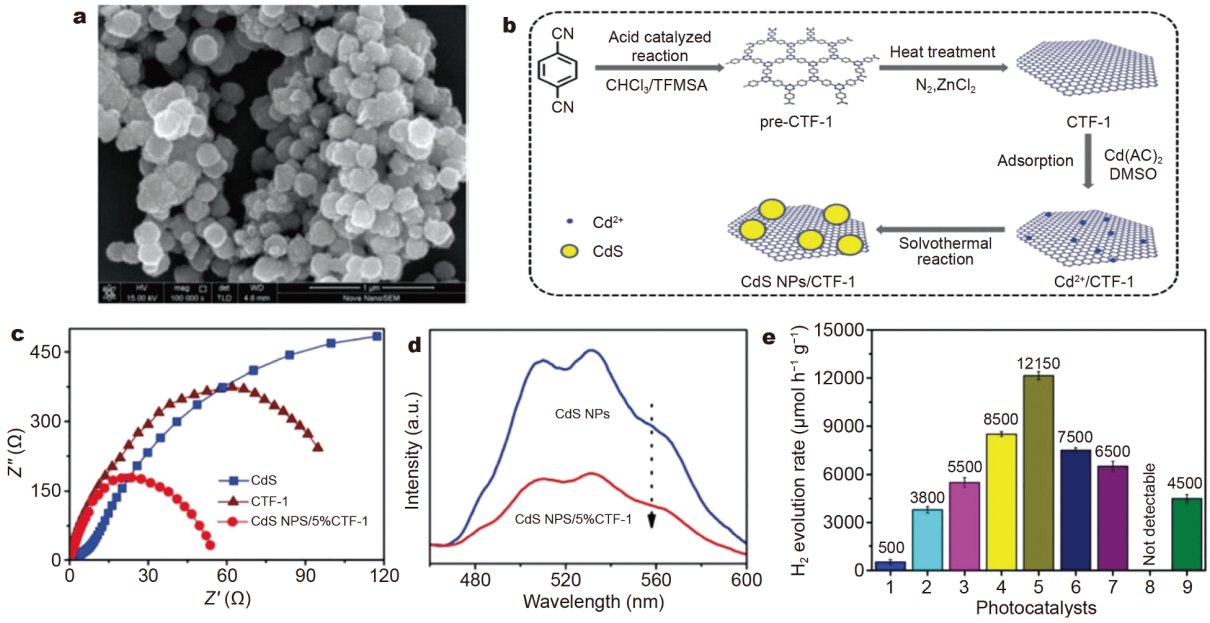

Figure 8 (a) SEM image of CdS, (b) schematic of the formation of 0D CdS NPs/CTF-1, (c) Nyquist plots, (d) PL spectra, and (e) amount of H_2 evolved over CTF-1 (1), CdS (2), CdS NPs/0.5%CTF (3), CdS NPs/1%CTF (4), CdS NPs/3%CTF (5), CdS NPs/5%CTF (6), CdS NPs/10%CTF (7), without catalyst or visible-light irradiation (8), and physically mixed CdS and CTF-1 (9). Reprinted with permission from Ref. [265]. Copyright 2018, Royal Society of Chemistry.

that of the bare 0D CdS NPs, suggesting that the charge recombination rate decreased in the nanocomposites. The photocatalytic H_2 generation performance of the as-fabricated CdS/CTF-1 was investigated using Pt as a cocatalyst in a lactic acid medium under visible-light irradiation. Fig. 8e shows that the H_2 generation rate of CdS/5%CTF-1 was better than those of bare CdS NPs and CTF-1. An insignificant amount of H_2 was released when bare CTF-1 was used as the catalyst. Hydrogen could not be detected without photocatalysts or visible-light irradiation, which suggested that H_2 generation was induced by irradiating CdS/5%CTF-1.

Construction of 1D nanostructures

Generally, 1D CdS NRs with improved charge transport properties compared with the 0D CdS quantum dots displayed quantum constraint effects and directional charge carrier transport. This reduced the recombination losses at the grain boundaries and enhanced the light harvesting capability [266–268]. The visible-light absorption occurred along the longer dimensions (microns or more) of the 1D NSs, while carrier separation through diffusion took place over a short radial distance [269]. The enhanced light absorption, combined with the merits of long distance as well as fast charge transfer, makes the 1D NS a promising candidate for solar energy conversion. There is increasing attention on the fabrication of 1D photocatalytic NSs, such as NWs, NRs, and their core–shell structures [270–273].

In 1D CdS NRs, the transfer velocity of the carrier is different in the axial and radial directions. Generally, the carrier moves much faster in the radial direction than in the axial one [274]. Thus, it is particularly vital to construct the morphology of CdS nano-semiconductors for 1D NR semiconductors with ideal diameters and high aspect ratios. Several methods, including ion-exchange [163], ligand-assisted growth [275,276], and metal particle-seeded growth [277], have been developed to fabricate 1D rod-shaped semiconductor materials. For example, Wu *et al.* [278] prepared 1D CdS NRs using the seeded growth method and studied the effects of 1D CdS and CdS–Pt NRs with different diameters on the dissociation kinetics and exciton localization. They studied the excitation dynamics and electronic structure of the photocatalytic 1D CdS–Pt NRs. In the presence of Pt, e^- were efficiently transferred from CdS to Pt, and photoexcited e^--h^+ pair recombination was suppressed. The tips of 1D CdS NRs can offer selective deposition sides for Pt, wherein the selectively tip-deposited Pt can promote the charge separation of 1D CdS NRs and CdS-based NSs. These results demonstrate that 1D CdS NRs with larger diameters possess more specific properties than tradi-

tional CdS NR structures. Many factors, including reaction time and temperature, as well as reactant and surfactant amounts, influence the synthesis of 1D CdS NSs.

Construction of 2D nanostructures

The photochemical, optical, and photoelectrical properties of the photo-semiconductors can be indirectly influenced by their morphology, size, and structure [279–281]. Since the discovery of 2D photocatalytic nanomaterials, 2D CdS NSs have attracted much attention because of their unique phase characteristics, and excellent photocatalytic properties, larger surface area and lower recombination rate of e^--h^+ pairs [171,246,282,283]. To synthesize 2D CdS photo-semiconductors, it is important to seek a low-cost and environment-friendly process that can control the formation of reasonable sizes and predictable shapes.

Apparently, the decreased thickness of 2D semiconductor nanosheets can effectively reduce the migration distance of photogenerated e^- from the bulk phase to the semiconductor photocatalyst surface, thereby preventing the recombination of photogenerated e^--h^+ pairs inside the semiconductor. For instance, in 2013, Xu *et al.* [170] synthesized ultrathin CdS nanosheets with thickness of ~4 nm *via* ultrasonic-induced aqueous exfoliation of lamellar CdS–diethylenetriamine hybrid nanosheets using *L*-cysteine as a stabilizing agent. The as-obtained CdS ultrathin nanosheets achieved H_2 production rates of 41.1 mmol g^{-1} h^{-1} with an AQE of 1.38% at 420 nm. In 2018, Bie *et al.* [171] synthesized the thinnest CdS nanosheets (1.5-nm-thick) through a simple and low-cost oil-bath method using sodium citrate as the structure-directing agent. They exhibited a photocatalytic H_2 production rate of 2.155 mmol g^{-1} h^{-1}, which was approximately 3.7 times higher than that of CdS NPs (0.582 mmol g^{-1} h^{-1}). More recently, Xie *et al.* [172] constructed five-layer ultrathin Cd_4S_5 nanosheets with unsaturated surface S anions *via* chemical vapor deposition. The thickness of the CdS nanosheet was approximately 1 nm. The average H_2 evolution rate of the ultrathin nanosheets was 29.44 mmol g^{-1} h^{-1}. Evidently, this unique structure induces a higher CB position than that of their thicker counterparts, which can fundamentally improve electrical conductivity, reduce recombination rate, and eventually enhance the driving force for the H_2 evolution reaction (HER). Consequently, ultrathin CdS nanosheets achieve a high AQE of 4.15% under 420-nm light irradiation.

Meanwhile, exposing the reactive facets on the surface of 2D CdS nanosheets is another strategy to boost the photocatalytic H_2 evolution. For instance, Li *et al.* [284] synthesized flake-like hexagonal phase CdS micro-/nano-leaves with exposed (0001) facets to promote the photocatalytic activity toward H_2 generation (Fig. 9a). The growth process of the dendrites is shown in Fig. 9b. Compared with CdS NPs, the photocatalytic H_2 generation activity of CdS micro-/nano-leaves with NR-branched NSs was significantly enhanced (468.4 mmol h^{-1}) (Fig. 9c). The average H_2 evolution rate of photocatalytic reactions reached 740.9 mmol h^{-1}, which was more than 6 times that of spheroidal particles under visible-light irradiation. The catalysts also evinced good stability (Fig. 9d). The enhanced activity of the CdS micro-/nano-leaves was partly due to the unique 2D micro-/NS and the exposure of high surface energy facets (0001) [284].

Additionally, constructing a 2D/2D NS coupled with layered composite photocatalysts could further boost charge separation between the CdS nanosheets and the other 2D cocatalysts owing to strongly coupled contact interfaces [179,285,286]. For example, Ma *et al.* [66] successfully synthesized 2D/2D layered hybrid CdS/MoS_2 nanocomposites *via* a one-step hydrothermal method. The coupling of 2D MoS_2 NSs as cocatalysts boosted the photocatalytic H_2 evolution performance of CdS NSs (Fig. 10). It was confirmed that the 2D CdS/1%MoS_2 nanocomposites exhibited the highest photocatalytic H_2 generation activity (1.75 mmol g^{-1} h^{-1}) in an aqueous solution containing sulfite and sulfide under visible light. The loading of ultrathin 2D MoS_2 NSs and the tight 2D/2D coupling interfaces led to excellent H_2 generation performances owing to the effectively boosted separation and migration of charge carriers as well as improved surface H_2 evolution kinetics. In our previous study, we demonstrated that the 2D/2D CdS/Cu_7S_4 nanocomposite could serve as advanced photocatalysts for photocatalytic water splitting toward H_2 generation [246]. The highest achieved H_2 generation rate of the 2D/2D CdS/2%Cu_7S_4 nanocomposites was 27.8 mmol g^{-1} h^{-1}, which was approximately 11 times higher than that of pure CdS NSs (2.6 mmol g^{-1} h^{-1}). The construction of the 2D/2D CdS/Cu_7S_4 heterojunction not only promoted photoexcited e^--h^+ pair separation, boosted photoexcited e^- transfer, and prolonged the lifetime of the photoexcited e^-, but also increased the visible-light absorption and H_2 generation kinetics.

Compared with the interfaces of 0D/1D, 0D/2D, 1D/1D, and 1D/2D, the 2D/2D coupled nanocomposites display a larger contact surface, which is conducive to more efficient interfacial charge migration [285]. Therefore, the construction of unique interfaces with tight 2D/

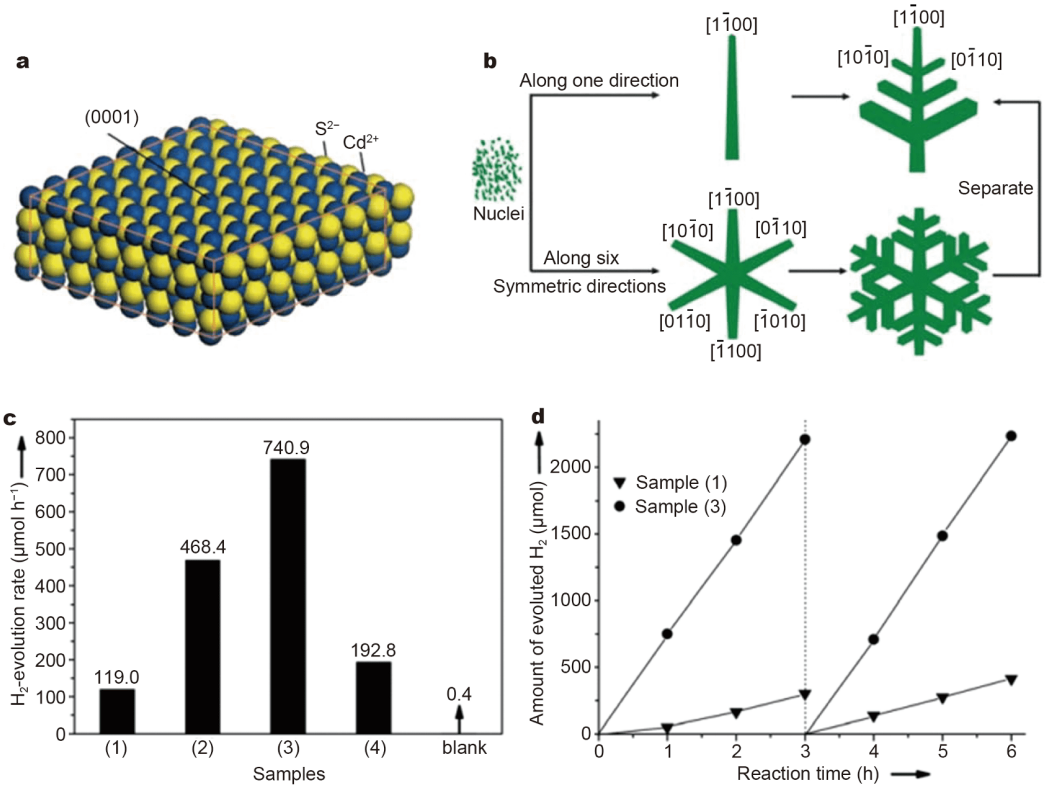

Figure 9 (a) Crystal structure of the hexagonal CdS. (b) Schematic of the growth process of CdS. (c) Average photocatalytic H_2 generation rate of CdS. (d) Time courses of photocatalytic H_2 generation on CdS, (1) without HF, and with (2) 0.125 mol L^{-1} HF, (3) 0.200 mol L^{-1} HF, and (4) 0.500 mol L^{-1} HF. Reprinted with permission from Ref. [284]. Copyright 2012, Royal Society of Chemistry.

2D coupling and large surface areas is critical for achieving efficient charge separation and photocatalytic H_2 generation activity.

Construction of 3D nanostructures

CdS photocatalysts with 3D NSs, such as hierarchical dendritic CdS, porous CdS flowers, and hollow spheres, have been widely studied [284,287–291]. Because of their unique structural characteristics, such as low material density and high surface/volume ratio, constructing 3D CdS NSs has been considered as a useful strategy to boost the photocatalytic activity. For example, to overcome the shortcomings of traditional non-porous CdS/TiO_2 spherical nanocomposites (rapid recombination of e^--h^+ pairs and inferior light absorption), Wu *et al.* [292] designed non-noble metal cocatalysts covered in hollow core–shell NSs for photocatalytic H_2 evolution. The unique hollow structure enhanced the absorption in the visible spectral range, while the non-noble metal cocatalysts provided active sites for H_2 evolution. The coupling of these three components reduced photogenerated e^--h^+ recombination. The synergistic effects of photocatalysts and e^--h^+ separation were preliminarily studied. Chen *et al.* [293] synthesized hollow core–shell CdS/TiO_2/Ni_2P photocatalysts for H_2 production with SiO_2 spheres as sacrificial templates (Fig. 11a and b). The formation of CdS/TiO_2 nanocomposites extended the absorption range of TiO_2 into the visible-light region, while the outer TiO_2 layer protected the CdS core from photocorrosion. The hollow structure improved the transmission capacity of light and reduced the reflectance of visible light. The H_2 generation rate of CdS@TiO_2 (4.65 mmol g^{-1} h^{-1}) showed significant improvement compared with that of CdS/TiO_2/Ni_2P nanocomposites (13.91 mmol g^{-1} h^{-1}). The H_2 generation rate for the CdS/TiO_2/Pt nanocomposite was 16.81 mmol g^{-1} h^{-1}, which was slightly higher than that of CdS/TiO_2/Ni_2P (Fig. 11c and d). The activity of CdS/Ni_2P and CdS/TiO_2/Ni_2P remained rather unchanged after 5 cycles. However, CdS/Pt and CdS/TiO_2/Pt exhibited a diminishing photocatalytic activity after each recovery cycle due to photocorrosion and poor stability of the Pt deposit (Fig. 11e) [293]. In the future, it is expected that more 3D CdS-based NS photocatalysts can be constructed through the self-assembly of promising 2D ultrathin CdS

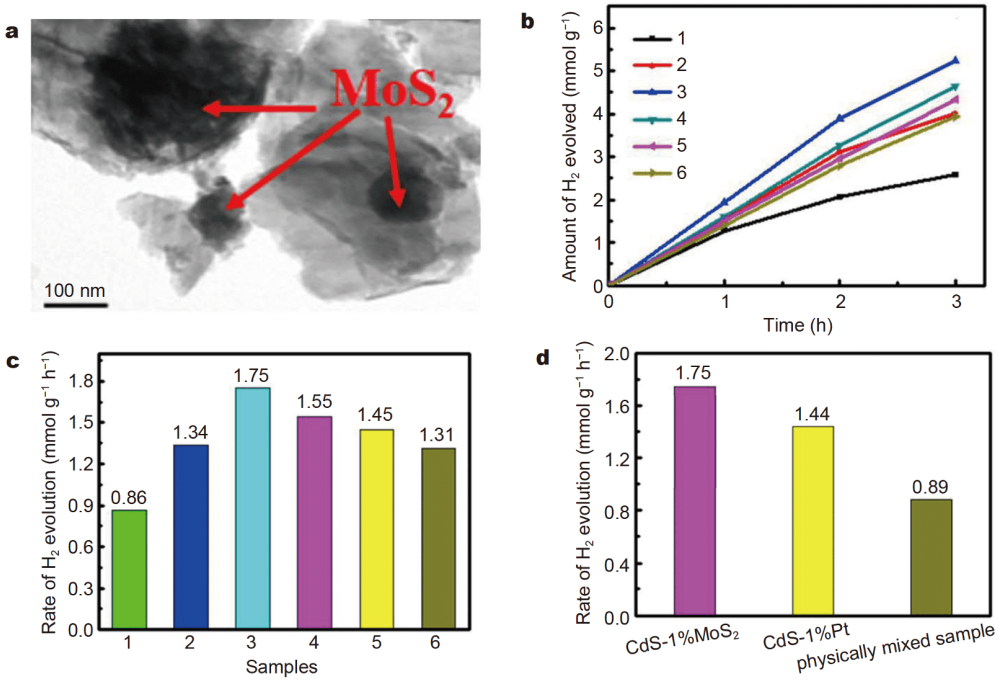

Figure 10 (a) TEM image of CdS/1%MoS_2, (b) time-dependent of H_2 generation (1: CdS NSs, 2: CdS-0.5% MoS_2, 3: CdS-1% MoS_2, 4: CdS-2% MoS_2, 5: CdS-3% MoS_2, 6: CdS-5% MoS_2) , (c) the average rate of photocatalytic H_2 generation over the photocatalysts, and (d) comparison of H_2 generation activities of CdS/1%MoS_2, CdS/1%Pt, and physically mixed sample of CdS/1% MoS_2. Reprinted with permission from Ref. [66]. Copyright 2017, Elsevier.

nanosheets, which could maximize all the advantages of 2D nanosheets by circumventing their unfavorable stacking.

BOOSTING INTERFACIAL CHARGE SEPARATION IN NANOSTRUCTURED CdS

Boosting the interfacial charge transfer of CdS-based photocatalysts can also be achieved by constructing semiconductor heterojunctions, which induce an internal electrical field for interfacial charge transfer [10]. Usually, semiconductor heterojunctions are categorized into the Schottky junction, as well as carbon-based, direct Z-scheme, Type I, Type II, and Type III heterojunctions. The Schottky and Type II junctions are beneficial for constructing efficient CdS-based photocatalysts. For instance, heterojunctions between CdS and other semiconductors (such as Fe_2O_3 [179], TiO_2 [63,226,294,295], g-C_3N_4 [296,297], $NiWO_4$ [298,299], BiOBr [300], WO_3 [165,178,222,301], MoO_2 [302], ZnO [150,303–306], $LaFeO_3$ [307], SiC [308], Bi_2WO_6 [309], and Co_3O_4 [310]) have been widely used in photocatalytic H_2 evolution.

However, there are still debatable aspects associated with the separation mechanism of photogenerated e^--h^+ pairs in these heterojunctions [311]. In addition, the reduction and oxidation potentials will be compromised after forming the Type II heterojunction, restricting their activity enhancement. Therefore, various favorable heterojunctions, such as p-n, Z-scheme, Schottky-based, carbon-based, and multicomponent heterojunctions, have also been studied to improve the photocatalytic performance of CdS-based photocatalysts.

p–n heterojunction

The p–n heterojunction has been widely applied toward enhancing the photocatalytic performance of CdS-based photocatalysts. The formation mechanism of the p–n heterojunction is shown in Fig. 12 [311]. Under visible-light illumination, the e^- from the n-type semiconductor are transferred to the p-type semiconductor owing to the larger work function of the latter. This results in the formation of a built-in electric field, which is beneficial for the transfer of photogenerated e^- between p-type and n-type semiconductors.

Ai *et al.* [224] designed novel CdS/boron carbon nitride nanotubes (BCNNTs) using a new band-matching transformation strategy. In this system, they realized the heterojunction transformation from Type I to Type II by tuning the carbon content of BCNNTs (Fig. 13a). The rational design of the band-matching process played an important role in constructing efficient photocatalysts *via*

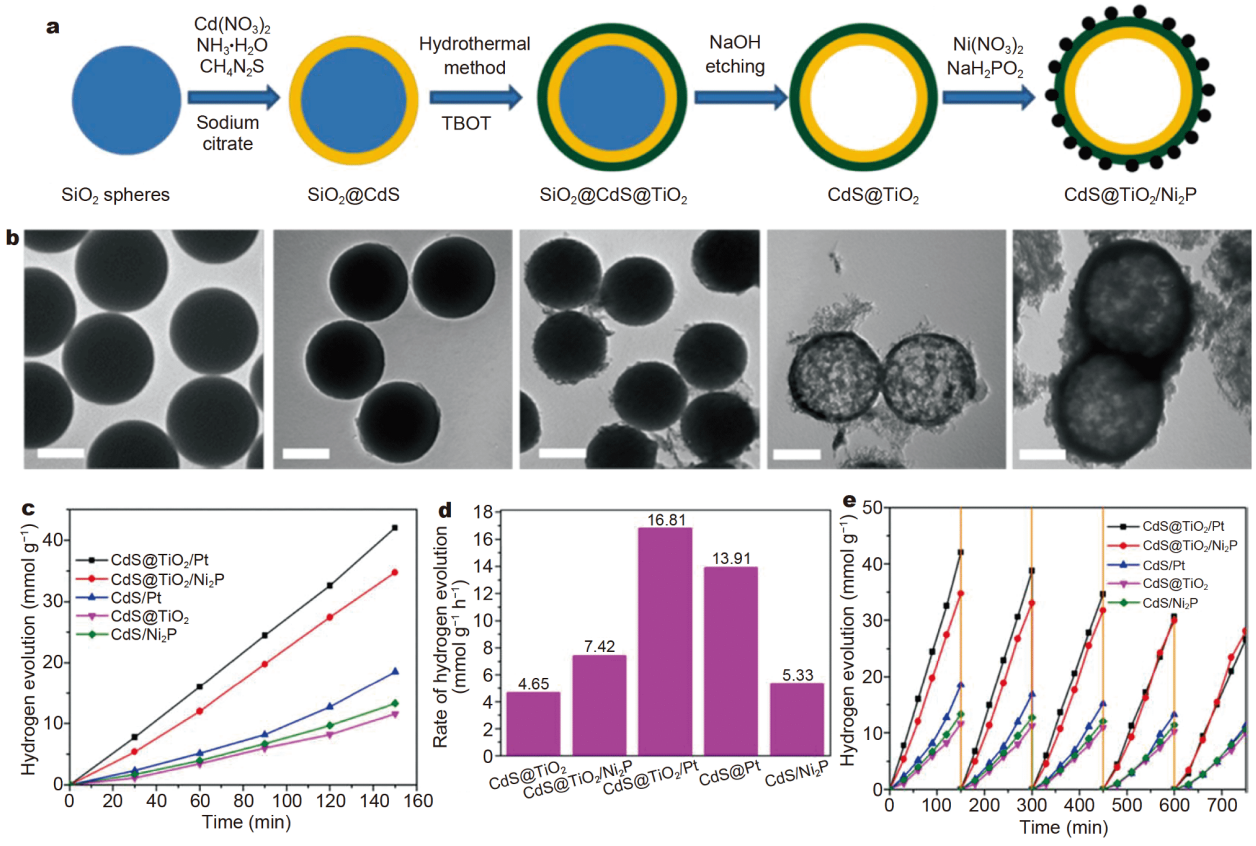

Figure 11 (a) Schematics of $CdS@TiO_2/Ni_2P$ preparation, (b) TEM images of SiO_2, SiO_2/CdS, SiO_2/CdS/TiO_2, CdS/TiO_2, and CdS/TiO_2/Ni_2P, (c) photocatalytic H_2 evolution, (d) rate of H_2 evolution and (e) stability of H_2 evolution. Reprinted with permission from Ref. [292]. Copyright 2019, Elsevier.

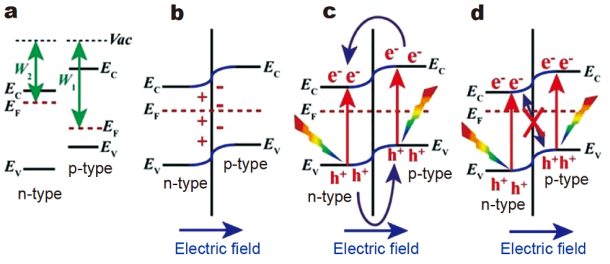

Figure 12 Formation mechanism of the p–n heterojunction: (a) before contact, (b) in contact, (c) photogenerated charge transfer, and (d) unsuccessful direct Z-scheme transfer of photogenerated charge carriers. Reprinted with permission from Ref. [311]. Copyright 2018, Elsevier.

the formation of a strong internal electric field to guarantee rapid charge separation and transfer. As the C content increased, the bandgap of BCNNTs decreased from 2.79 to 2.05 eV. At low C content, the CdS/BCNNTs belong to the Type I heterojunction, and all of the photogenerated e^- and h^+ were transferred to the CB and VB of CdS, respectively. With a high C content, the CB potential of BCNNTs was more positive than that of CdS, and VB was negative relative to CdS. This composite also belongs to the Type I heterojunction, wherein the CdS photogenerated e^- and h^+ were all transferred to BCNNTs. However, with moderate C-doping, both the CB and VB of BCNNTs were more positive than those of pure CdS, thereby fulfilling the requirement for the formation of Type II heterojunctions (Fig. 13c). The internal electric field between the CdS and BCNNTs could boost the separation of photogenerated e^--h^+ pairs. Hence, the photocatalytic performance of the Type II heterojunctions exceeded that of the Type I heterojunction between CdS and BCNNTs (Fig. 13b) [224]. Zhang *et al.* [310] constructed a ZIF-67(Co)-derived Co_3O_4 framework modified with a CdS p–n heterojunction photocatalyst (Fig. 14a–c). The formation of p–n heterojunctions could effectively reduce the bandgap of the composite, enhance the light absorption intensity, shorten the fluorescence lifetime (2.61 ns), accelerate the electron injection rate ($K_{ET} = 1.17 \times 10^8\ s^{-1}$), and improve electron injection efficiency ($\eta_{inj} = 30.6\%$) (Fig. 14d–f). The hollow structure of the Co_3O_4 framework served not only as a h^+ collector

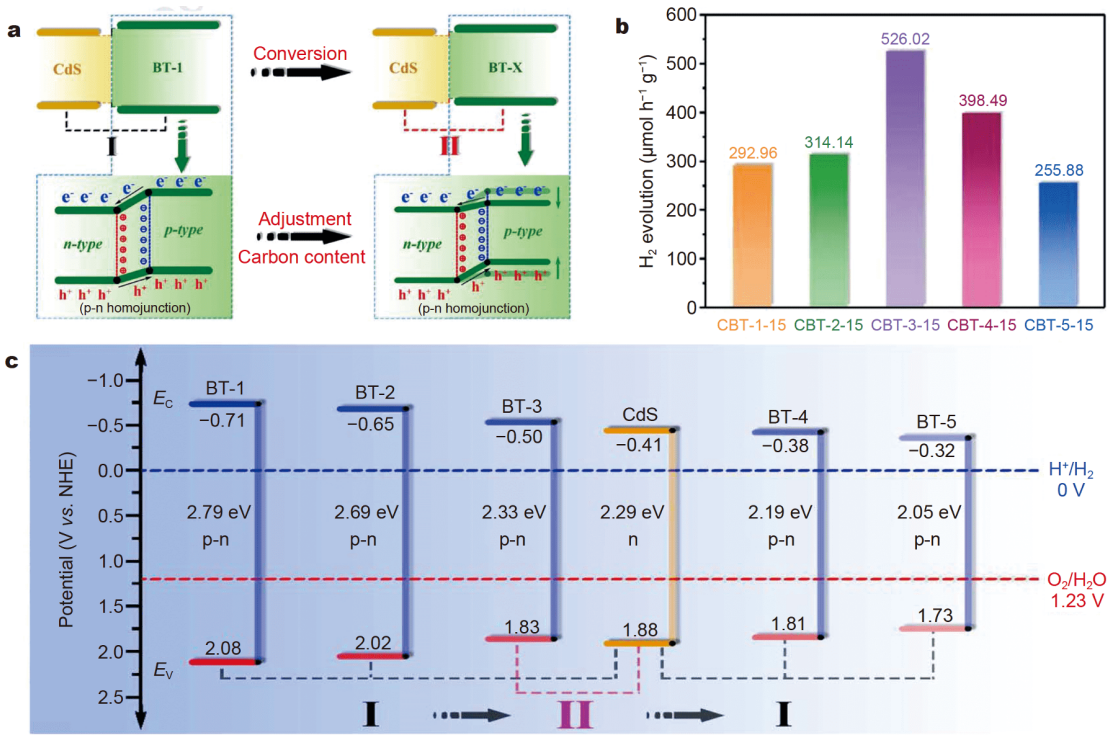

Figure 13 (a) Schematic for band-matching transformation of the CdS/BCNNTs photocatalytic system, (b) average H_2 evolution rate of CdS/BCNNTs, (c) schematic of the band-matching transformation process between BCNNTs (X= 1, 2, 3, 4, 5) and CdS. Reprinted with permission from Ref. [224]. Copyright 2020, Elsevier.

but also as a supporting material for CdS, thus increasing the specific surface area of the catalyst [310]. The results further confirmed the key roles of the p–n heterojunction toward achieving efficient charge separation and transfer across the heterojunction interface as well as the prolonged lifetime of the charge carriers.

Schottky junctions

Enhancing the photocatalytic activity of CdS-based semiconductors could also be realized by constructing Schottky junction-based internal electrical fields [4,87]. The Schottky junction can boost the spatial separation of e^- and h^+, thus delaying their recombination and lengthening their lifetime. Usually, for metal photo-semiconductor systems, because of the higher work function (Φ_m) of the metal than that of the semiconductor (Φ_s), the photoexcited e^- in the photo-semiconductor migrate to the metal and realign their Fermi levels; this leads to the formation of a Schottky barrier with an upward band bending and depletion layer (Fig. 15). As an effective method to trap photogenerated e^-, Schottky-based heterojunctions can promote e^--h^+ separation in photocatalysis [312].

When photo-semiconductors are coupled with metal, the e^- in the CB of the photo-semiconductor approach the metal until the two Fermi energy levels are in equilibrium. A space–charge layer is formed on the surface of the metal, resulting in efficient separation of photoexcited e^--h^+ pairs and migration of the charge carriers. For example, the work functions of metallic Cd clusters and CdS are 4.08 and 5.18 eV, respectively (Fig. 16a and b) [313]. After contact, the e^- in Cd migrate to the CdS until the Fermi levels are realigned, triggered by the higher Fermi level in metallic Cd than CdS. When CdS is excited by visible-light irradiation, the built-in field drives the migration of the photoexcited e^- on the CdS to the Cd sites. Thus, the construction of a Schottky junction can enhance visible-light-driven water splitting for H_2 generation. Similarly, Shang *et al.* [314] decorated CdS NPs on Cd nanosheets to form Schottky junctions by the polyol reduction method and oxidation–sulfurization process (Fig. 16c and d). The Cd nanosheets that served as a support were evidently better than those of carbon nanotubes and graphene in that study because the work function of Cd is much higher than that of the nanocarbon materials (Fig. 16e). More importantly, the black

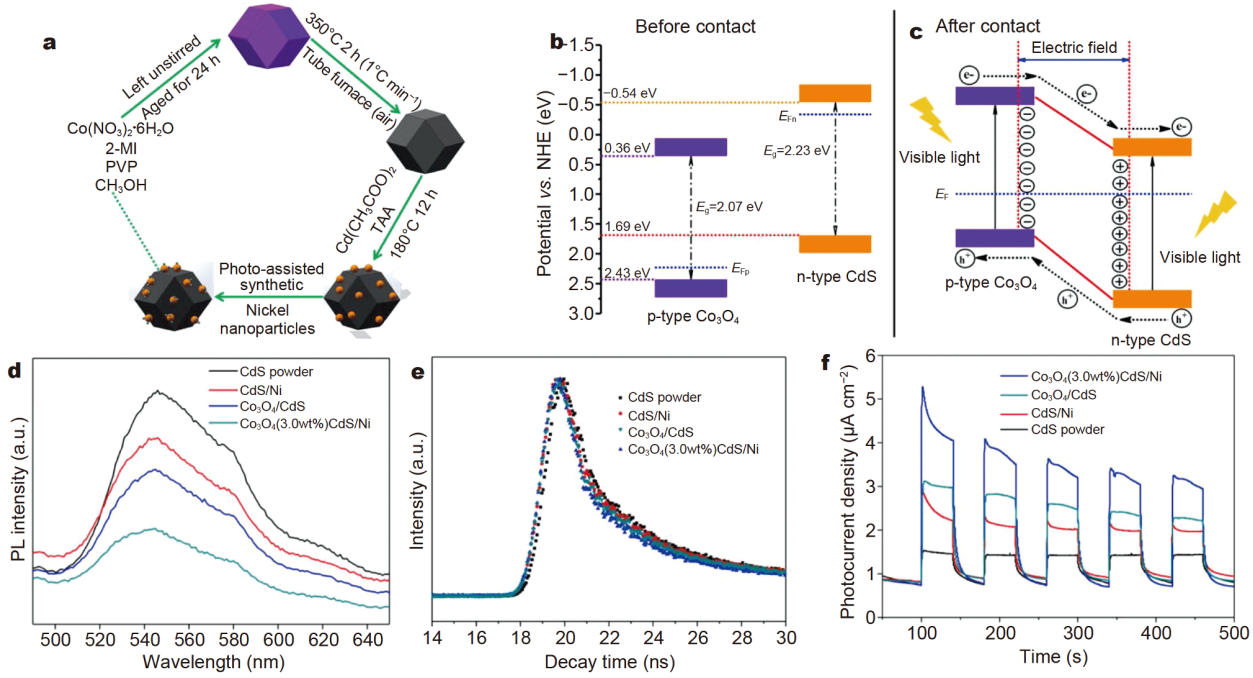

Figure 14 (a) Schematic of the fabrication of [Co_3O_4/CdS/Ni]. Schematics for energy bands of p-CdS and n-Co_3O_4 (b) before contact and (c) after the formation of the p–n heterojunction. (d) PL spectra, (e) time-resolved PL spectra, and (f) photocurrent of the as-prepared photocatalysts. Reprinted with permission from Ref. [310]. Copyright 2018, Elsevier.

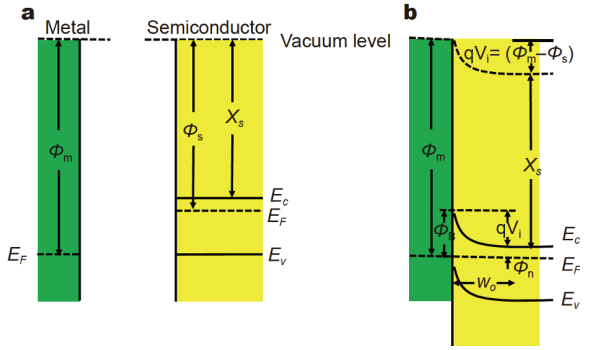

Figure 15 Schematic for the formation of the Schottky barrier ($\Phi_m > \Phi_s$): (a) before contact and (b) thermal equilibrium after contact (E_g, Φ, E_F, and χ represent the bandgap energy, work function, Fermi level, and electron affinity, respectively).

color of the nanocarbon shields a fraction of the visible light from reaching CdS [314]. Xiao *et al.* [238] demonstrated that a 1D CdS NR/2D MXene nanosheet with Schottky junctions reached an excellent photocatalytic H_2 evolution rate of 2407 μmol g^{-1} h^{-1}, which was attributed to the high charge carrier mobility of highly conducting metallic Ti_3C_2 and strong interfacial coupling between CdS and Ti_3C_2 [238].

Additionally, it is well known that nanocarbon materials (e.g., graphene [291,315–319], carbon quantum dots [211,236,257,320,321], carbon black [322], carbon fiber [323–325] and carbon nanotubes [78,326–328]) have been considered as outstanding promoters for photocatalytic performances. The attraction is attributed to their superior adsorption capacity, unique electronic conductivity, nontoxicity, low cost, high stability, and large surface area. The formation of carbon-based Schottky junctions and the narrowing bandgap by carbon doping are both beneficial to photocatalytic reactions.

Direct Z-scheme heterojunction

Biomimetic artificial photosynthesis by constructing direct Z-scheme photocatalysts represents a feasible strategy for improving the photocatalytic performance [46,204,306,329–332]. Specifically, the direct Z-scheme photocatalytic system has a charge carrier transfer pathway similar to the letter "Z" (Fig. 17) [333]. During the photocatalytic reaction, the photoexcited e^- (with lower reduction capacity) in semiconductor A recombine with the photoexcited h^+ (with lower oxidation capacity) in semiconductor B. Therefore, the photoexcited e^- (with high reduction capacity) in semiconductor B and photoexcited h^+ (with high oxidation capacity) in semiconductor A can be utilized. The direct Z-scheme

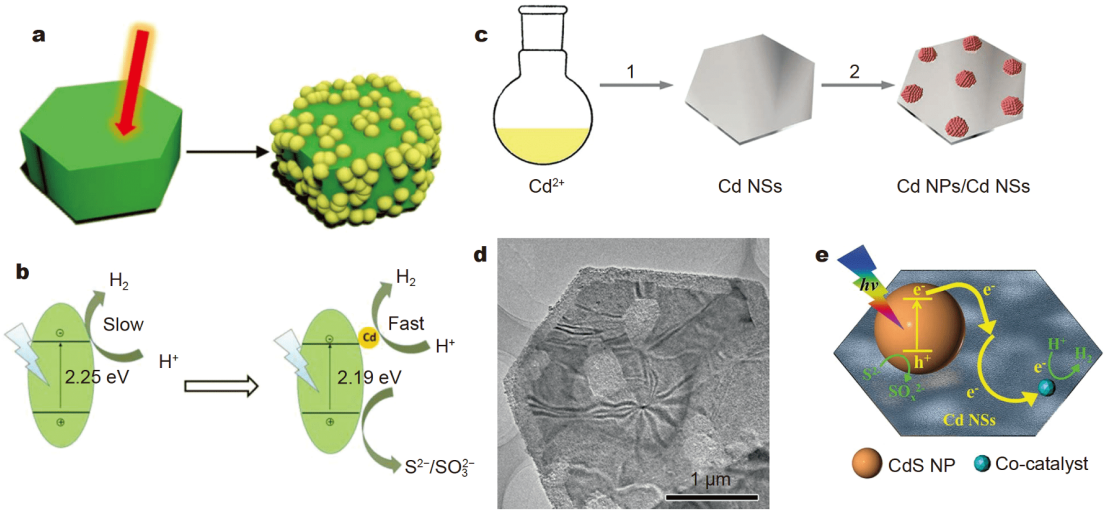

Figure 16 (a) Schematic of the laser irradiation-induced formation of a CdS/Cd Schottky junction, (b) synthesis process [313], (c) schematic of photocatalytic H_2 generation performance, (d) TEM image and (e) charge transfer mechanisms in CdS/Cd photocatalysts. Reprinted with permission from Ref. [314]. Copyright 2016, Wiley-VCH.

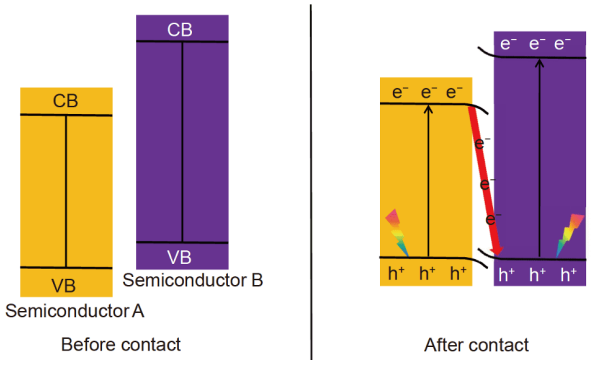

Figure 17 Mechanisms of charge carrier separation in the Z-scheme system.

photocatalyst possesses an enlarged and stronger redox capacity. Furthermore, the charge carrier transport for direct Z-scheme nanocomposites is more physically feasible because the transport of photoexcited e^- from the CB of photo-semiconductor A to the photoexcited h^+-rich VB of photo-semiconductor B is favorable due to the electrostatic attraction between h^+ and e^-.

In 2009, Cheng's group [177] reported the direct Z-scheme of CdS/ZnO heterostructure photocatalysts. They found that the formation of Z-scheme heterostructures between ZnO and CdS could effectively prolong the lifetime of photogenerated e^-, reaching a 14-fold improvement in H_2 evolution performance compared with that of pure CdS. Since then, numerous direct Z-scheme CdS-based photocatalysts have been applied in photocatalytic H_2 generation applications [334], including CdS/WO_{3-x} [222], $FeC_2O_4{\cdot}2H_2O$/CdS [335], CdS/WO_3 [165,301], CdS/MoO_{3-x} [336], CdS/g-C_3N_4 [337,338], $CoWO_4$/CdS [44], CdS/Fe_2O_3 [179], CdS/$BiVO_4$ [339], TiO_2/CdS [329,340,341], CdS/$CdWO_4$ [219,342], ZnO/CdS [306] and CdS/PI [217]. In our previous study, we reported the fabrication of 2D/2D CdS/g-C_3N_4 direct Z-scheme heterojunction nanocomposites through the *in-situ* growth of 2D CdS NSs on 2D g-C_3N_4 NSs [338]. As shown in Fig. 18a and b, the direct Z-scheme CdS/g-C_3N_4 nanocomposites displayed improved photocatalytic H_2 generation activity compared with pure g-C_3N_4 and CdS. The highest H_2 generation rate is realizable with the CdS/0.7 g-C_3N_4 direct Z-scheme heterostructures at 15.3 mmol g^{-1} h^{-1}, which is 3000 and 4 times higher than those of bare g-C_3N_4 and CdS, respectively. After 21 h of continuous visible-light irradiation, the 2D/2D CdS/0.7 g-C_3N_4 maintained excellent photocatalytic H_2 generation activities without noticeable decay (Fig. 18c). The apparent efficiency of the direct Z-scheme CdS/0.7 g-C_3N_4 was 6.86% at 420 nm (Fig. 18d). Based on the calculations and experimental results, a schematic for photocatalytic H_2 generation with CdS/g-C_3N_4 nanocomposite photocatalysts was suggested (Fig. 18e). This work highlights the synergistic effect between the direct Z-scheme and the 2D/2D NS in promoting photocatalytic H_2 generation reactions.

Shen *et al.* [179] reported 2D/2D Z-scheme nanocomposites fabricated *via* the *in-situ* growth of CdS NSs on α-Fe_2O_3 NSs (Fig. 19a). In addition, the modification

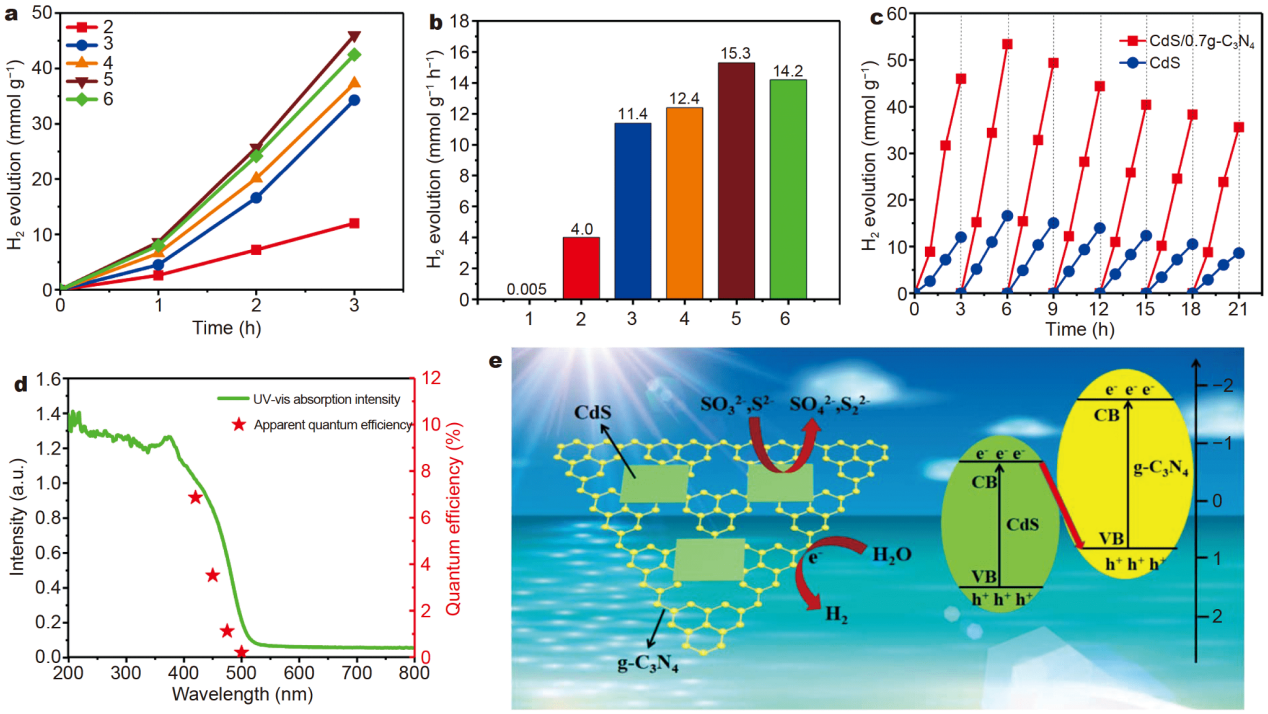

Figure 18 (a) Time-dependent photocatalytic H_2 evolution, (b) average H_2 evolution rates for different samples (1: g-C_3N_4, 2: CdS, 3: CdS/0.5g-C_3N_4, 4: CdS/0.6g-C_3N_4, 5: CdS/0.7g-C_3N_4, 6: CdS/0.8g-C_3N_4), (c) repeated time courses of photocatalytic H_2 evolution, (d) apparent quantum efficiency for CdS/0.7 g-C_3N_4, and (e) proposed schematic for 2D/2D CdS/g-C_3N_4 S-scheme heterostructures. Reprinted with permission from Ref. [338]. Copyright 2020, Wiley-VCH.

of CdS/α-Fe_2O_3 Z-scheme nanocomposites could be performed with metallic β-NiS, which continued to construct an ohmic junction as H_2-generation active sites (Fig. 19b). The CdS/α-Fe_2O_3/NiS ultrathin 2D/2D heterojunction exhibited an outstanding H_2 generation rate (45 mmol g^{-1} h^{-1}) with high AQEs at 420 nm (46.9%). The outstanding photocatalytic performance was ascribed to: (1) ohmic-based heterojunction that offered a large number of H_2-evolution sites; (2) large and intimate interfaces, which facilitated charge transfer; and (3) boosted charge migration in the direct Z-scheme heterojunction (Fig. 19c–e).

Besides 2D/2D Z-scheme nanocomposites, those with core–shell structures also offer advantages in photocatalytic water splitting. Compared to 2D/2D structures, core–shell structures can better protect CdS from photocorrosion. Ma *et al.* [304] synthesized CdS@ZnO core–shell structured photocatalysts *via* atomic layer deposition (ALD) (Fig. 20a). The growth of ZnO along certain facets was effectively controlled by the number of ALD cycles (Fig. 20b and c). The formation of core–shell structures in the Z-scheme composite could suppress the recombination of photogenerated e^--h^+ pairs and induce strong and intimate heterojunction interfacial contact between CdS and ZnO. Upon loading Pt and PdS as cocatalysts on the CdS@ZnO surface, the photocatalytic H_2 evolution rate reached 98.82 mmol g^{-1} h^{-1} with an AQE of 69.59% at 420 nm (Fig. 20d–f) [304].

These results highlight the promising performance of the 2D/2D layered Z-scheme heterojunctions with larger contact area for fast separation of photoexcited charge carriers across their interfaces with respect to the 0D/2D and 1D/2D coupling systems. Notably, coupling semiconductors at their active facets are apparently more promising for efficient photogenerated e^- transfer. It is expected that CdS-based composites with 2D/2D layered Z-scheme heterojunctions coupled with their active facets can be rationally fabricated for photocatalytic H_2 evolution [179,338].

ACCELERATING SURFACE CHARGE UTILIZATION OF NANOSTRUCTURED CdS

Structural defects in CdS may result in fast recombination of photo-excited e^--h^+ pairs [257,343]. As photocatalytic H_2 generation from water is a thermodynamically unfavorable reaction, the sluggish kinetics on the CdS surface need to be addressed. It is common to use suitable

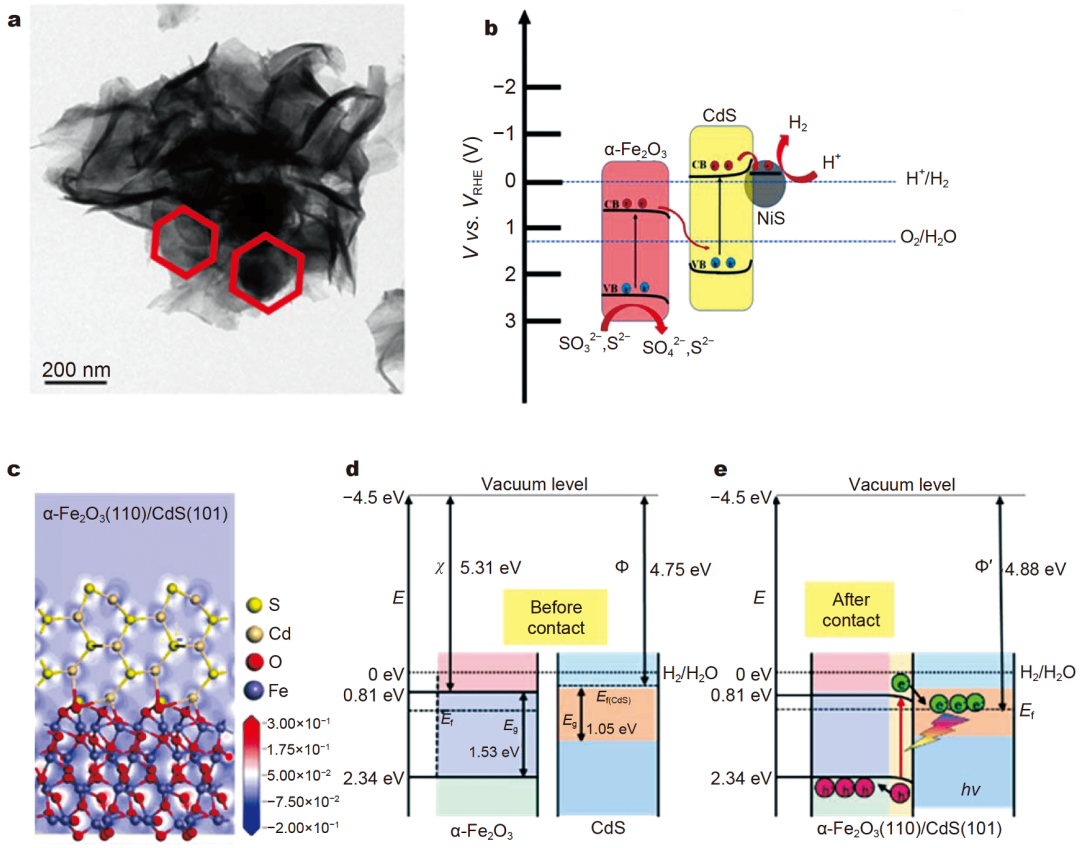

Figure 19 (a) TEM image of CdS/α-Fe_2O_3, (b) photocatalytic mechanism of CdS/α-Fe_2O_3/NiS, (c) simulated charge density difference distribution at the CdS/α-Fe_2O_3 heterojunction interface, (d) and (e) the band bending in the space charge region at the interface before and after coupling α-Fe_2O_3 and CdS. Reprinted with permission from Ref. [179]. Copyright 2020, Elsevier.

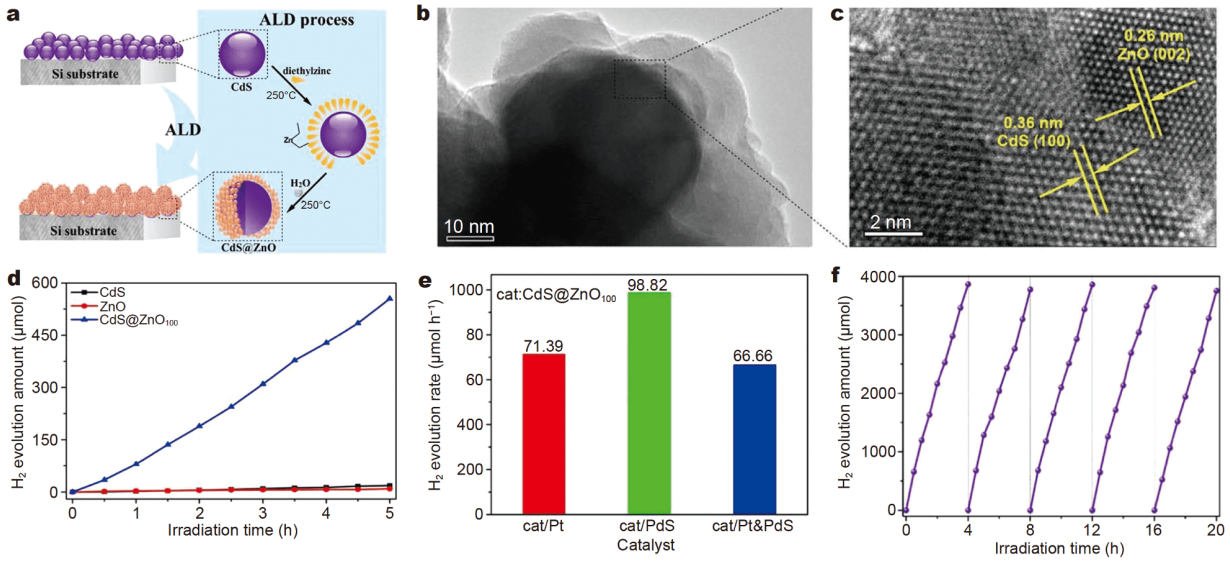

Figure 20 (a) Synthesis process, (b) TEM image, and (c) HRTEM image of CdS@ZnO core–shell photocatalysts. (d) H_2 evolution over CdS, ZnO, and CdS@ZnO; (e) average H_2 evolution rate; (f) cyclic runs for photocatalytic H_2 evolution over the CdS@ZnO-PdS. Reprinted with permission from Ref. [304]. Copyright 2017, Elsevier.

cocatalysts to promote the kinetics of photocatalytic H_2 generation. To date, various cocatalysts, such as Au [344,345], Pt [321,346,347], Ag_2S [348], MXenes [238,349–352], $CoMoS_x$ [353], MoO_xS_y [354], MoS_2 [222,355–358], Ni_3C[176], Ni_2P [359,360], NiS_x [63,322,361], NiCoP [362], CoP_x [199,363], CuS_x [212,246], and WS_2 [364,365], have been coupled with CdS-based semiconductors for photocatalytic H_2 evolution. Typically, noble metals (Pt, Ag, and Au) are known as excellent cocatalysts for this application. For example, Liu *et al.* [232] demonstrated a facile and rapid ultrasonic-chemistry-based approach to load Pt onto CdS NRs, and the resulting Pt/CdS showed efficient H_2 evolution performances. The maximum H_2 evolution rate could reach 24.15 mmol g^{-1} h^{-1} over 0.5 wt.% Pt/CdS. Bao *et al.* [169] reported a facile aqueous solution process for the large-scale synthesis of nanoporous CdS NSs and CdS hollow NRs by the air-insensitive inorganic reactants of $Na_2S{\cdot}9H_2O$ and $CdCl_2{\cdot}2.5H_2O$ at room temperature. The obtained CdS/Pt exhibited the highest AQEs (60.34%) at 420 nm for photocatalytic H_2 generation.

However, the scarcity and high cost of noble metals restrict their large-scale applications in photocatalytic H_2 generation. Therefore, earth-abundant-metal-based and noble-metal-free cocatalysts have received increasing attention [4,18,366,367]. For example, Li *et al.* [229] found that a 0.2 molar ratio of NiS improved the average charge carrier lifetime of CdS by 97 times, potentially leading to more efficient charge separation and transfer. They synthesized CdS NWs and NiS with tight connections using a two-pot solvothermal synthesis. Tight interfaces between CdS and NiS with a smaller intrinsic bandgap led to significantly enhanced photocatalytic H_2 evolution activities. As the content increased, NiS aggregated on the surface of CdS and unfavorably caused fast recombination of photogenerated e^--h^+ pairs. An evident decay was observed in the broad transient bleach signal after loading NiS, which indicated that the NiS improved the separation of CdS photogenerated e^- and h^+ pairs. CdS with a NiS molar ratio of 20 reached an optimal photocatalytic H_2 evolution rate of 1512.4 μmol g^{-1} h^{-1} in lignin and lactic acid aqueous solution, which was 5041 times higher than that of pristine CdS [229]. The resulting CdS/NiS also exhibited excellent stability for 900 min of experiments in the lignin and lactic acid solution [229].

Cocatalysts supported on semiconductors can facilitate the prompt separation and migration of photoexcited charge carriers. For example, we reported a novel strategy to form 2D/2D nanocomposites by coupling Ni_2SP NSs with CdS NSs [286]. Fig. 21a depicts the ultrathin 2D NS of CdS/Ni_2SP. The as-fabricated 2D/2D CdS/Ni_2SP photocatalysts displayed an outstanding H_2 generation performance under visible light ($\lambda \geq 420$ nm). The CdS/2%Ni_2SP yielded the highest H_2 generation rate of 18.96 mmol g^{-1} h^{-1}, which was approximately threefold higher than that of bare 2D CdS without the cocatalysts (Fig. 21b). As shown in Fig. 21c, the highest AQE was 4.8% at 420 nm. The *I*–*t* curve of CdS/2%Ni_2SP composites is obviously higher than that of nanostructured CdS, indicating that the 2D Ni_2SP cocatalysts promoted interfacial charge migration and accelerated charge utilization of nanostructured CdS (Fig. 21d). The interfacial coupling effects between the 2D Ni_2SP cocatalyst and 2D CdS enhanced photocatalytic H_2 generation by increasing the number of active sites, thereby facilitating rapid charge separation and transfer, while enhancing H_2 generation kinetics (Fig. 21e).

Recently, single metal atoms (serving as active sites) have shown excellent performances in photocatalytic and electrocatalytic reactions. The atomically dispersed single metal atoms on the semiconductor surface exhibit unique catalytic performances. For example, Zhang *et al.* [368] designed atomically dispersed Ni single atoms anchored on the surface of CdS NRs. Under visible light, the photocatalytic H_2 rate reached 630.1 mmol g^{-1} h^{-1}. The single Ni atoms were stabilized by the Ni–O bonds. Density functional theory calculations revealed that the Ni atoms could optimize H_2 binding and electronic properties, thus improving the separation of photogenerated e^--h^+ pairs. Meanwhile, Ni–CdS composites showed a stabilized photocatalytic performance during 16 h of irradiation. Some examples of CdS photocatalysts modified with cocatalysts are presented in Table 2.

In future, dual cocatalysts that combine different types of cocatalysts [369,370], including metal, metal oxide/sulfide/carbide/phosphide, and nanocarbons, might attract increasing attention in photocatalytic H_2 evolution over CdS-based photocatalysts. Additionally, apart from loading H_2 evolution cocatalysts, it should be noted that the oxidation cocatalysts are also expected to be loaded on CdS-based photocatalysts to boost charge separation and suppress photocorrosion, thereby fundamentally enhancing photocatalytic H_2 evolution [371].

SUPPRESSING CHARGE-INDUCED PHOTOCORROSION IN NANOSTRUCTURED CdS

Presently, research on the reaction mechanism and the fundamental carrier dynamics in CdS-based nanocomposite half-reaction systems has seen meaningful

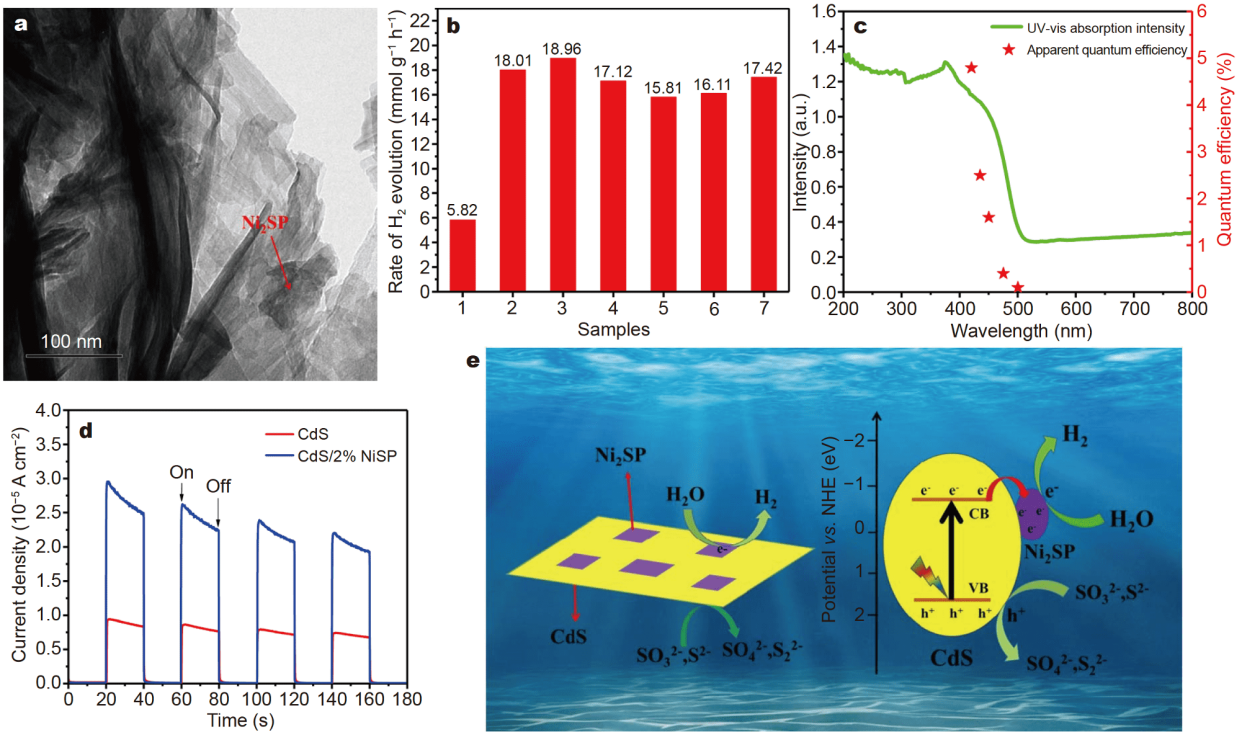

Figure 21 (a) HRTEM image of CdS/Ni_2SP, (b) average rate of H_2 evolution (1: CdS, 2: CdS/1%Ni_2SP, 3: CdS/2%Ni_2SP, 4: CdS/3%Ni_2SP, 5: CdS/4%Ni_2SP, 6: Ni_2SP, 7: CdS/2% NiS, 8: CdS/2%Ni_2SP nanoparticles), (c) AQEs of CdS/2%Ni_2SP, (d) photocurrent responses, and (e) proposed mechanistic scheme: (a) CdS; (b) CdS/1%Ni_2SP; (C) CdS/2%Ni_2SP; (d) CdS/3%Ni_2SP; (e) CdS/4%Ni_2SP; (f) Ni_2SP; (g) CdS/2%NiS; (h) CdS/2%Ni_2SP nanoparticles. Reprinted with permission from Ref. [286]. Copyright 2020, Elsevier.

progress. However, due to the photocorrosion phenomenon of CdS-based nanocomposites, the stability and durability of most reported CdS-based photocatalysts need further improvement. The accumulation of photoexcited h^+ in its VB can induce the self-oxidation of S^{2-} in CdS, which results in the dissolution of Cd^{2+}. Apparently, the effective removal of photoexcited h^+ from the VB of CdS impedes the self-oxidation of S^{2-}, enhancing the durability and photostability of CdS. It is well known that the use of sacrificial reagents (such as Na_2S–Na_2SO_3, ethanol, and lactic acid) as e^- donors for CdS photocatalysts in photocatalytic H_2 generation systems is an effective strategy to suppress photocorrosion of CdS.

Furthermore, Z-scheme heterojunctions could reduce the accumulation of h^+ in the VB of CdS. Li *et al.* [381] found that the formation of CdS–MnS Z-scheme photocatalysts through a cation exchange process could maintain good stability over 42 h of measurement (Fig. 22a and b). The chopped photocurrent density–voltage measurements show that the pure CdS was photocorroded rapidly within 800 min of illumination (Fig. 22c). After the formation of the Z-scheme heterojunction between CdS and MnS, the photocorrosion phenomenon was suppressed. Moreover, the formation of Z-scheme heterojunctions also increased the light-absorption range from 520 to 800 nm (Fig. 22d). Consequently, the obtained CdS–MnS showed an optimal H_2 evolution rate of 1595 μmol g^{-1} h^{-1} with an AQE of 22.6% at 420 nm [381].

Constructing a p–n heterojunction is another strategy to transfer h^+ from the VB of CdS. After the formation of the p–n heterojunction, the h^+ in the VB of CdS could be transferred to the relatively positive VB of a p-type semiconductor, which effectively reduces h^+ accumulation in the VB of CdS. Ai *et al.* [382] designed CdS@Ti_3C_2@CoO with a hierarchical tandem p–n heterojunction for photocatalytic HER. The insertion of Ti_3C_2 on the surface of CdS served as a platform for the growth of CoO NPs, which were introduced as a bridge to consolidate CdS and CoO into a special tandem p–n heterojunction. Meanwhile, Ti_3C_2 also served as a bridge with a powerful unidirectional internal electric field wherein another internal electric field was generated between Ti_3C_2 and CoO, causing photogenerated carriers to transfer to Ti_3C_2 and restricting h^+ migration (Fig. 23a). Thus, CdS@

Table 2 Cocatalyst loading on CdS for photocatalytic H_2 production

Nanocomposites	Content of cocatalysts	Light source	Sacrificial reagent	HER (mmol g^{-1} h^{-1})	AQE (420 nm)	Ref.
Pt-PdS/CdS	0.3 wt.%	300 W Xe lamp	Na_2S–Na_2SO_3	29.23	93	[173]
MoS_2/CdS	0.2 wt.%	300 W Xe lamp	Lactic acid	5.4	-	[166]
WS_2/CdS	1 wt.%	300 W Xe lamp	Lactic acid	4.2	-	[364]
NiS/CDs/CdS	10 wt.%	350 W Xe lamp	Na_2S–Na_2SO_3	1.44	-	[257]
CdS/Co-MoS_x	2 mol%	300 W Xe lamp	Lactic acid	0.54	23.5	[263]
NiS/CdS	1.2 mol%	300 W Xe lamp	Lactic acid	2.18	51.3	[174]
CdS/WS_2/graphene	4.2 wt.%	300 W Xe lamp	Na_2S–Na_2SO_3	1.84	21.2	[240]
PdNi/CdS	2 wt.%	300 W Xe lamp	$(NH_4)_2SO_3$	32.4	63.97	[372]
$PtNi_x$/CdS	2.0 wt.%	300 W Xe lamp	$(NH_4)_2SO_3$	11.4	51.24	[373]
CdS/g-C_3N_4/CuS	10 wt.%	350 W Xe lamp	Na_2S–Na_2SO_3	1.15	16.5	[212]
CuS/CdS	25 wt.%	300 W Xe lamp	Lactic acid	5.62	19.7	[374]
Pt/CdS	0.5 wt.%	300 W Xe lamp	Lactic acid	24.15	-	[232]
MoS_2/CdS	3 wt.%	300 W Xe lamp	Na_2S–Na_2SO_3	11.4	-	[213]
Ni@NiO/CdS/g-C_3N_4	1 wt.%	300 W Xe lamp	Triethanolamine	1.26	-	[218]
Ni_2P/CdS	3.51 wt.%	300 W Xe lamp	Na_2S–Na_2SO_3	44.65	-	[256]
$Co(OH)_2$/CdS	6.5 mol%	350 W Xe lamp	Lactic acid	14.43	-	[375]
$NiSe_2$/CdS	5 wt.%	300 W Xe lamp	Na_2S–Na_2SO_3	167.1	1.5	[241]
VC/CdS	15 wt.%	300 W Xe lamp	TEOA	14.2	8.7	[215]
Cobalt–salen/CdS	0.015 mmol L^{-1}	300 W Xe lamp	Na_2S–Na_2SO_3	106	29	[235]
NiO_x/CdS	1 mol%	300 W Xe lamp	Methanol and $Ni(CH_3COO)_2$	5.9	8.6	[57]
NiS/CdS	20 mol%	300 W Xe lamp	Lignin and lactic acid	0.15	44.9	[229]
CDs/CdS-S	1 wt.%	300 W Xe lamp	Lactic acid	4.64	11.8	[236]
MoS_2/CdS	5 wt.%	300 W Xe lamp	Na_2S–Na_2SO_3	4.65	7.31	[255]
CdS/MnS	5 wt.%	300 W Xe lamp	Lactic acid	15.55	6.9	[233]
Cu_2MoS_4/CdS	5 wt.%	150 W Xe lamp	Lactic acid	15.56	-	[231]
Ni_2P/MCdS-DETA	0.4 wt.%	300 W Xe lamp	Na_2S–Na_2SO_3	6.84	26.4	[359]
Ni_xB/CdS	0.8 wt.%	300 W Xe lamp	Lactic acid	4.8	21	[376]
RhP/CdS	20 wt.%	5 W LED	Lactic acid	0.33	34.3	[221]
P-MoS_2/CdS	20 wt.%	300 W Xe lamp	Na_2S–Na_2SO_3	5.89	19	[220]
Mn_{13}-cluster/CdS	7 wt.%	White-light LED	Lactic acid	3.6	-	[377]
$Ni_{2-x}Co_xP$/CdS	40 wt.%	300 W Xe lamp	Ethanol-water	218	76.3	[378]
CdS/Ti_3C_2	10%	300 W Xe lamp	Lactic acid	2.407	35.6	[238]
CdS/MoN_2	-	300 W Xe lamp	Lactic acid	9.2	-	[379]
MXene@CdS	-	300 W Xe lamp	Na_2S–Na_2SO_3	12.34	-	[349]
CdS/SnO_2	5%	150 W Xe lamp	Lactic acid	20.2	-	[242]
CdS/Mo_2C	3%	300 W Xe lamp	Na_2S–Na_2SO_3	1.843	-	[380]
CdS-FeP	5%	300 W Xe lamp	Lactic acid	18.63	11.2	[250]

Ti_3C_2@CoO (CTC-5-5) maintained good stability over 10 cycles, which was significantly better than that of CdS@Ti_3C_2 (CT-5) and CdS @CoO (CC-5) (Fig. 23b and c). These results indicate that its combination with a p-type semiconductor to form a p–n heterojunction can suppress the extent of photocorrosion [382].

Besides constructing a heterojunction to avoid the accumulation of h^+ in the VB of CdS, coating a chemically inert shell could also prevent the undesirable photocorrosion. Ning *et al.* [383] constructed a thin shell layer of Al_2O_3 on CdS NPs, which could remove the dissolved O_2 to inhibit photocorrosion (Fig. 24a). During the photocatalytic reaction, the photogenerated h^+ are trapped by the $A1^{3+}$ cationic vacancy network in amorphous

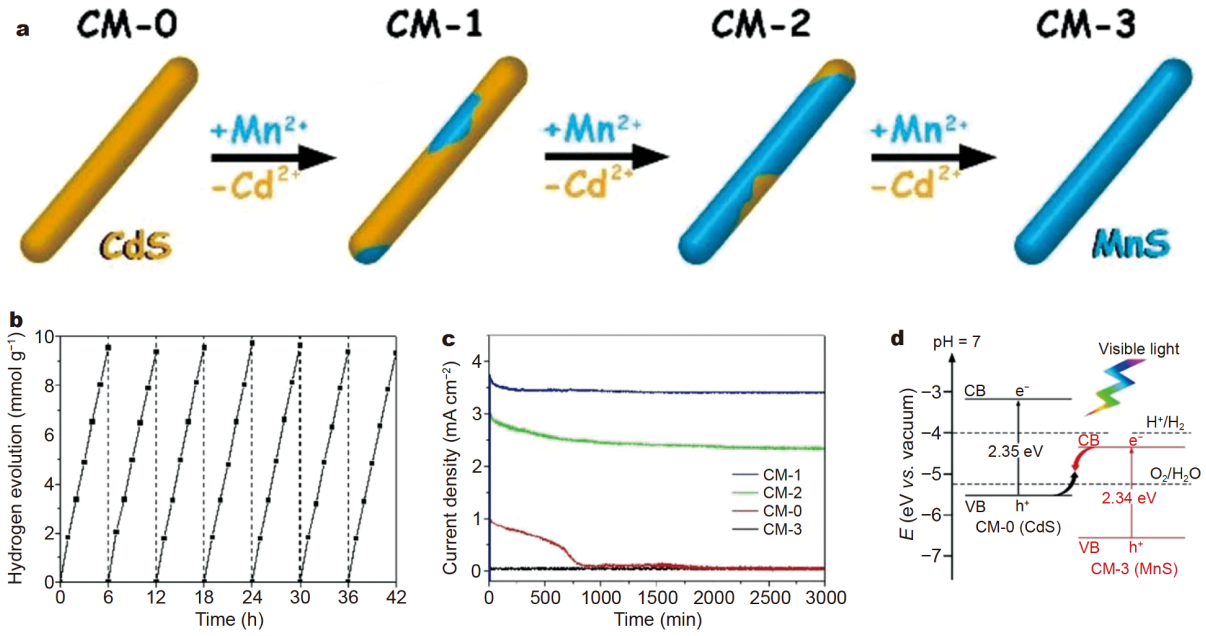

Figure 22 (a) Schematic of the synthesis process, (b) cyclic experiment of H_2 generation using CdS–MnS, (c) amperometric photocurrent density measurements (0.5 mol L^{-1} Na_2SO_4, 100 mW cm^{-2}, visible light), (d) Z-scheme electronic band structures between CdS and MnS heterojunction photocatalysts. Reprinted with permission from Ref. [381]. Copyright 2020, Wiley-VCH.

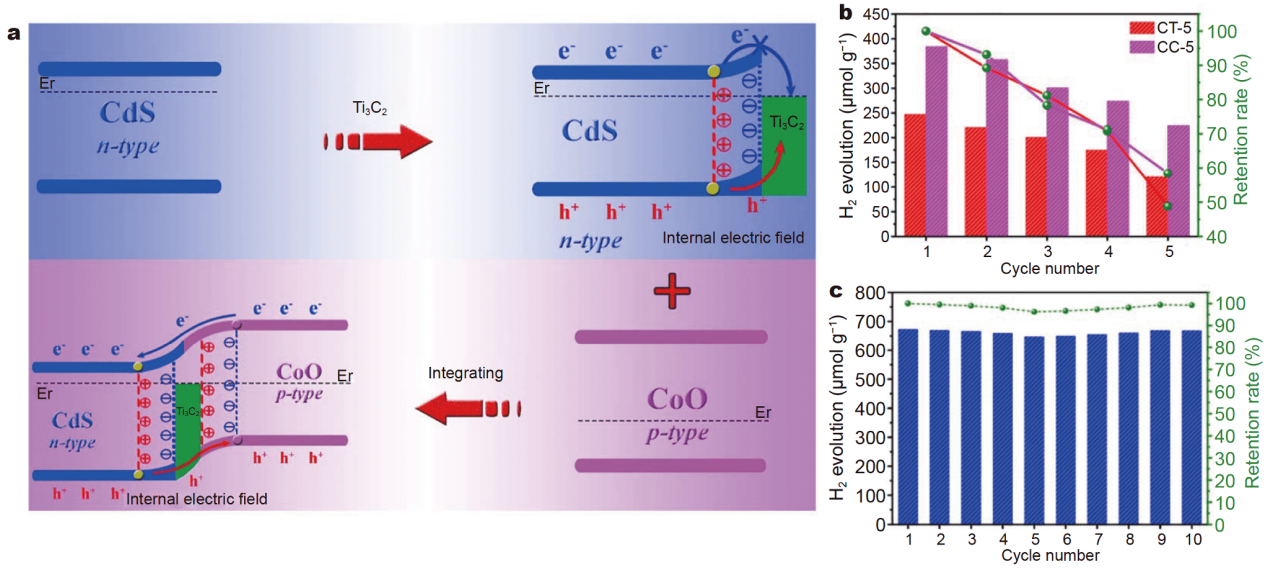

Figure 23 (a) Schematic of CdS@Ti_3C_2@CoO hierarchical tandem p–n heterojunction; recycling tests of photocatalytic H_2 evolution of (b) CT-5 and CC-5, (c) CTC-5-5. Reprinted with permission from Ref. [382]. Copyright 2020, Elsevier.

Al_2O_3. Compared with pure CdS, only trace amounts of Cd^{2+} were dissolved in the reaction solutions. Thus, CdS/Al_2O_3–Pt exhibited excellent stability during the photocatalytic HER (Fig. 24b and c). Moreover, CdS/Al_2O_3–Pt could induce overall water splitting by avoiding photocorrosion (Fig. 24d) [383].

CONCLUSIONS

In recent years, CdS-based nanostructured photocatalysts have been widely investigated. Significant progress has

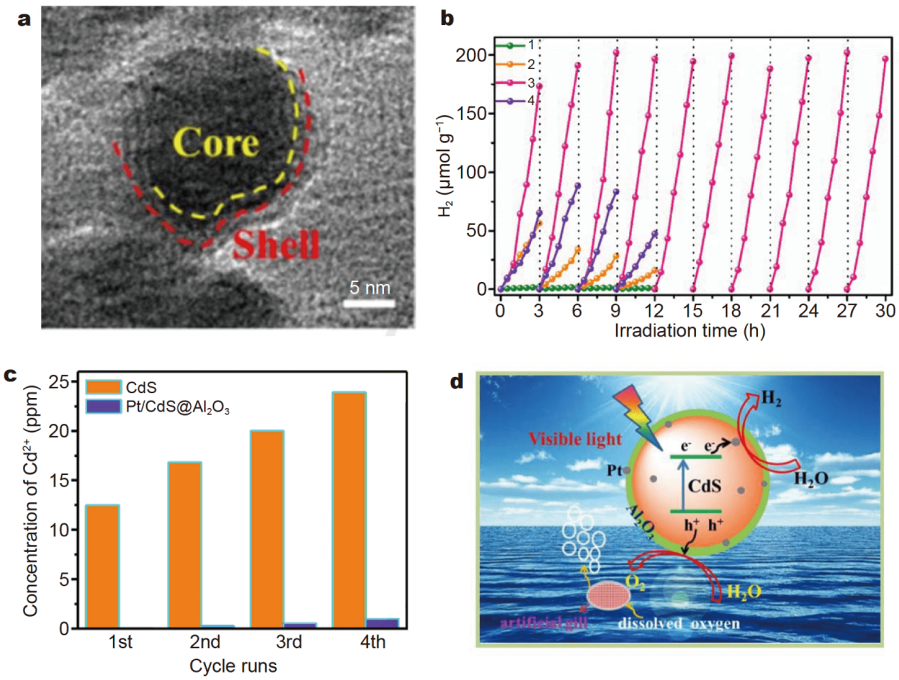

Figure 24 (a) TEM image of CdS@Al_2O_3, (b) cyclic runs of the photocatalytic H_2 evolution activity under visible light over various catalyst samples: (1) CdS NPs, (2) Pt/CdS, (3) Pt/CdS@Al_2O_3 with artificial gill and (4) Pt/CdS@Al_2O_3 without artificial gill, (c) the changes in cadmium ion concentration in the CdS NPs and Pt/CdS@Al_2O_3 composite solution with extended irradiation time, and (d) mechanism of overall water splitting over Pt/CdS@Al_2O_3 composite under visible illumination. Reprinted with permission from Ref. [383]. Copyright 2018, Elsevier.

been made in the field of solar–fuel conversion and environmental purification using CdS [15,213,364,384]. This review first systematically discusses the recent progress of CdS-based nanostructured photocatalysts with a detailed summary of the design strategies adopted to enhance H_2 generation efficiency. Although great advances have been made in recent years, many challenges remain, entailing the need for an in-depth understanding of the underlying mechanism for the observed H_2 evolution enhancement. Their intrinsic relations with modification routes should be unambiguously established [361,370,385,386].

Various strategies have been devised to increase photocatalytic H_2 generation using photocatalytic CdS-based nanomaterials: constructing multicomponent solid solutions, loading cocatalysts, constructing Z-scheme heterojunctions, designing 2D NSs, and reducing photocorrosion. These aspects are thoroughly highlighted and discussed. Notably, 2D nanomaterials possess many advantages, such as good chemical and physical stability, high interlayer adhesion, large surface area, high electron mobility, and rich surface-active sites, which facilitate photocatalytic H_2 evolution. In addition, bandgap tuning and heterojunction construction can be conveniently engineered by combining the strengths of different 2D nanomaterials in the form of 2D/2D layered nanocomposites [72,387]. Therefore, it is possible to obtain CdS photocatalysts with extended visible-light absorption and enhanced redox capacities, as well as better charge separation efficiencies. The durability and stability of photocatalysts remain an urgent problem that needs to be solved in the future.

A knowledge gap remains in the fundamental revelation of the actual active sites in CdS photocatalysts. Specifically, a far-reaching investigation into the detailed mechanisms of how CdS photocatalysts function through the advancement *in situ*/*operando* characterizations is highly sought. The e^- transfer mechanisms between the heterojunctions of CdS and other components are still debatable. Upon clarifying the transfer mechanism, targeted e^- transfer to the selected active sites can significantly improve the photocatalytic HER performance of CdS photocatalysts. In addition, shortening the migration distance is effective in increasing the consumption rate of the photogenerated e^--h^+ pairs. The construction of single-layer CdS nanosheets could minimize the charge migration distance from the bulk to the CdS surface. Therefore, developing methodologies to

synthesize ultrathin CdS is expected to continue to receive widespread attention.

A theoretical mechanistic study using computational methods is another important aspect to assist in the rational design of CdS photocatalysts with ideal electronic structures, species adsorption, and other properties. In addition, it could provide insights into the cocatalyst/semiconductor loading sites and interfacial interactions to guide the preparation of functional CdS. In summary, the exploration of new strategies to strengthen the overall performance of CdS-based nanocomposites, including their stability, can offer new opportunities toward the efficient utilization of solar energy for chemical fuel conversion.

Received 10 June 2020; accepted 6 July 2020; published online 10 October 2020

1 Xia Y, Yu J. Reaction: Rational design of highly active photocatalysts for CO_2 conversion. Chem, 2020, 6: 1039–1040
2 Fan X, Zhang L, Li M, *et al.* α-Ferrous oxalate dihydrate: a simple coordination polymer featuring photocatalytic and photo-initiated Fenton oxidations. Sci China Mater, 2016, 59: 574–580
3 Fan Y, Hu G, Yu S, *et al.* Recent advances in TiO_2 nanoarrays/graphene for water treatment and energy conversion/storage. Sci China Mater, 2019, 62: 325–340
4 Li X, Yu J, Jaroniec M, *et al.* Cocatalysts for selective photoreduction of CO_2 into solar fuels. Chem Rev, 2019, 119: 3962–4179
5 Li X, Xie J, Jiang C, *et al.* Review on design and evaluation of environmental photocatalysts. Front Environ Sci Eng, 2018, 12: 14
6 Tang Y, Zhou P, Chao Y, *et al.* Face-to-face engineering of ultrathin Pd nanosheets on amorphous carbon nitride for efficient photocatalytic hydrogen production. Sci China Mater, 2019, 62: 351–358
7 Zhang Y, Zhang Q, Xia T, *et al.* The influence of reaction temperature on the formation and photocatalytic hydrogen generation of (001) faceted TiO_2 nanosheets. ChemNanoMat, 2015, 1: 270–275
8 Ma Y, Wang X, Jia Y, *et al.* Titanium dioxide-based nanomaterials for photocatalytic fuel generations. Chem Rev, 2014, 114: 9987–10043
9 Chen X, Li C, Grätzel M, *et al.* Nanomaterials for renewable energy production and storage. Chem Soc Rev, 2012, 41: 7909–7937
10 Li X, Yu J, Low J, *et al.* Engineering heterogeneous semiconductors for solar water splitting. J Mater Chem A, 2015, 3: 2485–2534
11 Wen J, Xie J, Chen X, *et al.* A review on g-C_3N_4-based photocatalysts. Appl Surf Sci, 2017, 391: 72–123
12 Fu J, Yu J, Jiang C, *et al.* g-C_3N_4-based heterostructured photocatalysts. Adv Energy Mater, 2018, 8: 1701503
13 Liu L, Chen X. Titanium dioxide nanomaterials: Self-structural modifications. Chem Rev, 2014, 114: 9890–9918
14 Zhang Y, Zhao H, Zhao X, *et al.* Narrow-bandgap Nb_2O_5 nanowires with enclosed pores as high-performance photocatalyst. Sci China Mater, 2019, 62: 203–210
15 Zhao D, Sun B, Li X, *et al.* Promoting visible light-driven hydrogen evolution over CdS nanorods using earth-abundant CoP as a cocatalyst. RSC Adv, 2016, 6: 33120–33125
16 Cui X, Wang Y, Jiang G, *et al.* A photonic crystal-based CdS–Au–WO_3 heterostructure for efficient visible-light photocatalytic hydrogen and oxygen evolution. RSC Adv, 2014, 4: 15689–15694
17 Cheng L, Xiang Q, Liao Y, *et al.* CdS-based photocatalysts. Energy Environ Sci, 2018, 11: 1362–1391
18 Jiang D, Sun Z, Jia H, *et al.* A cocatalyst-free CdS nanorod/ZnS nanoparticle composite for high-performance visible-light-driven hydrogen production from water. J Mater Chem A, 2016, 4: 675–683
19 Chen X, Chen W, Lin P, *et al.* *In situ* photodeposition of nickel oxides on CdS for highly efficient hydrogen production *via* visible-light-driven photocatalysis. Catal Commun, 2013, 36: 104–108
20 Zhang GQ, Ou W, Xu YS. Fluorescein supramolecular nanosheets: A novel organic photocatalyst for visible-light-driven H_2 evolution from water. Sci China Mater, 2018, 61: 1001–1006
21 Yu Q, Lin R, Jiang L, *et al.* Fabrication and photocatalysis of ZnO nanotubes on transparent conductive graphene-based flexible substrates. Sci China Mater, 2018, 61: 1007–1011
22 Yang C, Chen JF, Zeng X, *et al.* Enhanced photochemical performance of hexagonal WO_3 by metal-assisted S–O coupling for solar-driven water splitting. Sci China Mater, 2018, 61: 91–100
23 Zhou M, Hou Z, Chen X. Graphitic-C_3N_4 nanosheets: synergistic effects of hydrogenation and n/n junctions for enhanced photocatalytic activities. Dalton Trans, 2017, 46: 10641–10649
24 Zhang X, Zhang P, Wang L, *et al.* Template-oriented synthesis of monodispersed SnS_2@SnO_2 hetero-nanoflowers for Cr(VI) photoreduction. Appl Catal B-Environ, 2016, 192: 17–25
25 Zhang P, Wang T, Chang X, *et al.* Effective charge carrier utilization in photocatalytic conversions. Acc Chem Res, 2016, 49: 911–921
26 Zhang P, Li X, Shao C, *et al.* Hydrothermal synthesis of carbon-rich graphitic carbon nitride nanosheets for photoredox catalysis. J Mater Chem A, 2015, 3: 3281–3284
27 Liu B, Ye L, Wang R, *et al.* Phosphorus-doped graphitic carbon nitride nanotubes with amino-rich surface for efficient CO_2 capture, enhanced photocatalytic activity, and product selectivity. ACS Appl Mater Interfaces, 2018, 10: 4001–4009
28 Ye S, Wang R, Wu MZ, *et al.* A review on g-C_3N_4 for photocatalytic water splitting and CO_2 reduction. Appl Surf Sci, 2015, 358: 15–27
29 Han C, Wu L, Ge L, *et al.* AuPd bimetallic nanoparticles decorated graphitic carbon nitride for highly efficient reduction of water to H_2 under visible light irradiation. Carbon, 2015, 92: 31–40
30 Saha M, Ghosh S, De SK. Nanoscale Kirkendall effect driven Au decorated CdS/CdO colloidal nanocomposites for efficient hydrogen evolution, photocatalytic dye degradation and Cr(VI) reduction. Catal Today, 2020, 340: 253–267
31 Wang R, Yan J, Zu M, *et al.* Facile synthesis of interlocking g-C_3N_4/CdS photoanode for stable photoelectrochemical hydrogen production. Electrochim Acta, 2018, 279: 74–83
32 Wang Q, Li J, Bai Y, *et al.* Photochemical preparation of Cd/CdS photocatalysts and their efficient photocatalytic hydrogen production under visible light irradiation. Green Chem, 2014, 16: 2728–2735
33 Zhu S, Liang S, Bi J, *et al.* Photocatalytic reduction of CO_2 with H_2O to CH_4 over ultrathin $SnNb_2O_6$ 2D nanosheets under visible light irradiation. Green Chem, 2016, 18: 1355–1363
34 Li X, Wen J, Low J, *et al.* Design and fabrication of semiconductor photocatalyst for photocatalytic reduction of CO_2 to solar fuel. Sci

China Mater, 2014, 57: 70–100
35 Muhammad NA, Wang Y, Muhammad FE, *et al.* Photoreduction of carbon dioxide using strontium zirconate nanoparticles. Sci China Mater, 2015, 58: 634–639
36 Wang H, Naghadeh SB, Li C, *et al.* Enhanced photoelectrochemical and photocatalytic activities of CdS nanowires by surface modification with MoS_2 nanosheets. Sci China Mater, 2018, 61: 839–850
37 Sun J, Xu J, Grafmueller A, *et al.* Self-assembled carbon nitride for photocatalytic hydrogen evolution and degradation of p-nitrophenol. Appl Catal B-Environ, 2017, 205: 1–10
38 Yang T, Peng J, Zheng Y, *et al.* Enhanced photocatalytic ozonation degradation of organic pollutants by ZnO modified TiO_2 nanocomposites. Appl Catal B-Environ, 2018, 221: 223–234
39 Zou L, Wang H, Wang X. High efficient photodegradation and photocatalytic hydrogen production of CdS/$BiVO_4$ heterostructure through *Z*-scheme process. ACS Sustain Chem Eng, 2017, 5: 303–309
40 Liu W, Liu Z, Wang G, *et al.* Carbon coated Au/TiO_2 mesoporous microspheres: a novel selective photocatalyst. Sci China Mater, 2017, 60: 438–448
41 Shenoy S, Jang E, Park TJ, *et al.* Cadmium sulfide nanostructures: Influence of morphology on the photocatalytic degradation of erioglaucine and hydrogen generation. Appl Surf Sci, 2019, 483: 696–705
42 Xiao F, Zhou W, Sun B, *et al.* Engineering oxygen vacancy on rutile TiO_2 for efficient electron-hole separation and high solar-driven photocatalytic hydrogen evolution. Sci China Mater, 2018, 61: 822–830
43 Wang X, Peng W, Li X. Photocatalytic hydrogen generation with simultaneous organic degradation by composite CdS–ZnS nanoparticles under visible light. Int J Hydrogen Energy, 2014, 39: 13454–13461
44 Cui H, Li B, Zhang Y, *et al.* Constructing Z-scheme based $CoWO_4$/CdS photocatalysts with enhanced dye degradation and H_2 generation performance. Int J Hydrogen Energy, 2018, 43: 18242–18252
45 Wen J, Xie J, Zhang H, *et al.* Constructing multifunctional metallic Ni interface layers in the g-C_3N_4 nanosheets/amorphous NiS heterojunctions for efficient photocatalytic H_2 generation. ACS Appl Mater Interfaces, 2017, 9: 14031–14042
46 Zhou P, Yu J, Jaroniec M. All-solid-state Z-Scheme photocatalytic systems. Adv Mater, 2014, 26: 4920–4935
47 Shen R, Xie J, Lu X, *et al.* Bifunctional Cu_3P decorated g-C_3N_4 nanosheets as a highly active and robust visible-light photocatalyst for H_2 production. ACS Sustain Chem Eng, 2018, 6: 4026–4036
48 Sun Z, Zhu M, Fujitsuka M, *et al.* Phase effect of Ni_xP_y hybridized with g-C_3N_4 for photocatalytic hydrogen generation. ACS Appl Mater Interfaces, 2017, 9: 30583–30590
49 Xiong T, Cen W, Zhang Y, *et al.* Bridging the g-C_3N_4 interlayers for enhanced photocatalysis. ACS Catal, 2016, 6: 2462–2472
50 Gu Q, Gao Z, Yu S, *et al.* Constructing Ru/TiO_2 heteronanostructures toward enhanced photocatalytic water splitting *via* a RuO_2/TiO_2 heterojunction and Ru/TiO_2 Schottky junction. Adv Mater Interfaces, 2016, 3: 1500631
51 Cui X, Shi J. Sn-based catalysts for Baeyer-Villiger oxidations by using hydrogen peroxide as oxidant. Sci China Mater, 2016, 59: 675–700
52 Shen R, Xie J, Zhang H, *et al.* Enhanced solar fuel H_2 generation over g-C_3N_4 nanosheet photocatalysts by the synergetic effect of noble metal-free Co_2P cocatalyst and the environmental phosphorylation strategy. ACS Sustain Chem Eng, 2018, 6: 816–826
53 Xiang Q, Cheng B, Yu J. Hierarchical porous CdS nanosheet-assembled flowers with enhanced visible-light photocatalytic H_2-production performance. Appl Catal B-Environ, 2013, 138: 299–303
54 Zheng D, Zhang G, Hou Y, *et al.* Layering MoS_2 on soft hollow g-C_3N_4 nanostructures for photocatalytic hydrogen evolution. Appl Catal A-General, 2016, 521: 2–8
55 Gu Q, Liao Y, Yin L, *et al.* Template-free synthesis of porous graphitic carbon nitride microspheres for enhanced photocatalytic hydrogen generation with high stability. Appl Catal B-Environ, 2015, 165: 503–510
56 Tian L, Yan X, Chen X. Electrochemical activity of iron phosphide nanoparticles in hydrogen evolution reaction. ACS Catal, 2016, 6: 5441–5448
57 Chen X, Chen W, Gao H, *et al. In situ* photodeposition of NiO_x on CdS for hydrogen production under visible light: Enhanced activity by controlling solution environment. Appl Catal B-Environ, 2014, 152: 68–72
58 He Z, Fu J, Cheng B, *et al.* $Cu_2(OH)_2CO_3$ clusters: Novel noble-metal-free cocatalysts for efficient photocatalytic hydrogen production from water splitting. Appl Catal B-Environ, 2017, 205: 104–111
59 Liu Y, Xiong J, Yang Y, *et al.* $HNb_xTa_{1-x}WO_6$ monolayer nanosheets solid solutions: Tunable energy band structures and highly enhanced photocatalytic performances for hydrogen evolution. Appl Catal B-Environ, 2017, 203: 798–806
60 He K, Xie J, Li M, *et al. In situ* one-pot fabrication of g-C_3N_4 nanosheets/NiS cocatalyst heterojunction with intimate interfaces for efficient visible light photocatalytic H_2 generation. Appl Surf Sci, 2018, 430: 208–217
61 Zhao Z, Xing Y, Li H, *et al.* Constructing CdS/Cd/doped TiO_2 Z-scheme type visible light photocatalyst for H_2 production. Sci China Mater, 2018, 61: 851–860
62 Akple MS, Low J, Wageh S, *et al.* Enhanced visible light photocatalytic H_2-production of g-C_3N_4/WS_2 composite heterostructures. Appl Surf Sci, 2015, 358: 196–203
63 Li N, Huang H, Bibi R, *et al.* Noble-metal-free MOF derived hollow CdS/TiO_2 decorated with NiS cocatalyst for efficient photocatalytic hydrogen evolution. Appl Surf Sci, 2019, 476: 378–386
64 He J, Chen L, Yi ZQ, *et al.* Fabrication of two-dimensional porous CdS nanoplates decorated with C_3N_4 nanosheets for highly efficient photocatalytic hydrogen production from water splitting. Catal Commun, 2017, 99: 79–82
65 Fujishima A, Honda K. Electrochemical photolysis of water at a semiconductor electrode. Nature, 1972, 238: 37–38
66 Ma S, Xie J, Wen J, *et al.* Constructing 2D layered hybrid CdS nanosheets/MoS_2 heterojunctions for enhanced visible-light photocatalytic H_2 generation. Appl Surf Sci, 2017, 391: 580–591
67 Yu J, Yu Y, Zhou P, *et al.* Morphology-dependent photocatalytic H_2-production activity of CdS. Appl Catal B-Environ, 2014, 156: 184–191
68 Chen X, Shen S, Guo L, *et al.* Semiconductor-based photocatalytic hydrogen generation. Chem Rev, 2010, 110: 6503–6570
69 Hu J, Wang L, Zhang P, *et al.* Construction of solid-state Z-scheme carbon-modified TiO_2/WO_3 nanofibers with enhanced photocatalytic hydrogen production. J Power Sources, 2016, 328:

28–36
70 Gao H, Zhang P, Hu J, *et al.* One-dimensional Z-scheme TiO_2/WO_3/Pt heterostructures for enhanced hydrogen generation. Appl Surf Sci, 2017, 391: 211–217
71 Liu Y, Zhang Y, Wang L, *et al.* Fast and large-scale anodizing synthesis of pine-cone TiO_2 for solar-driven photocatalysis. Catalysts, 2017, 7: 229
72 Lin B, Li H, An H, *et al.* Preparation of 2D/2D g-C_3N_4 nanosheet@$ZnIn_2S_4$ nanoleaf heterojunctions with well-designed high-speed charge transfer nanochannels towards high-efficiency photocatalytic hydrogen evolution. Appl Catal B-Environ, 2018, 220: 542–552
73 Zhou JJ, Wang R, Liu XL, *et al. In situ* growth of CdS nanoparticles on UiO-66 metal-organic framework octahedrons for enhanced photocatalytic hydrogen production under visible light irradiation. Appl Surf Sci, 2015, 346: 278–283
74 Li Q, Meng H, Yu J, *et al.* Enhanced photocatalytic hydrogen-production performance of graphene-$Zn_xCd_{1-x}S$ composites by using an organic S source. Chem Eur J, 2014, 20: 1176–1185
75 Gao H, Zhang P, Zhao J, *et al.* Plasmon enhancement on photocatalytic hydrogen production over the Z-scheme photosynthetic heterojunction system. Appl Catal B-Environ, 2017, 210: 297–305
76 Zhao J, Zhang P, Wang Z, *et al.* Direct evidence of multichannel-improved charge-carrier mechanism for enhanced photocatalytic H_2 evolution. Sci Rep, 2017, 7: 16116
77 He K, Xie J, Yang Z, *et al.* Earth-abundant WC nanoparticles as an active noble-metal-free co-catalyst for the highly boosted photocatalytic H_2 production over g-C_3N_4 nanosheets under visible light. Catal Sci Technol, 2017, 7: 1193–1202
78 Zhou X, Li X, Gao Q, *et al.* Metal-free carbon nanotube–SiC nanowire heterostructures with enhanced photocatalytic H_2 evolution under visible light irradiation. Catal Sci Technol, 2015, 5: 2798–2806
79 Yu J, Wang S, Cheng B, *et al.* Noble metal-free $Ni(OH)_2$–g-C_3N_4 composite photocatalyst with enhanced visible-light photocatalytic H_2-production activity. Catal Sci Technol, 2013, 3: 1782–1789
80 Hong Y, Zhang J, Huang F, *et al.* Enhanced visible light photocatalytic hydrogen production activity of CuS/ZnS nanoflower spheres. J Mater Chem A, 2015, 3: 13913–13919
81 Jin J, Yu J, Liu G, *et al.* Single crystal CdS nanowires with high visible-light photocatalytic H_2-production performance. J Mater Chem A, 2013, 1: 10927–10934
82 Shen S, Guo L, Chen X, *et al.* Effect of Ag_2S on solar-driven photocatalytic hydrogen evolution of nanostructured CdS. Int J Hydrogen Energy, 2010, 35: 7110–7115
83 Kudo A, Miseki Y. Heterogeneous photocatalyst materials for water splitting. Chem Soc Rev, 2009, 38: 253–278
84 Li X, Yu J, Jaroniec M. Hierarchical photocatalysts. Chem Soc Rev, 2016, 45: 2603–2636
85 Li X, Yu J, Wageh S, *et al.* Graphene in photocatalysis: A review. Small, 2016, 12: 6640–6696
86 Tanveer M, Wu Y, Qadeer MA, *et al.* Atypical BiOCl/Bi_2S_3 hetero-structures exhibiting remarkable photo-catalyst response. Sci China Mater, 2018, 61: 101–111
87 Shen R, Jiang C, Xiang Q, *et al.* Surface and interface engineering of hierarchical photocatalysts. Appl Surf Sci, 2019, 471: 43–87
88 Li Y, Jin Z, Zhang L, *et al.* Controllable design of Zn-Ni-P on g-C_3N_4 for efficient photocatalytic hydrogen production. Chin J Catal, 2019, 40: 390–402
89 Li Z, Ma Y, Hu X, *et al.* Enhanced photocatalytic H_2 production over dual-cocatalyst-modified g-C_3N_4 heterojunctions. Chin J Catal, 2019, 40: 434–445
90 Qi K, Lv W, Khan I, *et al.* Photocatalytic H_2 generation *via* CoP quantum-dot-modified g-C_3N_4 synthesized by electroless plating. Chin J Catal, 2020, 41: 114–121
91 Sun K, Shen J, Liu Q, *et al.* Synergistic effect of Co(II)-hole and Pt-electron cocatalysts for enhanced photocatalytic hydrogen evolution performance of P-doped g-C_3N_4. Chin J Catal, 2020, 41: 72–81
92 Xiao N, Li S, Liu S, *et al.* Novel PtPd alloy nanoparticle-decorated g-C_3N_4 nanosheets with enhanced photocatalytic activity for H_2 evolution under visible light irradiation. Chin J Catal, 2019, 40: 352–361
93 Wen J, Xie J, Shen R, *et al.* Markedly enhanced visible-light photocatalytic H_2 generation over g-C_3N_4 nanosheets decorated by robust nickel phosphide ($Ni_{12}P_5$) cocatalysts. Dalton Trans, 2017, 46: 1794–1802
94 Ma B, Zhao J, Ge Z, *et al.* 5 nm NiCoP nanoparticles coupled with g-C_3N_4 as high-performance photocatalyst for hydrogen evolution. Sci China Mater, 2020, 63: 258–266
95 Zhou X, Gao Q, Yang S, *et al.* Carbon nanotube@silicon carbide coaxial heterojunction nanotubes as metal-free photocatalysts for enhanced hydrogen evolution. Chin J Catal, 2020, 41: 62–71
96 Zhou X, Gao Q, Li X, *et al.* Ultra-thin SiC layer covered graphene nanosheets as advanced photocatalysts for hydrogen evolution. J Mater Chem A, 2015, 3: 10999–11005
97 Yuan YJ, Yu ZT, Li YH, *et al.* A MoS_2/6,13-pentacenequinone composite catalyst for visible-light-induced hydrogen evolution in water. Appl Catal B-Environ, 2016, 181: 16–23
98 Wang WN, Huang CX, Zhang CY, *et al.* Controlled synthesis of upconverting nanoparticles/$Zn_xCd_{1-x}S$ yolk-shell nanoparticles for efficient photocatalysis driven by NIR light. Appl Catal B-Environ, 2018, 224: 854–862
99 Chen M, Wu P, Zhu Y, *et al.* Enhanced photocatalytic H_2 production activity of CdZnS with stacking faults structure assisted by ethylenediamine and NiS. Int J Hydrogen Energy, 2018, 43: 10938–10949
100 Shi J, Islam IU, Chen W, *et al.* Two-dimensional ultrathin $Zn_xCd_{1-x}S$ nanosheet with exposed polar facet by using layered double hydroxide template for photocatalytic hydrogen generation. Int J Hydrogen Energy, 2018, 43: 19481–19491
101 Gao R, Cheng B, Fan J, *et al.* $Zn_xCd_{1-x}S$ quantum dot with enhanced photocatalytic H_2-production performance. Chin J Catal, 2021, 42: 15–24
102 Shen R, Ding Y, Li S, *et al.* Constructing low-cost Ni_3C/twin-crystal $Zn_{0.5}Cd_{0.5}S$ heterojunction/homojunction nanohybrids for efficient photocatalytic H_2 evolution. Chin J Catal, 2021, 42: 25–36
103 Xue W, Chang W, Hu X, *et al.* 2D mesoporous ultrathin $Cd_{0.5}Zn_{0.5}S$ nanosheet: Fabrication mechanism and application potential for photocatalytic H_2 evolution. Chin J Catal, 2021, 42: 152–163
104 Wang S, Guan BY, Wang X, *et al.* Formation of hierarchical Co_9S_8@$ZnIn_2S_4$heterostructured cages as an efficient photocatalyst for hydrogen evolution. J Am Chem Soc, 2018, 140: 15145–15148
105 Hou J, Yang C, Cheng H, *et al.* Ternary 3D architectures of CdS QDs/graphene/$ZnIn_2S_4$ heterostructures for efficient photocatalytic H_2 production. Phys Chem Chem Phys, 2013, 15: 15660–

15668
106 Zhang Z, Liu K, Feng Z, *et al.* Hierarchical sheet-on-sheet $ZnIn_2S_4$/g-C_3N_4 heterostructure with highly efficient photocatalytic H_2 production based on photoinduced interfacial charge transfer. Sci Rep, 2016, 6: 19221
107 Wang B, Ding Y, Deng Z, *et al.* Rational design of ternary NiS/CQDs/$ZnIn_2S_4$ nanocomposites as efficient noble-metal-free photocatalyst for hydrogen evolution under visible light. Chin J Catal, 2019, 40: 335–342
108 Zhang S, Duan S, Chen G, *et al.* MoS_2/$Zn_3In_2S_6$ composite photocatalysts for enhancement of visible light-driven hydrogen production from formic acid. Chin J Catal, 2021, 42: 193–204
109 Yu J, Lei SL, Chen TC, *et al.* A new CdS/Bi1−$InTaO_4$ heterostructured photocatalyst containing solid solutions for H_2 evolution from water splitting. Int J Hydrogen Energy, 2014, 39: 13105–13113
110 Estahbanati MRK, Feilizadeh M, Iliuta MC. Photocatalytic valorization of glycerol to hydrogen: Optimization of operating parameters by artificial neural network. Appl Catal B-Environ, 2017, 209: 483–492
111 Li L, Liu GN, Qi SP, *et al.* Highly efficient colloidal $Mn_xCd_{1-x}S$ nanorod solid solution for photocatalytic hydrogen generation. J Mater Chem A, 2018, 6: 23683–23689
112 Higashi M, Abe R, Takata T, *et al.* Photocatalytic overall water splitting under visible light using $ATaO_2N$ (A = Ca, Sr, Ba) and WO_3 in a IO_3^-/I^- shuttle redox mediated system. Chem Mater, 2009, 21: 1543–1549
113 Higashi M, Abe R, Ishikawa A, *et al.* Z-scheme overall water splitting on modified-TaON photocatalysts under visible light (λ<500 nm). Chem Lett, 2008, 37: 138–139
114 Chen G, Li F, Fan Y, *et al.* A novel noble metal-free ZnS–WS_2/CdS composite photocatalyst for H_2 evolution under visible light irradiation. Catal Commun, 2013, 40: 51–54
115 Jiang Z, Zhang X, Yang G, *et al.* Hydrogel as a miniature hydrogen production reactor to enhance photocatalytic hydrogen evolution activities of CdS and ZnS quantum dots derived from modified gel crystal growth method. Chem Eng J, 2019, 373: 814–820
116 Li K, Chen R, Li SL, *et al.* Self-assembly of a mesoporous ZnS/mediating interface/CdS heterostructure with enhanced visible-light hydrogen-production activity and excellent stability. Chem Sci, 2015, 6: 5263–5268
117 Xie YP, Yu ZB, Liu G, *et al.* CdS–mesoporous ZnS core–shell particles for efficient and stable photocatalytic hydrogen evolution under visible light. Energy Environ Sci, 2014, 7: 1895–1901
118 Li C, Du S, Wang H, *et al.* Enhanced visible-light-driven photocatalytic hydrogen generation using $NiCo_2S_4$/CdS nanocomposites. Chem Eng J, 2019, 378: 122089
119 Yuan M, Wang JL, Zhou WH, *et al.* Cu_2ZnSnS_4–CdS heterostructured nanocrystals for enhanced photocatalytic hydrogen production. Catal Sci Technol, 2017, 7: 3980–3984
120 Iervolino G, Vaiano V, Sannino D, *et al.* Enhanced photocatalytic hydrogen production from glucose aqueous matrices on Ru-doped $LaFeO_3$. Appl Catal B-Environ, 2017, 207: 182–194
121 Liu Y, Niu H, Gu W, *et al. In-situ* construction of hierarchical CdS/MoS_2 microboxes for enhanced visible-light photocatalytic H_2 production. Chem Eng J, 2018, 339: 117–124
122 Xu J, Cao X. Characterization and mechanism of MoS_2/CdS composite photocatalyst used for hydrogen production from water splitting under visible light. Chem Eng J, 2015, 260: 642–648
123 Zhao J, Zhang P, Fan J, *et al.* Constructing 2D layered MoS_2 nanosheets-modified Z-scheme TiO_2/WO_3 nanofibers ternary nanojunction with enhanced photocatalytic activity. Appl Surf Sci, 2018, 430: 466–474
124 Xu F, Zhang J, Zhu B, *et al.* $CuInS_2$ sensitized TiO_2 hybrid nanofibers for improved photocatalytic CO_2 reduction. Appl Catal B-Environ, 2018, 230: 194–202
125 Hu P, Ngaw CK, Tay YY, *et al.* A "uniform" heterogeneous photocatalyst: integrated p–n type $CuInS_2$/$NaInS_2$ nanosheets by partial ion exchange reaction for efficient H_2 evolution. Chem Commun, 2015, 51: 9381–9384
126 Liu B, Xue Y, Zhang J, *et al.* Study on photo-induced charge transfer in the heterointerfaces of $CuInS_2$/CdS co-sensitized mesoporous TiO_2 photoelectrode. Electrochim Acta, 2016, 192: 370–376
127 Luo J, Lin Z, Zhao Y, *et al.* The embedded $CuInS_2$ into hollow-concave carbon nitride for photocatalytic H_2O splitting into H_2 with S-scheme principle. Chin J Catal, 2020, 41: 122–130
128 Wang W, Jin C, Qi L. Hierarchical CdS nanorod@SnO_2 nanobowl arrays for efficient and stable photoelectrochemical hydrogen generation. Small, 2018, 14: 1801352
129 Cheng L, Zhang D, Liao Y, *et al.* One-step solid-phase synthesis of 2D ultrathin CdS nanosheets for enhanced visible-light photocatalytic hydrogen evolution. Sol RRL, 2019, 3: 1900062
130 Li X, Deng Y, Jiang Z, *et al.* Photocatalytic hydrogen production over CdS nanomaterials: An interdisciplinary experiment for introducing undergraduate students to photocatalysis and analytical chemistry. J Chem Educ, 2019, 96: 1224–1229
131 Meng R, Jiang J, Liang Q, *et al.* Design of graphene-like gallium nitride and WS_2/WSe_2 nanocomposites for photocatalyst applications. Sci China Mater, 2016, 59: 1027–1036
132 Mangiri R, Reddy DA, Subramanyam K, *et al.* Decorating MoS_2 and $CoSe_2$ nanostructures on 1D-CdS nanorods for boosting photocatalytic hydrogen evolution rate. J Mol Liquids, 2019, 289: 111164
133 Han HS, Han GS, Kim JS, *et al.* Indium–tin–oxide nanowire array based CdSe/CdS/TiO_2 one-dimensional heterojunction photoelectrode for enhanced solar hydrogen production. ACS Sustain Chem Eng, 2016, 4: 1161–1168
134 Vaneski A, Schneider J, Susha AS, *et al.* Aqueous synthesis of CdS and CdSe/CdS tetrapods for photocatalytic hydrogen generation. APL Mater, 2014, 2: 012104
135 Chang YS, Choi M, Baek M, *et al.* CdS/CdSe co-sensitized brookite H:TiO_2 nanostructures: Charge carrier dynamics and photoelectrochemical hydrogen generation. Appl Catal B-Environ, 2018, 225: 379–385
136 Chang Y, Yu K, Zhang C, *et al.* Ternary CdS/Au/3DOM-$SrTiO_3$ composites with synergistic enhancement for hydrogen production from visible-light photocatalytic water splitting. Appl Catal B-Environ, 2017, 215: 74–84
137 Chang Y, Xuan Y, Zhang C, *et al.* Z-Scheme Pt@CdS/3DOM-$SrTiO_3$ composite with enhanced photocatalytic hydrogen evolution from water splitting. Catal Today, 2019, 327: 315–322
138 Yin XL, Li LL, Li DC, *et al.* Room temperature synthesis of CdS/$SrTiO_3$ nanodots-on-nanocubes for efficient photocatalytic H_2 evolution from water. J Colloid Interface Sci, 2019, 536: 694–700
139 Yanagida T, Sakata Y, Imamura H. Photocatalytic decomposition of H_2O into H_2 and O_2 over Ga_2O_3 loaded with NiO. Chem Lett, 2004, 33: 726–727

140 She X, Wu J, Xu H, *et al.* High efficiency photocatalytic water splitting using 2D α-Fe_2O_3/g-C_3N_4 Z-scheme catalysts. Adv Energy Mater, 2017, 7: 1700025

141 Preethi V, Kanmani S. Photocatalytic hydrogen production using Fe_2O_3-based core shell nano particles with ZnS and CdS. Int J Hydrogen Energy, 2014, 39: 1613–1622

142 Mahadik MA, Subramanian A, Chung HS, *et al.* CdS/Zr:Fe_2O_3 nanorod arrays with Al_2O_3 passivation layer for photoelectrochemical solar hydrogen generation. ChemSusChem, 2017, 10: 2030–2039

143 Wang L, Wang W, Chen Y, *et al.* Heterogeneous p–n junction CdS/Cu_2O nanorod arrays: Synthesis and superior visible-light-driven photoelectrochemical performance for hydrogen evolution. ACS Appl Mater Interfaces, 2018, 10: 11652–11662

144 Cheng WY, Yu TH, Chao KJ, *et al.* Cu_2O-decorated CdS nanostructures for high efficiency visible light driven hydrogen production. Int J Hydrogen Energy, 2013, 38: 9665–9672

145 Sasikala R, Shirole AR, Bharadwaj SR. Enhanced photocatalytic hydrogen generation over ZrO_2–TiO_2–CdS hybrid structure. J Colloid Interface Sci, 2013, 409: 135–140

146 Shen J, Wang R, Liu Q, *et al.* Accelerating photocatalytic hydrogen evolution and pollutant degradation by coupling organic co-catalysts with TiO_2. Chin J Catal, 2019, 40: 380–389

147 Zhu Y, Zhang Z, Lu N, *et al.* Prolonging charge-separation states by doping lanthanide-ions into {001}/{101} facets-coexposed TiO_2 nanosheets for enhancing photocatalytic H_2 evolution. Chin J Catal, 2019, 40: 413–423

148 Wang P, Xu S, Chen F, *et al.* Ni nanoparticles as electron-transfer mediators and NiS as interfacial active sites for coordinative enhancement of H_2-evolution performance of TiO_2. Chin J Catal, 2019, 40: 343–351

149 Zhang W, Zhang H, Xu J, *et al.* 3D flower-like heterostructured TiO_2@$Ni(OH)_2$ microspheres for solar photocatalytic hydrogen production. Chin J Catal, 2019, 40: 320–325

150 Ma D, Shi JW, Zou Y, *et al.* Highly efficient photocatalyst based on a CdS quantum dots/ZnO nanosheets 0D/2D heterojunction for hydrogen evolution from water splitting. ACS Appl Mater Interfaces, 2017, 9: 25377–25386

151 Kuang PY, Su YZ, Xiao K, *et al.* Double-shelled CdS- and CdSe-cosensitized ZnO porous nanotube arrays for superior photoelectrocatalytic applications. ACS Appl Mater Interfaces, 2015, 7: 16387–16394

152 Zhao H, Dong Y, Jiang P, *et al.* Light-assisted preparation of a ZnO/CdS nanocomposite for enhanced photocatalytic H_2 evolution: An insight into importance of *in situ* generated ZnS. ACS Sustain Chem Eng, 2015, 3: 969–977

153 Xu L, Shi W, Guan J. Preparation of crystallized mesoporous CdS/Ta_2O_5 composite assisted by silica reinforcement for visible light photocatalytic hydrogen evolution. Catal Commun, 2012, 25: 54–58

154 Xu L, Guan J, Shi W. Enhanced interfacial charge transfer and visible photocatalytic activity for hydrogen evolution from a Ta_2O_5-based mesoporous composite by the incorporation of quantum-sized CdS. ChemCatChem, 2012, 4: 1353–1359

155 Liu Y, Ding S, Shi Y, *et al.* Construction of CdS/CoO_x core-shell nanorods for efficient photocatalytic H_2 evolution. Appl Catal B-Environ, 2018, 234: 109–116

156 Wu Q, Xiong S, Shen P, *et al.* Exceptional activity of sub-nm Pt clusters on CdS for photocatalytic hydrogen production: a combined experimental and first-principles study. Catal Sci Technol, 2015, 5: 2059–2064

157 Yu H, Huang Y, Gao D, *et al.* Improved H_2-generation performance of Pt/CdS photocatalyst by a dual-function TiO_2 mediator for effective electron transfer and hole blocking. Ceramics Int, 2019, 45: 9807–9813

158 Yu G, Geng L, Wu S, *et al.* Highly-efficient cocatalyst-free H_2-evolution over silica-supported CdS nanoparticle photocatalysts under visible light. Chem Commun, 2015, 51: 10676–10679

159 Zhang J, Zhu Z, Feng X. Construction of two-dimensional MoS_2/CdS p-n nanohybrids for highly efficient photocatalytic hydrogen evolution. Chem Eur J, 2014, 20: 10632–10635

160 Ma B, Xu H, Lin K, *et al.* Mo_2C as non-noble metal co-catalyst in Mo_2C/CdS composite for enhanced photocatalytic H_2 evolution under visible light irradiation. ChemSusChem, 2016, 9: 820–824

161 Wen J, Li X, Liu W, *et al.* Photocatalysis fundamentals and surface modification of TiO_2 nanomaterials. Chin J Catal, 2015, 36: 2049–2070

162 Unni SM, George L, Bhange SN, *et al.* Valorization of coffee bean waste: a coffee bean waste derived multifunctional catalyst for photocatalytic hydrogen production and electrocatalytic oxygen reduction reactions. RSC Adv, 2016, 6: 82103–82111

163 Yang C, Li M, Zhang WH, *et al.* Controlled growth, properties, and application of CdS branched nanorod arrays on transparent conducting oxide substrate. Sol Energy Mater Sol Cells, 2013, 115: 100–107

164 Li Q, Li X, Wageh S, *et al.* CdS/graphene nanocomposite photocatalysts. Adv Energy Mater, 2015, 5: 1500010

165 Zhang Y, Hao X, Ma X, *et al.* Special Z-scheme CdS@WO_3 hetero-junction modified with CoP for efficient hydrogen evolution. Int J Hydrogen Energy, 2019, 44: 13232–13241

166 Zong X, Yan H, Wu G, *et al.* Enhancement of photocatalytic H_2 evolution on CdS by loading MoS_2 as cocatalyst under visible light irradiation. J Am Chem Soc, 2008, 130: 7176–7177

167 Kalyanasundaram K, Borgarello E, Gráutzel M. Visible light induced water cleavage in CdS dispersions loaded with Pt and RuO_2, hole scavenging by RuO_2. HCA, 1981, 64: 362–366

168 Jang JS, Joshi UA, Lee JS. Solvothermal synthesis of CdS nanowires for photocatalytic hydrogen and electricity production. J Phys Chem C, 2007, 111: 13280–13287

169 Bao N, Shen L, Takata T, *et al.* Self-templated synthesis of nanoporous CdS nanostructures for highly efficient photocatalytic hydrogen production under visible light. Chem Mater, 2008, 20: 110–117

170 Xu Y, Zhao W, Xu R, *et al.* Synthesis of ultrathin CdS nanosheets as efficient visible-light-driven water splitting photocatalysts for hydrogen evolution. Chem Commun, 2013, 49: 9803–9805

171 Bie C, Fu J, Cheng B, *et al.* Ultrathin CdS nanosheets with tunable thickness and efficient photocatalytic hydrogen generation. Appl Surf Sci, 2018, 462: 606–614

172 Xie YM, Liu XH, Zhang R, *et al.* Ultrathin cadmium sulfide nanosheets for visible-light photocatalytic hydrogen production. J Mater Chem A, 2020, 8: 3586–3589

173 Yan H, Yang J, Ma G, *et al.* Visible-light-driven hydrogen production with extremely high quantum efficiency on Pt–PdS/CdS photocatalyst. J Catal, 2009, 266: 165–168

174 Zhang W, Wang Y, Wang Z, *et al.* Highly efficient and noble metal-free NiS/CdS photocatalysts for H_2 evolution from lactic acid sacrificial solution under visible light. Chem Commun, 2010, 46: 7631–7633

175 Ran J, Yu J, Jaroniec M. $Ni(OH)_2$ modified CdS nanorods for highly efficient visible-light-driven photocatalytic H_2 generation.

Green Chem, 2011, 13: 2708–2713
176 Ma S, Deng Y, Xie J, *et al.* Noble-metal-free Ni_3C cocatalysts decorated CdS nanosheets for high-efficiency visible-light-driven photocatalytic H_2 evolution. Appl Catal B-Environ, 2018, 227: 218–228
177 Wang X, Liu G, Chen ZG, *et al.* Enhanced photocatalytic hydrogen evolution by prolonging the lifetime of carriers in ZnO/CdS heterostructures. Chem Commun, 2009, 23: 3452
178 Zhang LJ, Li S, Liu BK, *et al.* Highly efficient CdS/WO_3 photocatalysts: Z-scheme photocatalytic mechanism for their enhanced photocatalytic H_2 evolution under visible light. ACS Catal, 2014, 4: 3724–3729
179 Shen R, Zhang L, Chen X, *et al.* Integrating 2D/2D CdS/α-Fe_2O_3 ultrathin bilayer Z-scheme heterojunction with metallic β-NiS nanosheet-based ohmic-junction for efficient photocatalytic H_2 evolution. Appl Catal B-Environ, 2020, 266: 118619
180 Li Q, Guo B, Yu J, *et al.* Highly efficient visible-light-driven photocatalytic hydrogen production of CdS-cluster-decorated graphene nanosheets. J Am Chem Soc, 2011, 133: 10878–10884
181 Yuan YJ, Chen D, Yu ZT, *et al.* Cadmium sulfide-based nanomaterials for photocatalytic hydrogen production. J Mater Chem A, 2018, 6: 11606–11630
182 Lian Z, Xu P, Wang W, *et al.* C_{60}-decorated CdS/TiO_2 mesoporous architectures with enhanced photostability and photocatalytic activity for H_2 evolution. ACS Appl Mater Interfaces, 2015, 7: 4533–4540
183 Zhang LJ, Zheng R, Li S, *et al.* Enhanced photocatalytic H_2 generation on cadmium sulfide nanorods with cobalt hydroxide as cocatalyst and insights into their photogenerated charge transfer properties. ACS Appl Mater Interfaces, 2014, 6: 13406–13412
184 Qian XB, Peng W, Huang JH. Fluorescein-sensitized Au/g-C_3N_4 nanocomposite for enhanced photocatalytic hydrogen evolution under visible light. Mater Res Bull, 2018, 102: 362–368
185 Song T, Zhang P, Zeng J, *et al.* Boosting the photocatalytic H_2 evolution activity of Fe_2O_3 polymorphs (α-, γ- and β-Fe_2O_3) by fullerene [C_{60}]-modification and dye-sensitization under visible light irradiation. RSC Adv, 2017, 7: 29184–29192
186 Shen R, Xie J, Ding Y, *et al.* Carbon nanotube-supported Cu_3P as high-efficiency and low-cost cocatalysts for exceptional semiconductor-free photocatalytic H_2 evolution. ACS Sustain Chem Eng, 2019, 7: 3243–3250
187 Wang L, Gao Z, Li Y, *et al.* Photosensitization of CdS by acid red-94 modified alginate: Dual ameliorative effect upon photocatalytic hydrogen evolution. Appl Surf Sci, 2019, 492: 598–606
188 Zhang X, Xiao J, Hou M, *et al.* Robust visible/near-infrared light driven hydrogen generation over Z-scheme conjugated polymer/CdS hybrid. Appl Catal B-Environ, 2018, 224: 871–876
189 Lei Y, Yang C, Hou J, *et al.* Strongly coupled CdS/graphene quantum dots nanohybrids for highly efficient photocatalytic hydrogen evolution: Unraveling the essential roles of graphene quantum dots. Appl Catal B-Environ, 2017, 216: 59–69
190 Ma L, Chen YL, Yang DJ, *et al.* Multi-interfacial plasmon coupling in multigap (Au/AgAu)@CdS core–shell hybrids for efficient photocatalytic hydrogen generation. Nanoscale, 2020, 12: 4383–4392
191 Chiu YH, Naghadeh SB, Lindley SA, *et al.* Yolk-shell nanostructures as an emerging photocatalyst paradigm for solar hydrogen generation. Nano Energy, 2019, 62: 289–298
192 Li S, Zhang L, Jiang T, *et al.* Construction of shallow surface states through light Ni doping for high-efficiency photocatalytic hydrogen production of CdS nanocrystals. Chem Eur J, 2014, 20: 311–316
193 Wang P, Pu Z, Li Y, *et al.* Iron-doped nickel phosphide nanosheet arrays: An efficient bifunctional electrocatalyst for water splitting. ACS Appl Mater Interfaces, 2017, 9: 26001–26007
194 Murphy JR, Delikanli S, Scrace T, *et al.* Time-resolved photoluminescence study of CdSe/CdMnS/CdS core/multi-shell nanoplatelets. Appl Phys Lett, 2016, 108: 242406
195 Li H, Wang Z, He Y, *et al.* Rational synthesis of $Mn_xCd_{1-x}S$ for enhanced photocatalytic H_2 evolution: Effects of S precursors and the feed ratio of Mn/Cd on its structure and performance. J Colloid Interface Sci, 2019, 535: 469–480
196 Xue C, Li H, An H, *et al.* NiS_x quantum dots accelerate electron transfer in $Cd_{0.8}Zn_{0.2}S$ photocatalytic system *via* an rGO nanosheet "bridge" toward visible-light-driven hydrogen evolution. ACS Catal, 2018, 8: 1532–1545
197 Wu Y, Yue Z, Liu A, *et al.* p-Type Cu-doped $Zn_{0.3}Cd_{0.7}S$/graphene photocathode for efficient water splitting in a photoelectrochemical tandem cell. ACS Sustain Chem Eng, 2016, 4: 2569–2577
198 Zhang J, Qi L, Ran J, *et al.* Ternary NiS/$Zn_xCd_{1-x}S$/reduced graphene oxide nanocomposites for enhanced solar photocatalytic H_2-production activity. Adv Energy Mater, 2014, 4: 1301925
199 Dai D, Xu H, Ge L, *et al. In-situ* synthesis of CoP co-catalyst decorated $Zn_{0.5}Cd_{0.5}S$ photocatalysts with enhanced photocatalytic hydrogen production activity under visible light irradiation. Appl Catal B-Environ, 2017, 217: 429–436
200 Ye L, Han C, Ma Z, *et al.* Ni_2P loading on $Cd_{0.5}Zn_{0.5}S$ solid solution for exceptional photocatalytic nitrogen fixation under visible light. Chem Eng J, 2017, 307: 311–318
201 Zhang J, Xu Q, Qiao SZ, *et al.* Enhanced visible-light hydrogen-production activity of copper-modified $Zn_xCd_{1-x}S$. ChemSusChem, 2013, 6: 2009–2015
202 Moradlou O, Tedadi N, Banazadeh A, *et al.* Effect of RGO/$Zn_xCd_{1-x}S$ crystalline phase on solar photoactivation processes. RSC Adv, 2016, 6: 46282–46290
203 Li Y, Ruan Q, Lin H, *et al.* Unique $Cd_{1-x}Zn_xS$@WO_{3-x} and Cd_{1-x}-Zn_xS@WO_{3-x}/CoO_x/NiO_x Z-scheme photocatalysts for efficient visible-light-induced H_2 evolution. Sci China Mater, 2020, 63: 75–90
204 Mei F, Li Z, Dai K, *et al.* Step-scheme porous g-C_3N_4/$Zn_{0.2}Cd_{0.8}S$-DETA composites for efficient and stable photocatalytic H_2 production. Chin J Catal, 2020, 41: 41–49
205 Wang P, Geng Z, Gao J, *et al.* $Zn_xCd_{1-x}S$/bacterial cellulose bionanocomposite foams with hierarchical architecture and enhanced visible-light photocatalytic hydrogen production activity. J Mater Chem A, 2015, 3: 1709–1716
206 Lingampalli SR, Gautam UK, Rao CNR. Highly efficient photocatalytic hydrogen generation by solution-processed ZnO/Pt/CdS, ZnO/Pt/$Cd_{1-x}Zn_xS$ and ZnO/Pt/$CdS_{1-x}Se_x$ hybrid nanostructures. Energy Environ Sci, 2013, 6: 3589–3594
207 Han Z, Chen G, Li C, *et al.* Preparation of 1D cubic $Cd_{0.8}Zn_{0.2}S$ solid-solution nanowires using levelling effect of TGA and improved photocatalytic H_2-production activity. J Mater Chem A, 2015, 3: 1696–1702
208 Zhang X, Jing D, Liu M, *et al.* Efficient photocatalytic H_2 production under visible light irradiation over Ni doped $Cd_{1-x}Zn_xS$ microsphere photocatalysts. Catal Commun, 2008, 9: 1720–1724
209 Jiang Z, Qian K, Zhu C, *et al.* Carbon nitride coupled with CdS-TiO_2 nanodots as 2D/0D ternary composite with enhanced photocatalytic H_2 evolution: A novel efficient three-level electron

transfer process. Appl Catal B-Environ, 2017, 210: 194–204
210 Lv JX, Zhang ZM, Wang J, *et al.* *In situ* synthesis of CdS/graphdiyne heterojunction for enhanced photocatalytic activity of hydrogen production. ACS Appl Mater Interfaces, 2019, 11: 2655–2661
211 Shi W, Guo F, Li M, *et al.* N-doped carbon dots/CdS hybrid photocatalyst that responds to visible/near-infrared light irradiation for enhanced photocatalytic hydrogen production. Separation Purification Tech, 2019, 212: 142–149
212 Cheng F, Yin H, Xiang Q. Low-temperature solid-state preparation of ternary CdS/g-C_3N_4/CuS nanocomposites for enhanced visible-light photocatalytic H_2-production activity. Appl Surf Sci, 2017, 391: 432–439
213 Jiang L, Wang L, Xu G, *et al.* A microwave-assisted thermolysis route to single-step preparation of MoS_2/CdS composite photocatalysts for active hydrogen generation. Sustain Energy Fuels, 2018, 2: 430–435
214 Kang H, Kim JH. Utilization of a $ZnS(en)_{0.5}$ photocatalyst hybridized with a CdS component for solar energy conversion to hydrogen. Adv Powder Tech, 2017, 28: 2438–2444
215 Tian L, Min S, Wang F. Integrating noble-metal-free metallic vanadium carbide cocatalyst with CdS for efficient visible-light-driven photocatalytic H_2 evolution. Appl Catal B-Environ, 2019, 259: 118029
216 Zhao J, Li W, Liu H, *et al.* Yolk-shell CdS@void@TiO_2 composite particles with photocorrosion resistance for enhanced dye removal and hydrogen evolution. Adv Powder Tech, 2019, 30: 1965–1975
217 Hu Y, Hao X, Cui Z, *et al.* Enhanced photocarrier separation in conjugated polymer engineered CdS for direct Z-scheme photocatalytic hydrogen evolution. Appl Catal B-Environ, 2020, 260: 118131
218 Yue X, Yi S, Wang R, *et al.* Cadmium sulfide and nickel synergetic co-catalysts supported on graphitic carbon nitride for visible-light-driven photocatalytic hydrogen evolution. Sci Rep, 2016, 6: 22268
219 Jia X, Tahir M, Pan L, *et al.* Direct Z-scheme composite of CdS and oxygen-defected $CdWO_4$: An efficient visible-light-driven photocatalyst for hydrogen evolution. Appl Catal B-Environ, 2016, 198: 154–161
220 Xu J, Yan X, Qi Y, *et al.* Novel phosphidated MoS_2 nanosheets modified CdS semiconductor for an efficient photocatalytic H_2 evolution. Chem Eng J, 2019, 375: 122053
221 Song L, Li T, Zhang S, *et al.* Synthesis of rhodium phosphide cocatalyst and remarkably enhanced photocatalytic hydrogen evolution over CdS under visible light radiation. Chem Eng J, 2017, 314: 498–507
222 Li F, Hou Y, Yu Z, *et al.* Oxygen deficiency introduced to *Z*-scheme CdS/WO_{3-x} nanomaterials with MoS_2 as the cocatalyst towards enhancing visible-light-driven hydrogen evolution. Nanoscale, 2019, 11: 10884–10895
223 Nekouei F, Nekouei S, Pouzesh M, *et al.* Porous-CdS/Cu_2O/graphitic-C_3N_4 dual p-n junctions as highly efficient photo/catalysts for degrading ciprofloxacin and generating hydrogen using solar energy. Chem Eng J, 2020, 385: 123710
224 Ai Z, Zhang K, Shi D, *et al.* Band-matching transformation between CdS and BCNNTs with tunable p-n homojunction for enhanced photocatalytic pure water splitting. Nano Energy, 2020, 69: 104408
225 Lin Y, Zhang Q, Li Y, *et al.* The evolution from a typical type-I CdS/ZnS to type-II and Z-scheme hybrid structure for efficient and stable hydrogen production under visible light. ACS Sustain Chem Eng, 2020, 8: 4537–4546
226 Qin Y, Li H, Lu J, *et al.* Nitrogen-doped hydrogenated TiO_2 modified with CdS nanorods with enhanced optical absorption, charge separation and photocatalytic hydrogen evolution. Chem Eng J, 2020, 384: 123275
227 Jiang C, Zhang L, Gao F, *et al.* Promoting photocatalytic hydrogen production by a core–shell CdS@MoO_x photocatalyst connected by an S–Mo "bridge". Catal Sci Technol, 2020, 10: 1368–1375
228 Zhang J, Wang Y, Jin J, *et al.* Efficient visible-light photocatalytic hydrogen evolution and enhanced photostability of core/shell CdS/g-C_3N_4 nanowires. ACS Appl Mater Interfaces, 2013, 5: 10317–10324
229 Li C, Wang H, Naghadeh SB, *et al.* Visible light driven hydrogen evolution by photocatalytic reforming of lignin and lactic acid using one-dimensional NiS/CdS nanostructures. Appl Catal B-Environ, 2018, 227: 229–239
230 Zhang L, Fu X, Meng S, *et al.* Ultra-low content of Pt modified CdS nanorods: one-pot synthesis and high photocatalytic activity for H_2 production under visible light. J Mater Chem A, 2015, 3: 23732–23742
231 Hong S, Kumar DP, Reddy DA, *et al.* Excellent photocatalytic hydrogen production over CdS nanorods *via* using noble metal-free copper molybdenum sulfide (Cu_2MoS_4) nanosheets as co-catalysts. Appl Surf Sci, 2017, 396: 421–429
232 Liu S, Guo Z, Qian X, *et al.* Sonochemical deposition of ultrafine metallic Pt nanoparticles on CdS for efficient photocatalytic hydrogen evolution. Sustain Energy Fuels, 2019, 3: 1048–1054
233 Fang X, Cui L, Pu T, *et al.* Core-shell CdS@MnS nanorods as highly efficient photocatalysts for visible light driven hydrogen evolution. Appl Surf Sci, 2018, 457: 863–869
234 Zhang J, Qiao SZ, Qi L, *et al.* Fabrication of NiS modified CdS nanorod p–n junction photocatalysts with enhanced visible-light photocatalytic H_2-production activity. Phys Chem Chem Phys, 2013, 15: 12088–12094
235 Chen H, Sun Z, Ye S, *et al.* Molecular cobalt–salen complexes as novel cocatalysts for highly efficient photocatalytic hydrogen production over a CdS nanorod photosensitizer under visible light. J Mater Chem A, 2015, 3: 15729–15737
236 Zhu C, Liu C, Fu Y, *et al.* Construction of CDs/CdS photocatalysts for stable and efficient hydrogen production in water and seawater. Appl Catal B-Environ, 2019, 242: 178–185
237 Li Q, Shi T, Li X, *et al.* Remarkable positive effect of $Cd(OH)_2$ on CdS semiconductor for visible-light photocatalytic H_2 production. Appl Catal B-Environ, 2018, 229: 8–14
238 Xiao R, Zhao C, Zou Z, *et al.* *In situ* fabrication of 1D CdS nanorod/2D Ti_3C_2 MXene nanosheet Schottky heterojunction toward enhanced photocatalytic hydrogen evolution. Appl Catal B-Environ, 2020, 268: 118382
239 Zhou X, Fang Y, Cai X, *et al.* *In situ* photodeposited construction of Pt–CdS/g-C_3N_4–MnO_x composite photocatalyst for efficient visible-light-driven overall water splitting. ACS Appl Mater Interfaces, 2020, 12: 20579–20588
240 Xiang Q, Cheng F, Lang D. Hierarchical layered WS_2/graphene-modified CdS nanorods for efficient photocatalytic hydrogen evolution. ChemSusChem, 2016, 9: 996–1002
241 Chen Z, Gong H, Liu Q, *et al.* $NiSe_2$ nanoparticles grown *in situ* on CdS nanorods for enhanced photocatalytic hydrogen evolution. ACS Sustain Chem Eng, 2019, 7: 16720–16728
242 Rangappa AP, Kumar DP, Gopannagari M, *et al.* Highly efficient

hydrogen generation in water using 1D CdS nanorods integrated with 2D SnS_2 nanosheets under solar light irradiation. Appl Surf Sci, 2020, 508: 144803
243 Li K, Han M, Chen R, *et al.* Hexagonal@cubic CdS core@shell nanorod photocatalyst for highly active production of H_2 with unprecedented stability. Adv Mater, 2016, 28: 8906–8911
244 Chava RK, Son N, Kim YS, *et al.* Controlled growth and band-structure properties of one dimensional cadmium sulfide nanorods for visible photocatalytic hydrogen evolution reaction. Nanomaterials, 2020, 10: 619
245 Li Z, Zhang L, Liu Y, *et al.* Surface-polarity-induced spatial charge separation boosts photocatalytic overall water splitting on GaN nanorod arrays. Angew Chem Int Ed, 2020, 59: 935–942
246 Ren D, Shen R, Jiang Z, *et al.* Highly efficient visible-light photocatalytic H_2 evolution over 2D–2D CdS/Cu_7S_4 layered heterojunctions. Chin J Catal, 2020, 41: 31–40
247 Dai K, Hu T, Zhang J, *et al.* Carbon nanotube exfoliated porous reduced graphene oxide/CdS-diethylenetriamine heterojunction for efficient photocatalytic H_2 production. Appl Surf Sci, 2020, 512: 144783
248 Abbood HA, Alabadi A, Al-Hawash AB, *et al.* Square CdS micro/nanosheets as efficient photo/piezo-bi-catalyst for hydrogen production. Catal Lett, 2020, 150: 3059–3070
249 Pan Z, Li J, Zhou K. Wrinkle-free atomically thin CdS nanosheets for photocatalytic hydrogen evolution. Nanotechnology, 2018, 29: 215402
250 Sun K, Shen J, Yang Y, *et al.* Highly efficient photocatalytic hydrogen evolution from 0D/2D heterojunction of FeP nanoparticles/CdS nanosheets. Appl Surf Sci, 2020, 505: 144042
251 Lv J, Zhang J, Liu J, *et al.* Bi SPR-promoted Z-scheme Bi_2MoO_6/CdS-diethylenetriamine composite with effectively enhanced visible light photocatalytic hydrogen evolution activity and stability. ACS Sustain Chem Eng, 2018, 6: 696–706
252 Wu A, Tian C, Jiao Y, *et al.* Sequential two-step hydrothermal growth of MoS_2/CdS core-shell heterojunctions for efficient visible light-driven photocatalytic H_2 evolution. Appl Catal B-Environ, 2017, 203: 955–963
253 Yu H, Zhong W, Huang X, *et al.* Suspensible cubic-phase CdS nanocrystal photocatalyst: facile synthesis and highly efficient H_2-evolution performance in a sulfur-rich system. ACS Sustain Chem Eng, 2018, 6: 5513–5523
254 Chen J, Wu XJ, Yin L, *et al.* One-pot synthesis of CdS nanocrystals hybridized with single-layer transition-metal dichalcogenide nanosheets for efficient photocatalytic hydrogen evolution. Angew Chem Int Ed, 2015, 54: 1210–1214
255 Chai B, Xu M, Yan J, *et al.* Remarkably enhanced photocatalytic hydrogen evolution over MoS_2 nanosheets loaded on uniform CdS nanospheres. Appl Surf Sci, 2018, 430: 523–530
256 Yin XL, Li LL, Han SR, *et al.* Green and *in-situ* synthesis of noble-metal-free Ni_2P/CdS nanoheterostructure for enhanced photocatalytic H_2 generation activity. J Taiwan Institute Chem Engineers, 2019, 103: 110–117
257 Wei RB, Huang ZL, Gu GH, *et al.* Dual-cocatalysts decorated rimous CdS spheres advancing highly-efficient visible-light photocatalytic hydrogen production. Appl Catal B-Environ, 2018, 231: 101–107
258 Zubair M, Svenum IH, Rønning M, *et al.* Facile synthesis approach for core-shell TiO_2–CdS nanoparticles for enhanced photocatalytic H_2 generation from water. Catal Today, 2019, 328: 15–20
259 Yao X, Liu T, Liu X, *et al.* Loading of CdS nanoparticles on the (101) surface of elongated TiO_2 nanocrystals for efficient visible-light photocatalytic hydrogen evolution from water splitting. Chem Eng J, 2014, 255: 28–39
260 Zhou FQ, Fan JC, Xu QJ, *et al.* $BiVO_4$ nanowires decorated with CdS nanoparticles as Z-scheme photocatalyst with enhanced H_2 generation. Appl Catal B-Environ, 2017, 201: 77–83
261 Du J, Wang H, Yang M, *et al.* Pyramid-like CdS nanoparticles grown on porous TiO_2 monolith: An advanced photocatalyst for H_2 production. Electrochim Acta, 2017, 250: 99–107
262 Zhao L, Jia J, Yang Z, *et al.* One-step synthesis of CdS nanoparticles/MoS_2 nanosheets heterostructure on porous molybdenum sheet for enhanced photocatalytic H_2 evolution. Appl Catal B-Environ, 2017, 210: 290–296
263 Lei Y, Hou J, Wang F, *et al.* Boosting the catalytic performance of MoS_x cocatalysts over CdS nanoparticles for photocatalytic H_2 evolution by Co doping *via* a facile photochemical route. Appl Surf Sci, 2017, 420: 456–464
264 Girginer B, Galli G, Chiellini E, *et al.* Preparation of stable CdS nanoparticles in aqueous medium and their hydrogen generation efficiencies in photolysis of water. Int J Hydrogen Energy, 2009, 34: 1176–1184
265 Wang D, Li X, Zheng LL, *et al.* Size-controlled synthesis of CdS nanoparticles confined on covalent triazine-based frameworks for durable photocatalytic hydrogen evolution under visible light. Nanoscale, 2018, 10: 19509–19516
266 Weng B, Liu S, Zhang N, *et al.* A simple yet efficient visible-light-driven CdS nanowires-carbon nanotube 1D–1D nanocomposite photocatalyst. J Catal, 2014, 309: 146–155
267 Wu K, Zhu H, Lian T. Ultrafast exciton dynamics and light-driven H_2 evolution in colloidal semiconductor nanorods and Pt-tipped nanorods. Acc Chem Res, 2015, 48: 851–859
268 Appell D. Wired for success. Nature, 2002, 419: 553–555
269 Bierman MJ, Jin S. Potential applications of hierarchical branching nanowires in solar energy conversion. Energy Environ Sci, 2009, 2: 1050–1059
270 Shieh F, Saunders AE, Korgel BA. General shape control of colloidal CdS, CdSe, CdTe quantum rods and quantum rod heterostructures. J Phys Chem B, 2005, 109: 8538–8542
271 Fatahi P, Roy A, Bahrami M, *et al.* Visible-light-driven efficient hydrogen production from CdS nanorods anchored with co-catalysts based on transition metal alloy nanosheets of NiPd, NiZn, and NiPdZn. ACS Appl Energy Mater, 2018, 1: 5318–5327
272 Han B, Liu S, Zhang N, *et al.* One-dimensional CdS@MoS_2 core-shell nanowires for boosted photocatalytic hydrogen evolution under visible light. Appl Catal B-Environ, 2017, 202: 298–304
273 Li Q, Qiao XQ, Jia Y, *et al.* Noble-metal-free amorphous $CoMoS_x$ modified CdS core-shell nanowires for dramatically enhanced photocatalytic hydrogen evolution under visible light irradiation. Appl Surf Sci, 2019, 498: 143863
274 Shabaev A, Efros AL. 1D exciton spectroscopy of semiconductor nanorods. Nano Lett, 2004, 4: 1821–1825
275 Sitt A, Salant A, Menagen G, *et al.* Highly emissive nano rod-in-rod heterostructures with strong linear polarization. Nano Lett, 2011, 11: 2054–2060
276 Peng CY, Manning L, Albertson R, *et al.* The tumour-suppressor genes lgl and dlg regulate basal protein targeting in Drosophila neuroblasts. Nature, 2000, 408: 596–600
277 Tongying P, Vietmeyer F, Aleksiuk D, *et al.* Double heterojunction nanowire photocatalysts for hydrogen generation. Nanoscale, 2014, 6: 4117–4124

278 Wu K, Rodríguez-Córdoba W, Lian T. Exciton localization and dissociation dynamics in CdS and CdS–Pt quantum confined nanorods: Effect of nonuniform rod diameters. J Phys Chem B, 2014, 118: 14062–14069
279 Park J, Lee E, Hwang NM, *et al.* One-nanometer-scale size-controlled synthesis of monodisperse magnetic iron oxide nanoparticles. Angew Chem Int Ed, 2005, 44: 2872–2877
280 Pileni MP. Self-assemblies of nanocrystals: fabrication and collective properties. Appl Surf Sci, 2001, 171: 1–14
281 Wang X, Zhuang J, Peng Q, *et al.* A general strategy for nanocrystal synthesis. Nature, 2005, 437: 121–124
282 Gai Q, Zheng X, Liu W, *et al.* 2D-2D heterostructured CdS–CoP photocatalysts for efficient H_2 evolution under visible light irradiation. Int J Hydrogen Energy, 2019, 44: 27412–27420
283 Liu C, Xiong M, Chai B, *et al.* Construction of 2D/2D Ni_2P/CdS heterojunctions with significantly enhanced photocatalytic H_2 evolution performance. Catal Sci Technol, 2019, 9: 6929–6937
284 Li C, Han L, Liu R, *et al.* Controlled synthesis of CdS micro/nano leaves with (0001) facets exposed: enhanced photocatalytic activity toward hydrogen evolution. J Mater Chem, 2012, 22: 23815–23820
285 Low J, Cao S, Yu J, *et al.* Two-dimensional layered composite photocatalysts. Chem Commun, 2014, 50: 10768–10777
286 Ren D, Liang ZZ, Ng YH, *et al.* Strongly coupled 2D-2D nanojunctions between P-doped Ni_2S (Ni_2SP) cocatalysts and CdS nanosheets for efficient photocatalytic H_2 evolution. Chem Eng J, 2020, 390: 124496
287 Cui X, Jiang G, Zhu M, *et al.* TiO_2/CdS composite hollow spheres with controlled synthesis of platinum on the internal wall for the efficient hydrogen evolution. Int J Hydrogen Energy, 2013, 38: 9065–9073
288 Xu M, Wei Z, Liu J, *et al.* One-pot synthesized visible-light-responsive MoS_2@CdS nanosheets-on-nanospheres for hydrogen evolution from the antibiotic wastewater: Waste to energy insight. Int J Hydrogen Energy, 2019, 44: 21577–21587
289 Yuan W, Zhang Z, Cui X, *et al.* Fabrication of hollow mesoporous CdS@TiO_2@Au microspheres with high photocatalytic activity for hydrogen evolution from water under visible light. ACS Sustain Chem Eng, 2018, 6: 13766–13777
290 Zheng XL, Song JP, Ling T, *et al.* Strongly coupled nafion molecules and ordered porous CdS networks for enhanced visible-light photoelectrochemical hydrogen evolution. Adv Mater, 2016, 28: 4935–4942
291 Bie C, Zhu B, Xu F, *et al. In situ* grown monolayer N-doped graphene on CdS hollow spheres with seamless contact for photocatalytic CO_2 reduction. Adv Mater, 2019, 31: 1902868
292 Wu K, Wu P, Zhu J, *et al.* Synthesis of hollow core-shell CdS@TiO_2/Ni_2P photocatalyst for enhancing hydrogen evolution and degradation of MB. Chem Eng J, 2019, 360: 221–230
293 Chen Z, Xu YJ. Ultrathin TiO_2 layer coated-CdS spheres core–shell nanocomposite with enhanced visible-light photoactivity. ACS Appl Mater Interfaces, 2013, 5: 13353–13363
294 Yoo I, Kalanur SS, Seo H. A nanoscale p–n junction photoelectrode consisting of an NiO_x layer on a TiO_2/CdS nanorod core-shell structure for highly efficient solar water splitting. Appl Catal B-Environ, 2019, 250: 200–212
295 Wang M, Cui Z, Yang M, *et al.* Core/shell structured CdS/polydopamine/TiO_2 ternary hybrids as highly active visible-light photocatalysis. J Colloid Interface Sci, 2019, 544: 1–7
296 Wu H, Meng S, Zhang J, *et al.* Construction of two-dimensionally relative p-n heterojunction for efficient photocatalytic redox reactions under visible light. Appl Surf Sci, 2020, 505: 144638
297 Wang Y, Zhang X, Liu Y, *et al.* Crystallinity and phase controlling of g-C_3N_4/CdS hetrostructures towards high efficient photocatalytic H_2 generation. Int J Hydrogen Energy, 2019, 44: 30151–30159
298 Liu H, Yan T, Jin Z, *et al.* CoP nanoparticles as cocatalyst modified the CdS/$NiWO_4$ p–n heterojunction to produce hydrogen efficiently. New J Chem, 2020, 44: 1426–1438
299 Zhang Y, Jin Z. Accelerated charge transfer *via* a nickel tungstate modulated cadmium sulfide p–n heterojunction for photocatalytic hydrogen evolution. Catal Sci Technol, 2019, 9: 1944–1960
300 Majhi D, Das K, Mishra A, *et al.* One pot synthesis of CdS/BiOBr/$Bi_2O_2CO_3$: A novel ternary double Z-scheme heterostructure photocatalyst for efficient degradation of atrazine. Appl Catal B-Environ, 2020, 260: 118222
301 Hu T, Li P, Zhang J, *et al.* Highly efficient direct Z-scheme WO_3/CdS-diethylenetriamine photocatalyst and its enhanced photocatalytic H_2 evolution under visible light irradiation. Appl Surf Sci, 2018, 442: 20–29
302 Wei W, Tian Q, Sun H, *et al.* Efficient visible-light-driven photocatalytic H_2 evolution over MoO_2-C/CdS ternary heterojunction with unique interfacial microstructures. Appl Catal B-Environ, 2020, 260: 118153
303 Tang Y, Traveerungroj P, Tan HL, *et al.* Scaffolding an ultrathin CdS layer on a ZnO nanorod array using pulsed electrodeposition for improved photocharge transport under visible light illumination. J Mater Chem A, 2015, 3: 19582–19587
304 Ma D, Shi JW, Zou Y, *et al.* Rational design of CdS@ZnO core-shell structure *via* atomic layer deposition for drastically enhanced photocatalytic H_2 evolution with excellent photostability. Nano Energy, 2017, 39: 183–191
305 Wu H, Zheng Z, Tang Y, *et al.* Pulsed electrodeposition of CdS on ZnO nanorods for highly sensitive photoelectrochemical sensing of copper(II) ions. Sustain Mater Technol, 2018, 18: e00075
306 Wang S, Zhu B, Liu M, *et al.* Direct Z-scheme ZnO/CdS hierarchical photocatalyst for enhanced photocatalytic H_2-production activity. Appl Catal B-Environ, 2019, 243: 19–26
307 Hoseini AA, Farhadi S, Zabardasti A, *et al.* A novel n-type CdS nanorods/p-type $LaFeO_3$ heterojunction nanocomposite with enhanced visible-light photocatalytic performance. RSC Adv, 2019, 9: 24489–24504
308 Han X, Wang D, Guo Z, *et al.* Excellent visible light absorption by adopting mesoporous SiC in SiC/CdS for enhanced photocatalytic hydrogen generation. mat express, 2019, 9: 65–72
309 Arif M, Min Z, Yuting L, *et al.* A Bi_2WO_6-based hybrid heterostructures photocatalyst with enhanced photodecomposition and photocatalytic hydrogen evolution through Z-scheme process. J Industrial Eng Chem, 2019, 69: 345–357
310 Zhang Y, Jin Z, Yuan H, *et al.* Well-regulated nickel nanoparticles functional modified ZIF-67 (Co) derived Co_3O_4/CdS p-n heterojunction for efficient photocatalytic hydrogen evolution. Appl Surf Sci, 2018, 462: 213–225
311 Xu Q, Zhang L, Yu J, *et al.* Direct Z-scheme photocatalysts: Principles, synthesis, and applications. Mater Today, 2018, 21: 1042–1063
312 Li X, Shen R, Ma S, *et al.* Graphene-based heterojunction photocatalysts. Appl Surf Sci, 2018, 430: 53–107
313 Zhong W, Shen S, He M, *et al.* The pulsed laser-induced Schottky junction *via in-situ* forming Cd clusters on CdS surfaces toward efficient visible light-driven photocatalytic hydrogen evolution.

Appl Catal B-Environ, 2019, 258: 117967
314 Shang L, Tong B, Yu H, *et al.* CdS nanoparticle-decorated Cd nanosheets for efficient visible light-driven photocatalytic hydrogen evolution. Adv Energy Mater, 2016, 6: 1501241
315 Lang D, Shen T, Xiang Q. Roles of MoS_2 and graphene as co-catalysts in the enhanced visible-light photocatalytic H_2 production activity of multiarmed CdS nanorods. ChemCatChem, 2015, 7: 943–951
316 Xu J, Wang L, Cao X. Polymer supported graphene–CdS composite catalyst with enhanced photocatalytic hydrogen production from water splitting under visible light. Chem Eng J, 2016, 283: 816–825
317 Kuang P, Sayed M, Fan J, *et al.* 3D graphene-based H_2-production photocatalyst and electrocatalyst. Adv Energy Mater, 2020, 10: 1903802
318 Xia Y, Cheng B, Fan J, *et al.* Unraveling photoexcited charge transfer pathway and process of CdS/graphene nanoribbon composites toward visible-light photocatalytic hydrogen evolution. Small, 2019, 15: 1902459
319 Xia Y, Cheng B, Fan J, *et al.* Near-infrared absorbing 2D/3D $ZnIn_2S_4$/N-doped graphene photocatalyst for highly efficient CO_2 capture and photocatalytic reduction. Sci China Mater, 2020, 63: 552–565
320 Wang Y, Chen J, Liu L, *et al.* Novel metal doped carbon quantum dots/CdS composites for efficient photocatalytic hydrogen evolution. Nanoscale, 2019, 11: 1618–1625
321 Qiu S, Shen Y, Wei G, *et al.* Carbon dots decorated ultrathin CdS nanosheets enabling *in-situ* anchored Pt single atoms: A highly efficient solar-driven photocatalyst for hydrogen evolution. Appl Catal B-Environ, 2019, 259: 118036
322 Ma S, Xu X, Xie J, *et al.* Improved visible-light photocatalytic H_2 generation over CdS nanosheets decorated by NiS_2 and metallic carbon black as dual earth-abundant cocatalysts. Chin J Catal, 2017, 38: 1970–1980
323 Kim YK, Lim SK, Park H, *et al.* Trilayer CdS/carbon nanofiber (CNF) mat/Pt-TiO_2 composite structures for solar hydrogen production: Effects of CNF mat thickness. Appl Catal B-Environ, 2016, 196: 216–222
324 Zhang J, Huang F. Enhanced visible light photocatalytic H_2 production activity of g-C_3N_4 *via* carbon fiber. Appl Surf Sci, 2015, 358: 287–295
325 Kim YK, Kim M, Hwang SH, *et al.* CdS-loaded flexible carbon nanofiber mats as a platform for solar hydrogen production. Int J Hydrogen Energy, 2015, 40: 136–145
326 Gopannagari M, Kumar DP, Park H, *et al.* Influence of surface-functionalized multi-walled carbon nanotubes on CdS nanohybrids for effective photocatalytic hydrogen production. Appl Catal B-Environ, 2018, 236: 294–303
327 Li H, Xiao S, Zhou J, *et al.* A flexible CdS nanorods-carbon nanotubes/stainless steel mesh photoanode for boosted photoelectrocatalytic hydrogen evolution. Chem Commun, 2019, 55: 2741–2744
328 Kim YK, Park H. Light-harvesting multi-walled carbon nanotubes and CdS hybrids: Application to photocatalytic hydrogen production from water. Energy Environ Sci, 2011, 4: 685–694
329 Meng A, Zhu B, Zhong B, *et al.* Direct Z-scheme TiO_2/CdS hierarchical photocatalyst for enhanced photocatalytic H_2-production activity. Appl Surf Sci, 2017, 422: 518–527
330 Yu W, Zhang S, Chen J, *et al.* Biomimetic Z-scheme photocatalyst with a tandem solid-state electron flow catalyzing H_2 evolution. J Mater Chem A, 2018, 6: 15668–15674
331 He F, Meng A, Cheng B, *et al.* Enhanced photocatalytic H_2-production activity of WO_3/TiO_2 step-scheme heterojunction by graphene modification. Chin J Catal, 2020, 41: 9–20
332 He K, Xie J, Luo X, *et al.* Enhanced visible light photocatalytic H_2 production over Z-scheme g-C_3N_4 nansheets/WO_3 nanorods nanocomposites loaded with Ni(OH)$_x$ cocatalysts. Chin J Catal, 2017, 38: 240–252
333 Low J, Jiang C, Cheng B, *et al.* A review of direct Z-scheme photocatalysts. Small Methods, 2017, 1: 1700080
334 Di T, Xu Q, Ho WK, *et al.* Review on metal sulphide-based Z-scheme photocatalysts. ChemCatChem, 2019, 11: 1394–1411
335 Zhang L, Hao X, Jian Q, *et al.* Ferrous oxalate dehydrate over CdS as Z-scheme photocatalytic hydrogen evolution. J Solid State Chem, 2019, 274: 286–294
336 Peng J, Shen J, Yu X, *et al.* Construction of LSPR-enhanced 0D/2D CdS/MoO_3–S-scheme heterojunctions for visible-light-driven photocatalytic H_2 evolution. Chin J Catal, 2021, 42: 87–96
337 Ren Y, Zeng D, Ong WJ. Interfacial engineering of graphitic carbon nitride (g-C_3N_4)-based metal sulfide heterojunction photocatalysts for energy conversion: A review. Chin J Catal, 2019, 40: 289–319
338 Ren D, Zhang W, Ding Y, *et al. In situ* fabrication of robust cocatalyst-free CdS/g-C_3N_4 2D-2D step-scheme heterojunctions for highly active H_2 evolution. Sol RRL, 2020, 4: 1900423
339 Yang R, Zhu R, Fan Y, *et al.* Construction of an artificial inorganic leaf CdS–$BiVO_4$ Z-scheme and its enhancement activities for pollutant degradation and hydrogen evolution. Catal Sci Technol, 2019, 9: 2426–2437
340 Low J, Dai B, Tong T, *et al. In situ* irradiated X-ray photoelectron spectroscopy investigation on a direct Z-scheme TiO_2/CdS composite film photocatalyst. Adv Mater, 2019, 31: 1802981
341 Ge H, Xu F, Cheng B, *et al.* S-scheme heterojunction TiO_2/CdS nanocomposite nanofiber as H_2-production photocatalyst. ChemCatChem, 2019, 11: 6301–6309
342 Cui H, Li B, Li Z, *et al.* Z-scheme based CdS/$CdWO_4$ heterojunction visible light photocatalyst for dye degradation and hydrogen evolution. Appl Surf Sci, 2018, 455: 831–840
343 Yin C, Cui L, Pu T, *et al.* Facile fabrication of nano-sized hollow-CdS@g-C_3N_4 core-shell spheres for efficient visible-light-driven hydrogen evolution. Appl Surf Sci, 2018, 456: 464–472
344 Yu G, Wang X, Cao J, *et al.* Plasmonic Au nanoparticles embedding enhances the activity and stability of CdS for photocatalytic hydrogen evolution. Chem Commun, 2016, 52: 2394–2397
345 Oros-Ruiz S, Hernández-Gordillo A, García-Mendoza C, *et al.* Comparative activity of CdS nanofibers superficially modified by Au, Cu, and Ni nanoparticles as co-catalysts for photocatalytic hydrogen production under visible light. J Chem Technol Biotechnol, 2016, 91: 2205–2210
346 Zhou X, Chen H, Sun Y, *et al.* Highly efficient light-induced hydrogen evolution from a stable Pt/CdS NPs-co-loaded hierarchically porous zeolite beta. Appl Catal B-Environ, 2014, 152: 271–279
347 Feng J, An C, Dai L, *et al.* Long-term production of H_2 over Pt/CdS nanoplates under sunlight illumination. Chem Eng J, 2016, 283: 351–357
348 Di T, Cheng B, Ho W, *et al.* Hierarchically CdS–Ag_2S nanocomposites for efficient photocatalytic H_2 production. Appl Surf Sci, 2019, 470: 196–204
349 Yin J, Zhan F, Jiao T, *et al.* Facile preparation of self-assembled

MXene@Au@CdS nanocomposite with enhanced photocatalytic hydrogen production activity. Sci China Mater, 2020, 63: 2228–2238
350 Ran J, Gao G, Li FT, *et al.* Ti_3C_2 MXene co-catalyst on metal sulfide photo-absorbers for enhanced visible-light photocatalytic hydrogen production. Nat Commun, 2017, 8: 13907
351 Li K, Zhang S, Li Y, *et al.* MXenes as noble-metal-alternative co-catalysts in photocatalysis. Chin J Catal, 2021, 42: 3–14
352 Cheng L, Li X, Zhang H, *et al.* Two-dimensional transition metal MXene-based photocatalysts for solar fuel generation. J Phys Chem Lett, 2019, 10: 3488–3494
353 Liu W, Wang X, Yu H, *et al.* Direct photoinduced synthesis of amorphous $CoMoS_x$ cocatalyst and its improved photocatalytic H_2-evolution activity of CdS. ACS Sustain Chem Eng, 2018, 6: 12436–12445
354 Lu X, Toe CY, Ji F, *et al.* Light-induced formation of MoO_xS_y clusters on CdS nanorods as cocatalyst for enhanced hydrogen evolution. ACS Appl Mater Interfaces, 2020, 12: 8324–8332
355 Zhang ZW, Li QH, Qiao XQ, *et al.* One-pot hydrothermal synthesis of willow branch-shaped MoS_2/CdS heterojunctions for photocatalytic H_2 production under visible light irradiation. Chin J Catal, 2019, 40: 371–379
356 Liang Z, Shen R, Ng YH, *et al.* A review on 2D MoS_2 cocatalysts in photocatalytic H_2 production. J Mater Sci Tech, 2020, 56: 89–121
357 Wei Z, Xu M, Liu J, *et al.* Simultaneous visible-light-induced hydrogen production enhancement and antibiotic wastewater degradation using MoS_2@$Zn_xCd_{1-x}S$: Solid-solution-assisted photocatalysis. Chin J Catal, 2020, 41: 103–113
358 Chai B, Liu C, Wang C, *et al.* Photocatalytic hydrogen evolution activity over MoS_2/$ZnIn_2S_4$ microspheres. Chin J Catal, 2017, 38: 2067–2075
359 Hu T, Dai K, Zhang J, *et al.* Noble-metal-free Ni_2P as cocatalyst decorated rapid microwave solvothermal synthesis of inorganic-organic CdS-DETA hybrids for enhanced photocatalytic hydrogen evolution. Appl Surf Sci, 2019, 481: 1385–1393
360 Dai D, Wang L, Xiao N, *et al. In-situ* synthesis of Ni_2P co-catalyst decorated $Zn_{0.5}Cd_{0.5}S$ nanorods for high-quantum-yield photocatalytic hydrogen production under visible light irradiation. Appl Catal B-Environ, 2018, 233: 194–201
361 Yuan J, Wen J, Zhong Y, *et al.* Enhanced photocatalytic H_2 evolution over noble-metal-free NiS cocatalyst modified CdS nanorods/g-C_3N_4 heterojunctions. J Mater Chem A, 2015, 3: 18244–18255
362 Song L, Zhang S. A novel cocatalyst of NiCoP significantly enhances visible-light photocatalytic hydrogen evolution over cadmium sulfide. J Industr Eng Chem, 2018, 61: 197–205
363 Li S, Wang L, Liu S, *et al. In situ* synthesis of strongly coupled Co_2P-CdS nanohybrids: An effective strategy to regulate photocatalytic hydrogen evolution activity. ACS Sustain Chem Eng, 2018, 6: 9940–9950
364 Zong X, Han J, Ma G, *et al.* Photocatalytic H_2 evolution on CdS loaded with WS_2 as cocatalyst under visible light irradiation. J Phys Chem C, 2011, 115: 12202–12208
365 Zou Y, Shi JW, Ma D, *et al.* WS_2/graphitic carbon nitride heterojunction nanosheets decorated with CdS quantum dots for photocatalytic hydrogen production. ChemSusChem, 2018, 11: 1187–1197
366 Moniruddin M, Oppong E, Stewart D, *et al.* Designing CdS-based ternary heterostructures consisting of co-metal and CoO_x cocatalysts for photocatalytic H_2 evolution under visible light. Inorg Chem, 2019, 58: 12325–12333
367 Shen R, Xie J, Xiang Q, *et al.* Ni-based photocatalytic H_2-production cocatalysts. Chin J Catal, 2019, 40: 240–288
368 Zhang H, Dong Y, Zhao S, *et al.* Photochemical preparation of atomically dispersed nickel on cadmium sulfide for superior photocatalytic hydrogen evolution. Appl Catal B-Environ, 2020, 261: 118233
369 Meng A, Zhang L, Cheng B, *et al.* Dual cocatalysts in TiO_2 photocatalysis. Adv Mater, 2019, 31: 1807660
370 Huang L, Wang X, Yang J, *et al.* Dual cocatalysts loaded type I CdS/ZnS core/shell nanocrystals as effective and stable photocatalysts for H_2 evolution. J Phys Chem C, 2013, 117: 11584–11591
371 Di T, Zhu B, Zhang J, *et al.* Enhanced photocatalytic H_2 production on CdS nanorod using cobalt-phosphate as oxidation cocatalyst. Appl Surf Sci, 2016, 389: 775–782
372 Ba Q, Jia X, Huang L, *et al.* Alloyed Pd Ni hollow nanoparticles as cocatalyst of CdS for improved photocatalytic activity toward hydrogen production. Int J Hydrogen Energy, 2019, 44: 5872–5880
373 Ba Q, Jia X, Huang L, *et al.* Hollow structured PtNi alloy as cocatalyst of CdS for hydrogen generation under visible light irradiation. Int J Hydrogen Energy, 2019, 44: 28104–28112
374 Zhang F, Zhuang HQ, Zhang W, *et al.* Noble-metal-free CuS/CdS photocatalyst for efficient visible-light-driven photocatalytic H_2 production from water. Catal Today, 2019, 330: 203–208
375 Liu G, Zhao G, Zhou W, *et al. In situ* bond modulation of graphitic carbon nitride to construct p-n homojunctions for enhanced photocatalytic hydrogen production. Adv Funct Mater, 2016, 26: 6822–6829
376 Wang X, Yu H, Yang L, *et al.* A highly efficient and noble metal-free photocatalytic system using Ni_xB/CdS as photocatalyst for visible light H_2 production from aqueous solution. Catal Commun, 2015, 67: 45–48
377 Wen T, Zhang L, Schmitt W. A Mn_{13}-cluster based coordination polymer as a co-catalyst of CdS for enhanced visible-light driven H_2 evolution. Dalton Trans, 2018, 47: 10857–10860
378 Iqbal S. Spatial charge separation and transfer in *L*-cysteine capped NiCoP/CdS nano-heterojunction activated with intimate covalent bonding for high-quantum-yield photocatalytic hydrogen evolution. Appl Catal B-Environ, 2020, 274: 119097
379 Lian J, Qi Y, Bao Y, *et al.* Reversed configuration of photocatalyst to exhibit improved properties of basic processes compared to conventional one. Sci China Chem, 2020, 63: 771–776
380 You F, Wan J, Qi J, *et al.* Lattice distortion in hollow multi-shelled structures for efficient visible-light CO_2 reduction with a SnS_2/SnO_2 junction. Angew Chem Int Ed, 2020, 59: 721–724
381 Li J, Liu X, Zhang J. Smart assembly of sulfide heterojunction photocatalysts with well-defined interfaces for direct Z-scheme water splitting under visible light. ChemSusChem, 2020, 13: 2996–3004
382 Ai Z, Zhang K, Chang B, *et al.* Construction of CdS@Ti_3C_2@CoO hierarchical tandem p-n heterojunction for boosting photocatalytic hydrogen production in pure water. Chem Eng J, 2020, 383: 123130
383 Ning X, Zhen W, Wu Y, *et al.* Inhibition of CdS photocorrosion by Al_2O_3 shell for highly stable photocatalytic overall water splitting under visible light irradiation. Appl Catal B-Environ, 2018, 226: 373–383
384 Qian L, Hou Y, Yu Z, *et al.* Metal-induced Z-scheme CdS/Ag/g-C_3N_4 photocatalyst for enhanced hydrogen evolution under visible light: The synergy of MIP effect and electron mediator of

Ag. Mol Catal, 2018, 458: 43–51
385 Peng T, Zhang X, Zeng P, *et al.* Carbon encapsulation strategy of Ni co-catalyst: Highly efficient and stable Ni@C/CdS nanocomposite photocatalyst for hydrogen production under visible light. J Catal, 2013, 303: 156–163
386 Xiong J, Liu Y, Cao C, *et al.* An architecture of $CdS/H_2Ti_5O_{11}$ ultrathin nanobelt for photocatalytic hydrogenation of 4-nitroaniline with highly efficient performance. J Mater Chem A, 2015, 3: 6935–6942
387 Hou Y, Laursen AB, Zhang J, *et al.* Layered nanojunctions for hydrogen-evolution catalysis. Angew Chem Int Ed, 2013, 52: 3621–3625

Acknowledgements Li X thanks the National Natural Science Foundation of China (21975084 and 51672089) and the Ding Ying Talent Project of South China Agricultural University for their support. Ng Y thanks the Hong Kong Research Grant Council (RGC) General Research Fund GRF1305419 for financial support. Zhang P thanks the National Natural Science Foundation of China (51972287 and 51502269).

Author contributions Shen R and Li X proposed the topic and outline of the manuscript. Shen R, Ren D, Ding Y and Guan Y collected the related information needed in writing the paper; Shen R and Li X co-wrote the manuscript. Ng Y and Zhang P revised and polished this manuscript. All authors discussed and commented on the manuscript.

Conflict of interest The authors declare that they have no conflict of interest.

Rongchen Shen received his Bachelor degree from Huaibei Normal University in 2016 and Master degree from South China Agricultural University in 2019. He is a PhD candidate at South China Agricultural University. His research interests mainly focus on two-dimensional materials for photocatalytic application.

Yun Hau Ng is an associate professor at the School of Energy and Environment, City University of Hong Kong. He received his PhD from Osaka University in 2009. Before joining the City University of Hong Kong, he was a lecturer (2014) and senior lecturer (2016) in the School of Chemical Engineering, University of New South Wales. His research is focused on the development of novel photoactive semiconductors for solar energy conversion. He received the APEC ASPIRE Prize in 2019, Distinguished Lectureship Award from the Chemical Society of Japan in 2018, and Honda-Fujishima Prize by the Electrochemical Society of Japan in 2013.

Peng Zhang received his PhD in materials physics and chemistry from Northeast Normal University, China (2014). After postdoctoral research at Helmholtz-Zentrum Berlin, Germany, he joined the School of Materials Science and engineering at Zhengzhou University. His current research interests focus on micro- and nanotechnology including low-dimensional carbon-based materials (graphene, CNF, carbon layer, etc.) and their applications in the fields of environment remediation and energy storage. He has published more than 60 SCI papers in the above fields such as *Adv. Mater.*, *Adv. Func. Mater.*, *Energy Storage Mater.* His work has been cited more than 4,000 times, and his H-index is 33.

Xin Li received his BS and PhD degrees in chemical engineering from Zhengzhou University in 2002 and South China University of Technology in 2007, respectively. Then, he joined South China Agricultural University as a faculty staff member, and became an associate professor of applied chemistry in 2011. In 2017, he became a Professor at South China Agricultural University. During 2012–2013, he worked as a visiting scholar at the Electrochemistry Center, the University of Texas at Austin, USA. His research interests include photocatalysis, photoelectrochemistry, adsorption, and the development of nanomaterials and devices (see http://www.researcherid.com/rid/A-2698-2011).

纳米结构硫化镉光催化分解水产氢综述

沈荣晨[1†], 任豆豆[1†], 丁英娜[2], 关雅彤[2], 吴永豪[3*], 张鹏[4*], 李鑫[1*]

摘要 太阳能驱动光催化分解水制氢是实现可持续制氢气的一种有效策略. 硫化镉半导体光催化剂基于其较强的可见光响应、适宜的氧化还原反应带边位置以及优异的电荷传输性能而备受关注. 本文综述了近年来国内外在提高硫化镉基光催化剂制氢性能的设计、改性和制备等方面的研究进展. 首先简要介绍了光催化制氢的基本概念和机理, 阐述了硫化镉光催化制氢的基本性质、重要进展和瓶颈, 综述了该材料的发展前景. 随后, 重点讨论了硫化镉基光催化剂光催化分解水产氢的各种改性策略, 其中有效的策略是产生更多的载流子, 促进电荷的有效分离, 促进界面电荷转移, 加速电荷利用, 以及抑制电荷诱导的自光腐蚀. 针对每一种改性策略, 都详细讨论了影响光催化剂性能的重要因素和未来潜在的研究方向. 最后介绍了纳米结构硫化镉和硫化镉基纳米复合材料在光催化分解水产氢中的发展前景和面临的挑战. 本综述将为开发镉基半导体光催化剂提供重要和及时的理论指导, 并促进其在太阳能氢气生产中的应用.

